Generic Market Modelling for Future Grid Scenario Analysis

Shariq Riaz

Supervisor: Dr. Gregor Verbič

Co-supervisor: Archie C. Chapman

Centre for Future Energy Networks,
School of Electrical and Information Engineering,
Faculty of Engineering and IT,
The University of Sydney.

This thesis submitted in fulfilment of the requirements for the degree of
Doctor of Philosophy

School of EIE February 2018

Dedicated with love and gratitude to:

My Mother

A strong and persistent women, made a lot of sacrifices and faced many odd situations for me. My success is result of your love, care, affection and prayers.

My Father

My safety net, thanks for being a strong anchor point and showing me how to navigate the treacherous waters of life. Lessons I learned from your action have far greater impact in my life than anything else.

My Wife

Thanks for your understanding and sticking with me through thick and thin. I can always count on you.

Declaration

I hereby declare that except where specific reference is made to the work of others, the contents of this dissertation are original and have not been submitted in whole or in part for consideration for any other degree or qualification in this, or any other university. This dissertation is my own work and contains nothing which is the outcome of work done in collaboration with others, except as specified in the text and Acknowledgements. This dissertation contains fewer than 80,000 words including appendices, bibliography, footnotes, tables and equations and has fewer than 150 figures.

Shariq Riaz
February 2018

Acknowledgements

I would like to express my heartfelt gratitude and acknowledgement to my supervisors Dr. Gregor Verbič and Dr. Archie C. Chapman. You have been exceptional mentors for me during last three years. Thank you for your continuous support, time and relentless efforts both inside and outside academic domains. You comments, advice and encouragement have a positive influence on my thought process.

I would also like to thank Dr. Hesamoddin Marzooghi and Mr. Ahmad Shabir Ahmadyar at The University of Sydney who collaborated with me for Chapter 3 and Chapter 6, respectively.

Finally I would thank following for provided me with financial assistance:

- Faculty Development Program Scholarship, University of Engineering and Technology Lahore, Department of Electrical Engineering, Pakistan.
- Postgraduate Scholarship in Future Grids, The University of Sydney, School of Electrical and Information Engineering.
- Norman I Price Scholarship, The University of Sydney, School of Electrical and Information Engineering.

List of Publications

I made a number of contributions in the papers listed below where I was the lead author in two journal and three conference publications. The numbers in the tables represent percentage shares of each author's contribution. In each work, authors are arranged in ascending order based on their contributions.

Journal Articles

[JA1] "S. Riaz, H. Marzooghi, G. Verbič, A. Chapman, D. J. Hill "Generic Demand Model Considering the Impact of Prosumers for Future Grid Scenario Analysis," in *IEEE Transactions on Smart Grid*. doi: 10.1109/TSG.2017.2752712

Contribution made in this paper is incorporated in Chapter 3.

Contributors	Modelling	Analysing the results	Writing the paper
S. Riaz	60 %	50 %	30 %
Others	40 %	50 %	70 %

[JA2] S. Riaz, G. Verbič, A. Chapman "Computationally Efficient Market Simulation Tool for Future Grid Scenario Analysis," in *IEEE Transactions on Smart Grid*. doi: 10.1109/TSG.2017.2765662

Contribution made in this paper is incorporated in Chapter 5.

Contributors	Modelling	Analysing the results	Writing the paper
S. Riaz	90 %	90 %	70 %
Others	10 %	10 %	30 %

[JA3] A.S. Ahmadyar, S. Riaz, G. Verbič, A. Chapman, D. J. Hill "A Framework for Assessing Renewable Integration Limits with Respect to Frequency Performance," in *IEEE Transactions on Power Systems*. doi: 10.1109/TPWRS.2017.2773091

Contribution made in this paper is incorporated in Chapter 6.

Contributors	Modelling	Analysing the results	Writing the paper
S. Riaz	30 %	20 %	15 %
Others	70 %	80 %	85 %

Conference Papers

[CP1] S. Riaz, A. C. Chapman and G. Verbič, "Comparing utility and residential battery storage for increasing flexibility of power systems," *2015 Australasian Universities Power Engineering Conference (AUPEC)*, Wollongong, NSW, 2015, pp. 1-6. doi: 10.1109/AUPEC.2015.7324836

Contribution made in this paper is incorporated in Chapter 2.

Contributors	Modelling	Analysing the results	Writing the paper
S. Riaz	75 %	85 %	80 %
Others	25 %	15 %	20 %

[CP2] S. Riaz, A. C. Chapman and G. Verbič, "Evaluation of concentrated solar-thermal generation for provision of power system flexibility," *2016 Power Systems Computation Conference (PSCC)*, Genoa, 2016, pp. 1-7. doi: 10.1109/PSCC.2016.7540955

Contribution made in this paper is incorporated in Chapter 4.

Contributors	Modelling	Analysing the results	Writing the paper
S. Riaz	85 %	90 %	70 %
Others	15 %	10 %	30 %

[CP3] S. Riaz, H. Marzooghi, G. Verbič, A. C. Chapman and D. J. Hill, "Impact study of prosumers on loadability and voltage stability of future grids," 2016 IEEE International Conference on Power System Technology (POWERCON), Wollongong, NSW, 2016, pp. 1-6. doi: 10.1109/POWERCON.2016.7753922

Contribution made in this paper is incorporated in Chapter 3.

Contributors	Modelling	Analysing the results	Writing the paper
S. Riaz	70 %	80 %	70 %
Others	30 %	20 %	30 %

[CP4] A. S. Ahmadyar, S. Riaz, G. Verbič, J. Riesz and A. Chapman, "Assessment of minimum inertia requirement for system frequency stability," *2016 IEEE International Conference on Power System Technology (POWERCON)*, Wollongong, NSW, 2016, pp. 1-6. doi: 10.1109/POWERCON.2016.7753912

Contribution made in this paper is not included in this thesis.

Contributors	Modelling	Analysing the results	Writing the paper
S. Riaz	30 %	20 %	25 %
Others	70 %	80 %	75 %

Abstract

Power systems worldwide are moving away from being dominated by large-scale synchronous generation and passive consumers. Instead, in the future, new actors on both the generation and the load side will play an increasingly significant role. On the generation side, there are renewable energy resources (RES) such as wind generation (WG), photovoltaic (PV) and concentrated solar thermal (CST). On the load side, there are demand response (DR), energy storage and price responsive users equipped with a small-scale PV-battery system (called prosumers). The two sides will together shape future grids. However, if connected at a large scale without proper consideration of their effect, they can also jeopardise the reliability and security of electricity supply. For example, the addition of non-synchronous RES will jeopardise the frequency response of the future grids, while the intermittency and variability of RES threats the existing model of electricity supply (supply following demand), complicating balancing and stressing future grids' ramping capabilities. On the other hand, the inclusion of DR, prosumers and storage without proper consideration of the implications can cause significant changes to the demand profiles and may result in new stresses such as secondary peaks or excessive ramps. In summary, balancing, stability (frequency, voltage, transient) and ultimately reliability are affected by the changes introduced to the future grids' technology mix.

Given that the lifespan of power system assets is well over fifty years, laying out a roadmap to future grid development in an economical fashion without risking its security is a challenging task. The uncertainty of cost, availability and quality of new technologies requires power system planners and policy-makers to evaluate the feasibility and viability of future grids for a diverse range of technology options. To this end, a rigorous and systematic approach is developed in this dissertation to analyse the implications of prosumers, storage and CST on the balancing and stability of future grids. The best features of all these approaches are combined and presented in a single coherent framework. Computation time improvement techniques are then deployed to improve the computational efficiency and solution accuracy. Taken as a whole, the tool will fill the gap to explore the validity of emerging technologies to tackle balancing, stability, security and reliability issues, over a diverse scope of uncertain premises.

The tool is developed for an approach to future grids studies called *scenario analysis*. Traditionally, power systems are planned based on a handful of the most critical scenarios with an aim to find an optimal generation and/or transmission plan. In contradistinction, scenario analysis involves analysing possible evolutionary pathways to facilitate informed decision making by policy-makers and system planners. Specifically, the primary aim of future grids studies is to deal with the uncertainty of long-term decision making and providing outcomes that are technically possible, although explicit costing might be considered. To this end, for any future grids stability framework, the market model is a critical bottleneck. Existing future grids studies mostly look at simple balancing, ignore network constraints and include most of the emerging technologies in an ad hoc fashion. These simplifications are made to combat the high computation time requirement of accurate approaches.

Against this backdrop, this dissertation presents: i) a novel optimisation-based models to capture the effects of prosumers (Chapter 2, 3); ii) co-optimise dispatch of PV and CST aggregation to reduce ramping stress on the conventional generators (Chapter 4); iii) efficiently implemented market-based dispatch (Chapter 5); iv) framework for frequency performance assessment of future grids (Chapter 6).

In more detail, first, Chapter 2 and 3 develop a novel approach to explicitly model prosumers' demand in market dispatch (production cost) models. The key novelty of the method is its ability to capture the impact of prosumers without going into specific market structure or control mechanisms, which are computationally expensive. The model is formulated as a bi-level program in which the upper-level unit commitment (UC) problem minimises the total generation cost and the lower-level problem maximises prosumers' aggregate self-consumption. Unlike the existing bi-level optimisation frameworks that focus on the interaction between the wholesale market and an aggregator, the coupling is through the prosumers' demand, not through the electricity price. That renders the proposed model market structure agnostic, making it suitable for future grids studies where the market structure is potentially unknown. This model addresses some critical questions such as, How much flexibility can prosumer provide to help with large-scale RES integration?

Flexibility is the key to achieve a high RES penetration. One of the major problem in the integration of RES is their intermittent and variable nature. Concentrated solar thermal (CST) presents an excellent resource with inherent flexibility. In contrast to Chapter 2 and 3 (exploring flexibility through DSM), Chapter 4 examines flexibility options from a generation end. In particular, it proposes an RES aggregation (REA) scheme aiming to co-optimise the dispatch of intermittent and dispatchable RES. The principal aim is to keep in check the ramping stress imposed on the conventional generators due to the RES integration. A Stackelberg game is used to capture the interaction between an independent system operator

(ISO) and the REA when the ISO tries to minimise the generation cost, while REA seeks to maximise its revenue. This approach also highlights the potential of a ramping market, as proposed by some US studies.

In Chapter 5, the utility storage proposed in Chapter 2, prosumers model proposed in Chapter 3, the dispatch model of CST developed in Chapter 4 and inertia constraint detailed in Chapter 6 are combined into a single coherent framework. The addition of these emerging technologies in the energy market model significantly increases the computation burden. Also, to allow for a subsequent stability assessment, an accurate representation of the number of online generation units is required, which affects the power system inertia and the reactive power support capability. This renders a fully-fledged market model computationally intractable, so in Chapter 5 we deploy unit clustering, a rolling-horizon optimisation approach and constraint clipping to improve the computational efficiency. Together, these comprise a computationally efficient market simulation tool (MST) suitable for future grid stability analysis.

Finally, developed MST is used in Chapter 6 for a comprehensive frequency performance assessment of the Australian National Electricity Market (NEM). First, an assessment of minimum inertia requirements is presented, followed by a framework for frequency performance assessment of future grids. The maximum non-synchronous instantaneous range from a frequency performance point of view is established for the NEM. Also, to alleviate the deteriorating effects of the high RES penetration on frequency performance, different technical solutions are proposed and discussed. These efforts will empower policy-makers and system planners with the information on safe penetration levels of different technologies while ensuring reliability and security of future grids.

Table of contents

Nomenclature

Variables

b	Additional variable introduced to maintain complementarity
d^{cst}	Binary variable to indicate CST is turned off
δ_n	Voltage angle at node n
d_g	Shutdown variable of a unit of generator g
e_p^{b}	Battery state of charge of prosumer p
p^{es}	Electric power spillage
e_s	Energy stored in storage plant s
λ	Dual variables associated with equality constraints
μ	Dual variables associated with inequality constraints
p_p^{b}	Battery power flow of prosumer p
p^{cst}	Power dispatched from CST
$p_p^{\text{g+}}$	Grid power requirement of prosumer p
p_g	Power dispatched from supplier g
p_l	Power flow on line l
$p_p^{\text{g-}}$	Feed-in power from prosumer p
p^{pv}	Power dispatched from PV
p^{rea}	Power dispatch from REA

p_s	Power flow of storage plant s
$q^{\text{tes+/-}}$	TES thermal power in/out flow
q^{ts}	Thermal power spillage
s^{cst}	Binary variable to indicate on/off status of CST
s_g	Number of online units of generator g
e^{tes}	Thermal energy stored by TES
u^{cst}	Binary variable to indicate CST is turned on
u_g	Startup variable of a unit of generator g

Initial Conditions

$\hat{d}_{g,t}$	Minimum number of units of generator $g \in \mathcal{G}^{\text{syn}}$ required to remain offline for time $t < \tau_g^{\text{d}}$
$\hat{e}_g$	Energy stored in TES of $g \in \mathcal{G}^{\text{cst}}$ at start of horizon
$\hat{e}_p^{\text{b}}$	Battery state of charge for prosumer p at start of horizon
$\hat{e}_s$	Energy stored in storage plant s at start of horizon
$\hat{p}_g$	Power dispatch of generator g at start of horizon
$\hat{s}_g$	Number of online units of generator $g \in \mathcal{G}^{\text{syn}}$ at start of horizon
$\hat{u}_{g,t}$	Minimum number of units of generator $g \in \mathcal{G}^{\text{syn}}$ required to remain online for time $t < \tau_g^{\text{u}}$

Parameters

α	Percentage spinning reserves to be maintained by CST for PV
B_l	Susceptance of line l
c_g^{fix}	Fix cost of a unit of generator g
c_g^{sd}	Shutdown cost of a unit of generator g
c_g^{su}	Startup cost of a unit of generator g

c_g^{var}	Variable cost of a unit of generator g
η	Efficiency of component
H_g	Inertia constant of a power generating unit g
I	Synchronous inertia requirement (GW s)
M	Large enough coefficient, such that corresponding constraint is never binding if right hand of equation is non zero
λ^{rea}	REA bid
p	System load demand
$p^{'}$	System residual load demand
p_c	Power demand of consumer c
Δp_l	Power loss on line l
p_p	Underline load demand of prosumer p
p_p^{pv}	Aggregator PV power of prosumer p
r_g^+	Ramp-up rate of a unit of generator g
r_g^-	Ramp-down rate of a unit of generator g
p^{r}	Active power reserve requirement
S_g	MVA rating of a unit of generator g
τ_g^{d}	Minimum down time of a unit of generator g
$\tilde{t}$	Time slot offset index
τ_g^{u}	Minimum up time of a unit of generator g
$\overline{U}_g$	Total number of identical units of generator g

Sets

$\mathcal{C}$	Set of consumers c
$\mathcal{G}$	Set of generators g

$\mathcal{G}^{\text{cst}}$	Set of CST generators $\mathcal{G}^{\text{cst}} \subseteq \mathcal{G}$
$\mathcal{G}_r$	Set of generators in region r
$\mathcal{N}_r$	Set of nodes in region r
$\mathcal{N}$	Set of Nodes n
Ω	Set of decision variables
$\mathcal{P}$	Set of prosumers p
$\mathcal{R}$	Set of regions r
$\mathcal{S}$	Set of storage plants s
$\mathcal{G}^{\text{syn}}$	Set of synchronous generators $\mathcal{G}^{\text{syn}} \subseteq \mathcal{G}$
$\mathcal{T}$	Set of time slots t

Other Symbols

$\overline{\bullet}$	Maximum limit of variable $\bullet$
$\underline{\bullet}$	Minimum limit of variable $\bullet$
$\lvert\bullet\rvert$	Cardinality of set $\bullet$

Acronyms / Abbreviations

AEMO	Australian energy market operator
BAU	Business as usual
CC	Credible contingency
CCGT	Combine cycle gas turbine
CG	Conventional generators
CSIRO	Commonwealth scientific and industrial research organisation
CST	Concentrated solar thermal
DR	Demand Response
DSM	Demand side management

FG	Future grid
ISO	Independent system operator
KKT	Karush-Kuhn-Tucker
MILP	Mixed integer linear programming
MIP	Mixed integer programming
MPEC	Mathematical programming with equilibrium constraints
MST	Market simulation tool
MDT	Minimum down time
MUT	Minimum up time
MUDT	Minimum up/down time
NEM	National electricity market
NSAP	Non-synchronous annual penetration
NSIP	Non-synchronous instantaneous penetration
NSW	New South Wales
NTNDP	National transmission network development plan
O&M	Operation and maintenance
OCGT	Open cycle gas turbine
PV	Photovoltaic
QLD	Queensland
REA	Renewable energy resource aggregation
RES	Renewable energy resource
RoCoF	Rate of change of frequency
SA	South Australia
SOC	State of charge

SRMC	Short run marginal cost
TES	Thermal energy storage
UC	Unit commitment
VIC	Victoria
WG	Wind generator

Chapter 1

Introduction

Electricity is a commodity that can be traded like any other goods. However, unlike other goods, electricity is difficult to store, so supply and demand need to be perfectly balanced at all times. Thus, electricity has to be generated and dispatched to follow the system's demand, instantaneously. Reliable delivery of electric power is ensured by large generators connected to consumers through a vast electricity network. Any mismatch between supply and demand results in detrimental frequency variations jeopardising system stability. Real-time power dispatch is challenging as demand varies with external factors such as temperature, humidity, time of day and season. Transmission losses caused by network congestion adds to the complexity.

In order to manage this complexity, the commercial exchange of electric power between producers and consumers is managed through an electricity market. An electricity market is comprised of systems and rules enabling trade of electricity through different mechanisms, including but not limited to sale and purchase bids, short-term trades, future, spot, wholesale and day ahead trade obligations. Historically, until 1980, most power systems worldwide were state-owned vertically-integrated utilities. In traditional regulatory environments, one entity (usually the state) owns generation, transmission and distribution systems, holding a monopoly over a vast geographical area. For decades, the traditional models of state-owned vertically-integrated utilities worked well. Advancements in science and engineering improved reliability to the extent that, in most parts of the industrialised world, the average consumer was not deprived of electricity for more than a few minutes per year.

In the last two decades of the twentieth century, economists started to highlight the inefficacy of state regulations. They contended that state-owned monopolies did not leave customers with any choice, often encouraged unnecessary investments stifled new technologies and innovation and were prone to political interference. Also, it was possible that such regulated industries would act for their own benefit, adversely affecting investment

opportunities, consumers and the broader economy. They concluded that in a deregulated framework, fewer and simpler regulations would encourage competitiveness resulting in greater efficiencies and innovation, higher productivity and lower prices. Also, unlike in a regulated environment, the investment mistakes in a deregulated framework will not be passed down to consumers. For these reasons, the electric power industry has been primarily privatised, resulting in the emergence of electricity markets.

In deregulated environments, generation companies *(gencos)* own a portfolio of generators and sell electrical energy in a wholesale market. They also typically participate in voltage and frequency control, and in reserve and ancillary services markets. Transmission companies *(transcos)* and distribution companies *(discos)* own the transmission and distribution infrastructure. *Small consumers* buy electrical energy from a *retailer*. Retailers buy electrical energy from the wholesale market and sell it to the consumers, who typically do not participate in the wholesale market. Retailers usually do not own any transmission or distribution infrastructure. However, some retailers do own generators and knowns as *gentailers*. In a deregulated environment, the energy cost determined in the wholesale market and network costs (i.e., the costs of operating, maintaining and developing the networks) are separated. The responsibility for ensuring the fair, efficient and coherent operation of the electricity sector is a held by a regulator, which is typically a government body that sets rules and investigates cases of market abuse. Small consumers typically choose the preferred retailer. In contrast, large consumers can actively participate in the electricity market and can purchase power directly in the wholesale market or use bilateral contracts with gencos. All wholesale market participants, both suppliers and buyers of energy, must register with the *market operator* who is responsible for the settlement of sale and purchase bids, which sometimes also includes consideration of bilateral agreements between gencos and retailers. *Independent system operator* (ISO) has the primary responsibility of dispatching power in real-time while ensuring the security of the power system and determining the market clearance price. In Australia, with its gross pooled market, energy is traded in the pool market only, and this is the responsibility of Australian Electricity Market Operator (AEMO). Contracts for supply and derivatives are used to manage the allocation of price risk between parties but are typically enacted as over-the-counter exchanges, although there is an energy futures market on the Australian Securities Exchange.

In order to fulfil demand requirements efficiently, power from generating units is scheduled in an optimally. Given that, at any time, several tens of units are available, economic dispatch is a challenging and computationally expensive task. A dispatch decision is constrained by technical and operational limits of the units and system wide constraints. Furthermore, some constraints have intertemporal dependence and require sufficiently long solution

horizons to schedule the available units well in advance. The resultant mathematical market models are referred to as *unit commitment* (UC) as explained in Section 1.2. The efficient formulations of and solutions to the UC problem is one of the technical focuses of this thesis.

1.1 Emerging Challenges

Contemporary power systems are designed around the concept of passive consumers, predictable demand with acceptable forecast accuracy and economical large-scale dispatchable generation. Thus, in an ideal situation, consumers vary their power consumption based on their needs (irrespective of price, network congestion and other factors), which can be predicted considering past consumption behaviours and patterns, temperature, seasons, etc. Generation then can be dispatched in anticipation of the demand requirements. Usually, only a small amount of power reserve is maintained to overcome any variation between predicted and actual demand. This model of *supply-following-demand* is currently dominant in most of the power systems worldwide.

However, emerging technologies are now challenging the status quo and have started to influence power systems in new ways. First are the renewable generation resources. Their intermittent, variable and non-synchronous nature requires new operational strategies, as discussed in Chapter 3, 4 and 6. A quick solution to the variable nature of renewable is large-scale storage, as presented in Chapter 2. Advancements in the small scale generation and storage technologies enabled small consumers to generate their electricity partially and more actively interact with the grid either by shifting their power consumption or through demand-side management programs. Hence, day ahead demand prediction models are becoming increasingly inefficient and new models are required to capture the effect of small-scale generation and storage, as discussed in Chapters 2 and 3. The inherent flexibility provided by concentrated solar thermal plants and their synchronous nature highlights their importance in the wake of decreasing system inertia, as explored in Chapter 4. A brief elaboration of these changes to the existing power systems is given below.

1.1.1 Renewable energy resources

In the last decade, raising environmental concerns, global warming, dwindling fossil fuels and increasing energy demand led to the introduction of renewable energy targets. These targets aim to decrease the global carbon footprint by reducing the world's dependency on fossil fuels and encouraging the uptake of alternative sustainable energy resources. Consequently, in the

electrical power domain, *renewable energy sources* (RES) have started to push power systems worldwide away from domination by large-scale fossil fuel based generation. However, integrating RES into existing grids has its challenges. In particular, including RES in the existing electricity network without proper measures can jeopardise stability and security of power systems, due to their variable and non-synchronous nature.

First, the challenge in realising a sustainable future is to develop technologies that enable flexible integration and control of RES in existing power systems. Inherently, the variable nature of matured RES technologies such as photovoltaic (PV), concentrated solar thermal (CST) and wind generation (WG) have challenged the traditional electricity model of supply-following-demand. RES can only provide energy when their primary resource is available. Hence, to minimise demand generation mismatch, power systems need to be more flexible to utilise energy when it is available.

Second, the output of RES fluctuates in the order of seconds because of the various natural phenomena (e.g. cloud moving above a PV). To ensure a balance between demand and supply, a more substantial amount of reserve power is required to overcome RES variability. Also, because of sudden power shortfall or excesses, the ramping capability of power systems needs to be increased to counter RES dispatch variations. Presently, power systems are dominated by large coal generators, which are not flexible enough to alter their dispatch as quickly as the variability in RES requires.

Third, currently dominating RES like PV and WG are connected to the power system through power electronic interface. So, they are non-synchronous and cannot contribute towards system inertia. Traditionally in power systems, an immediate imbalance between supply and demand are countered by kinetic energy stored in the rotating masses of synchronous generators. Higher penetration levels of RES will drive large coal synchronous generators out of the merit order, resulting in a decrease in system inertia. Lower inertia has a significant detrimental effect on the power system frequency performance.

The dream of 100% energy from RES cannot be achieved without overcoming the above three challenges. From the financial point of view, it is also desirable to integrate RES without having to rebuild the existing infrastructure completely . Hence, finding a solution that allows flexible integration of RES into the existing grid are becoming imperative.

1.1.2 Utility scale storage

Advancements in utility-scale storage such as chemical batteries, pumped hydro, compressed air, gravity storage, flywheels and thermal storage can support power systems as they increase their penetration of RES. However, most of these technologies are either not mature, too expensive or geographically limited. Thus, finding the best methods for determining the size

and location of storage for grid flexibility requires extensive studies regarding its impact on power system stability.

1.1.3 Small-scale generation and storage

In a power system, consumers' choices are limited to the selection of retailers. However, technological advancements in rooftop-PV, distributed generation and household battery systems make it economically viable for consumers to become *prosumers*[1], enabling them to participate actively and influence the electricity market by changing their consumption patterns. These technologies enable prosumers to generate, store and even send excess energy back to the grid, which is known as *feed-in power*. Thus, with their ability to respond to altering prices, prosumers can no longer be considered passive. These changes are invalidating traditional demand predictions and drive the need to incorporate the behaviour and impact of small-scale generation and storage on the operation of power system.

1.1.4 Demand side management

Demand side management (DSM) consists of programs encouraging the reduction or alteration of consumption patterns based on incentives and prices. DSM can improve the load factor and efficiency of a power system through peak clipping, load shifting, valley filling, flexible load shaping, energy conservation and strategic growth.

The concept of DSM is not new, although early versions of DSM mostly consist of load shedding and direct load control. DSM aims can be classified into three main categories. First are the targets inspired to fulfil economic needs. These programs are designed to reduce electricity production and transmission costs, increase reserve margins and mitigate price volatility. Second, environment-based programs aimed to decrease electricity usage through efficient devices, the commitment of environmentally friendly units and greenhouse effect reduction. Third, network-driven arrangements are designed to improve system reliability, stability and reduce the peak to average demand ratio.

DSM can be implemented either through incentive-based programs or indirect mechanisms. Direct load control and demand bidding are examples of incentive-based DSM. In incentive-based programs, benefits are paid to the participating customers for allowing utility to control their loads. Whereas indirect mechanisms including demand response (DR), encourage consumers to alter their demand to support power system and reduce their electricity cost. These mechanisms can be either implemented through pricing signals including time of use pricing, real-time pricing, critical peak pricing, extreme day pricing, and extreme day

[1] Consumer with generation (e.g. rooftop-PV) and/or battery (**pro**ducer-con**sumer**)

critical peak pricing, or supporting consumers to leverage flexibility from their batteries, hot water system and thermal inertia of building.

Modern communication and control infrastructure empowers consumers to react to changing prices and decrease electricity costs by shifting non-critical loads from peak to off-peak intervals. This action not only challenges the traditional demand prediction but also provides an opportunity for the design of *demand-following-supply* models. These models enable flexibility obtained from the demand to be used to integrate RES in power systems. However, to exploit the full potential of DSM, policies and mechanisms needed to be designed carefully. Otherwise, it might create more problems than one sought to solve. For example, if a selected mechanism gives rise to secondary peaks by shifting midday peak to afternoon, it will result in more severe line congestion. Less apparent, it is also undesirable for a mechanism to result in either high ramp rates or lower system inertia. Hence, careful studies need to be carried out to access the impact of DSM on power systems fully. Note that as prosumers are also capable of shifting their demand requirement, so, they can be considered under the umbrella of DSM.

1.1.5 Concentrated solar thermal

CST plant represents an RES with an integrated thermal energy storage system. In regions with an excellent solar resource, e.g., Australia, California and Chile it provides the cornerstone of future electric energy supply systems. It is different from the other ready-to-deploy RES in that it is synchronous and has dispatchable power, with thermal storage and backup fuel sources providing flexibility in its operation. As such, CST can overcome the intermittent nature of its primary energy source. The use of CST in future grids is not only advantageous from the power balancing point of view, but it will also provide spinning reserves and inertia required for power system security.

1.2 Unit Commitment

The Design of existing power systems revolves around the idea of controllable generation and passive consumers. Integration of RES, increasing penetration of prosumers, greater amounts of storage and other emerging technologies challenge the basic principles of network planning. Traditionally, the electricity grid is planned as an extension to the existing system with an aim to fulfil the demand over the next decade or so. However, the choice of a particular technology and its penetration level plays a crucial role in the design of future grids. Thus, traditional network planning (where only the most critical contingency cases are

identified and analysed) has to evolve and step in the realm of *scenario analysis*. In contrast to planning problems, the aim in scenario analysis is to analyse possible evolutionary pathways to guide power system planning and policy making over the long term, and subject to much higher levels of uncertainty about the available technologies and their costs. Furthermore, to study the impact of these new technologies on future grids, we need models that generate dispatch decisions, which provide the basis of power flow, and ultimately, the starting point of future grid scenario analysis. UC is one such candidate. The UC problem is an umbrella term for a large class of problems in power system operation and planning whose aim is to schedule and dispatch power generation at minimum cost to meet the anticipated demand while meeting a set of system-wide constraints. In smart grids, problems with a similar structure arise in the area of energy management for load-side applications, and they are sometimes also called UC [1]. But here we refer to the system-level coordinated dispatch of large generators and storage elements in an entire grid. Before deregulation, UC was used in vertically-integrated utilities for generation scheduling to minimise production costs. After deregulation, UC is still used by an ISO to maximise social welfare, but the underlying optimisation model is mostly the same.

Mathematically, UC is a large-scale, nonlinear, non-convex, mixed-integer optimisation problem under uncertainty. With some abuse of notation, the UC optimisation problem can be represented in the following compact formulation [2]:

$$\begin{aligned}
\underset{\mathbf{x}_\mathrm{c},\mathbf{x}_\mathrm{b}}{\text{minimise}} \quad & f_\mathrm{c}(\mathbf{x}_\mathrm{c}) + f_\mathrm{b}(\mathbf{x}_\mathrm{b}) && (1.1)\\
\text{subject to} \quad & g_\mathrm{c}(\mathbf{x}_\mathrm{c}) \leq \mathbf{b} && (1.2)\\
& g_\mathrm{b}(\mathbf{x}_\mathrm{b}) \leq \mathbf{c} && (1.3)\\
& h_\mathrm{c}(\mathbf{x}_\mathrm{c}) + h_\mathrm{b}(\mathbf{x}_\mathrm{b}) \leq \mathbf{d} && (1.4)\\
& \mathbf{x}_\mathrm{c} \in \mathbb{R}^+,\, \mathbf{x}_\mathrm{b} \in \{0,1\}
\end{aligned}$$

Due to the time-couplings, the UC problem needs to be solved over a sufficiently long horizon. The decision vector $\mathbf{x} = \{\mathbf{x}_\mathrm{c}, \mathbf{x}_\mathrm{b}\}$ for each time interval consist of continuous and binary variables. The continuous variables, $\mathbf{x}_\mathrm{c}$, include generation dispatch levels, load levels, transmission power flows, storage levels, and transmission voltage magnitudes and phase angles. The binary variables, $\mathbf{x}_\mathrm{b}$, includes scheduling decisions for generation and storage, and logical decisions that ensure consistency of the solution. The objective (1.1) captures the total production cost, including fuel costs, start-up costs and shut-down costs. The constraints include dispatch related constraints such as energy balance, reserve requirements, transmission limits, and ramping constraints (1.2); commitment variables, including minimum up and down, and start-up/shut-down constraints (1.3); and constraints

coupling commitment and dispatch decisions, including minimum and maximum generation capacity constraints (1.4).

The complexity of the problem stems from the following: i) Specific generation technologies (e.g. coal-fired steam units) require long start-up and shut-down times, which requires a sufficiently long solution horizon. ii) Generators are interconnected, which introduces couplings through the power flow constraints. iii) On/off decisions introduce a combinatorial structure. iv) Some constraints (e.g. AC load flow constraints) and parameters (e.g., production costs) are non-convex. v) The increasing penetration of variable renewable generation and the emergence of demand-side technologies introduce uncertainty. As a result, an exact UC formulation is computationally intractable, so many approximations and heuristics have been proposed to strike a balance between computational complexity and functional requirements. For example, power flow constraints can be neglected altogether (a copper plate model), can be replaced with simple network flow constraints to represent critical inter-connectors, or, instead of (non-convex) AC, a simplified (linear) DC load flow may be used.

In summary, UC is a computationally challenging problem. In practice, the difference between a computationally efficient method generating a good solution and an accurate method that takes a long time to converge is a vital decision parameter. In power systems, the requirements and formulations of UC used for operations and planning are quite distinct, and employ diverse levels of detail. UC formulations in operation and planning studies along with its solution methods are detailed below. Building on these existing approximations and methods, this thesis presents a UC based simulation tool suitable for studying the impact of emerging technologies as mentioned in Section 1.1, in a new setting, that of *scenario studies*, discussed in more detail in Section 1.3.

1.2.1 UC in power system operation

Operational UC involves the scheduling of units over a horizon, typically spanning from 24 hours to 48 hours. In a system with dominated by thermal units a good approximation of the UC problem can be obtained by considering exponential startup and shutdown costs and a quadratic variable cost function to model the thermal behaviour and fuel efficiency. However, to strike a balance between the computation time and accuracy in operational studies, some non-linear constraints, for example, ramping, minimum up/down time (MUDT) and thermal limits are typically linearised; startup and shutdown exponential costs are discretised, and; non-convex and non-differentiable variable cost functions are expressed either as a quadratic or a piecewise linear function [3–5]. These simplifications are performed to simplify the problem and to avoid using computationally expensive non-linear solution methods.

1.2.2 UC in power system planning

In planning studies, due to the extended time horizon lengths (typically spanning from weeks to months), the UC model is even more computationally challenging and requires further simplification for a better trade-off between the solution time and accuracy. For example, the combinatorial structure is reduced by aggregating all the units installed at one location [6–9]; piecewise linear cost functions and constraints are represented by one segment only; some costs (e.g. startup, shutdown and fix costs) are ignored, a deterministic UC with perfect foresight is used, and; non-critical constraints are omitted [10–12]. The resulting model is mostly mixed integer linear model and requires significantly less computation time as compared to the non-linear counterpart.

1.2.3 UC solution methods

Because of its importance, UC has been an area of interest for several decades. The accurate solution of the UC problem can be achieved through complete enumeration. However, this method is not suitable for a large power system because of the computation time requirement [13, 14]. Other approaches include heuristic or priority listing [15, 16], dynamic programming [17], integer and linear programming [4, 18], simulated annealing [19], Lagrangian relaxation [20] and other artificial learning, fuzzy logic and biological phenomenon inspired decision-making techniques [21–25]. Among UC solution techniques, mixed integer programming (MIP) approach provides a flexible and accurate modelling framework [4]. Development of efficient MIP solvers like branch-and-bound and their incorporation in commercial optimisation solver have made this approach convenient to study emerging aspects of power systems.

MIP was first introduced to solve generator scheduling problems in [26]. This model was based on three sets of binary variables, namely start indicators, shutdown indicators and on-off indicators and one continuous set of variables to indicate power dispatch of each unit. In [18] this model was extended to make it computationally practical for realistic power systems and to include representations of reserves. In [3] optimal response of one thermal unit is studied considering both energy and spinning reserve contribution in the spot market. This work has also examined the effect of intertemporal binding constraints like ramp rate limitation and MUDT requirements. Furthermore, they use MIP for modelling of non-convex and non-differentiable costs and exponential startup costs. All these upgrades came with the burden of an increased number of variables and thus the computation time requirement is increased. To avoid the computation complexity associated with the mixed integer formulation, recent work [27] has proposed a linear relaxation of the UC formulation

for flexibility studies, with an accuracy comparable to the full binary mixed integer linear formulation.

1.3 Future Grid Studies

Power systems worldwide are moving away from domination by large-scale synchronous generation and passive consumers. Instead, in future grids[2] (FG) new actors, such as variable RES, price-responsive users equipped with small-scale PV-battery systems (called prosumers), DR, and energy storage will play an increasingly significant role, as explained in Section 1.1. Given this, for policy-makers and power system planners to evaluate the integration of high-penetrations of these new elements into FGs, new simulation tools need to be developed. Specifically, there is a pressing need to understand the effects of technological change on FGs, regarding energy balance, stability, security and reliability, over a wide range of highly-uncertain future scenarios. This is complicated by the inherent and unavoidable uncertainty surrounding the availability, quality and cost of new technologies (e.g., battery or PV system costs, or CST generation operating characteristics) and the policy choices driving their uptake. The recent blackout in South Australia (SA) [28] serves as a reminder that things can go wrong when the uptake of new technologies is not planned carefully.

FG planning thus requires a significant departure from conventional power system planning, where only a handful of the most critical scenarios are analysed. To account for a wide range of potential future evolutions, scenario analysis has been proposed in many industries, e.g. in finance and economics [29], and in energy [30, 31]. In contradistinction to power system planning, where the aim is to find an optimal transmission and/or generation expansion plan, the aim in scenario analysis is to analyse possible evolutionary pathways to inform power system planning and policy making. Given the uncertainty associated with long-term projections, the focus of FG scenario analysis is limited to the analysis of what is technically possible, although it might also consider an explicit costing [32]. In contrast to operation and planning studies, the computation burden of future grid scenario analysis is even more significant, due to a sheer number of scenarios that need to be analysed, which requires further simplifications.

[2]We interpret a *future grid* to mean the study of national grid type structures with the transformational changes over the long-term out to 2050.

1.3.1 Existing FG studies

Existing future grid feasibility studies have shown that the balance between demand and supply can be maintained even with high penetration of RESs by using large-scale storage, flexible generation, and diverse RES technologies [33–37]. They, however, only focus on balancing and use simplified transmission network models (such as copper plate). This ignores network related issues, which limits these models' applicability for stability assessment. Also, most of these studies did not take into account emerging technologies such as prosumers or DSM within the optimisation framework. A few notable FG studies that either consider DC power flow or stability assessment are [31, 33, 38, 39].

The *European project e-highway2050* [31] acknowledged the size and the complexity of the optimisation framework in long-term planning, and plan to develop new tools with a simplified network representation. Also, it emphasised on including DSM within its optimisation framework, but did not do so due to the computation time requirement. This study did include DC power flow but used a relaxed linear model of UC for dispatch.

The *Zero carbon Australia* [33] put forward a ten year plan for 100% renewable energy for the Australia National Electricity Market (NEM). This study proposes large-scale RES for covering base load power requirement and advises biomass and hydroelectric for backup. More specifically, WGs and CSTs are proposed to provide 40% and 60% of annual energy, respectively. RES sites are chosen based on the high probability of wind speed and solar radiation and minimum changes are proposed to the existing grid for integrating new RES. This study relies mostly on economic aspects and lacks any stability or security assessment. Also, fixed and mobile storage is considered for flexibility. However, this study had neglected DSM altogether.

The *Greenpeace study* [38], aims to determine a Europe 100% renewable vision. This study shows that large-scale integration of RES in European grid is economically and technically feasible. They concluded that by 2030, there would be no room for base load plants and gas units will provide most of the flexible backup for RES, which will eventually be replaced by CST, geothermal and biomass by 2050. This study also explored the effects of storage and included DSM heuristically while considering DC load flow constraints. The Greenpeace [38] study uses an optimal power flow for generation dispatch and thus ignores UC decisions.

The Irish *All island grid study* [39] explored an Ireland 2020 vision of renewable energy. This study investigated least-cost scenario considering the impacts of RES variability and predictability on grid security. This study considers pumped hydro for positive spinning reserves. They do put forward an FG stability accessing framework. However, put no restriction on a minimum number of online synchronous generators to avoid RES spillage

which can lead to poor frequency response in high RES scenarios. Also, a simple merit order dispatch is used based on load and no power flow constraints are considered.

A second Australian study, *100% renewable in Australia* [34] exploring minimum cost generation portfolio argues that the cost-effectiveness of non-synchronous RES and found CST to be an expensive solution. This study proposes least cost scenario of the NEM dispatching most of the power from WGs (upto 80% of energy) and PV. Authors on [34] argue that portfolios with lower wind participation will be less economical. They emphasise on policy frameworks and stable market environments to minimise the uncertainty in RES investment to reduce the cost of RES generation. They also propose a small amount of flexible biofuel, hydro and CST generation with DSM to cater periods of low wind and solar generation.

North American studies [35, 40, 41] also explored least-cost generation portfolios for high RES integration. These studies mostly use simple balancing between generation and load. Most of them lack commitment decisions, network constraints and stability analysis. In [40] researchers explored different generation mixes of non-dispatchable RESs to fulfil 80 % of the power demand of the Texas, USA (ERCOT) grid. This study shows that 80% power from RES can be achieved with less than 20% of curtailment. However, reducing curtailment to less than 10% requires an enormous amount of storage in the system. They proposed network upgrades and increase in connection capacity to adjacent grids to take advantage of DSM and diverse RES. This study also neglects the network and does not consider the commitment decisions.

Another North American study for California [41] uses a Monte Carlo approach to least cost generation portfolio planning and variable renewables. This study proposes that the California ISO operating area can achieve 80% reduction in electric power sector emission from 2005 level. Furthermore, it can deliver 99% of energy from RES, and moreover, technologies such as electric vehicles, DSM and storage may help reduce emissions even to a lower level. This study again ignored the network, DSM and the impact of RES on system stability.

Authors of [35] assessed the feasibility of RES integration in the PJM network in eastern USA. They analysed 28 billion scenarios for different mixes of RES technologies and storage to calculate the least cost mix of technologies. They concluded that PJM could be powered up to 99.9% of the time from RES, at a cost comparable to present day scenario. A combination of 9-72 h of electrochemical storage and fossil fuel generation is used as a backup to cover periods of low generation from RES. This study shows that least-cost combinations result in excessive RES, almost three times more than demand requirement. Similarly to [34], this study mainly focuses on finding the least cost generation mix with simple balancing and

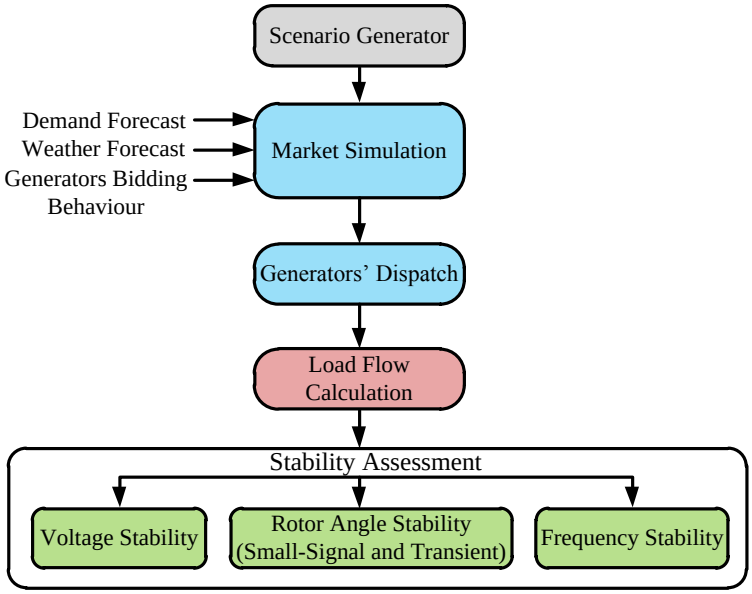

Fig. 1.1 Simulation platform for the performance and stability assessment of future grid scenarios.

neglected network issues, does not considered impact of DSM and possible adverse effects on system frequency response. However, this study is interesting because it put forward the need to evaluate a large number of scenarios (28 billion in this case) for sufficient long time horizons (four years in this study) to get a fairly clear picture of FG scenario. This highlights the scale and the sheer number of scenarios to be considered.

To the best of our knowledge, the Future Grid Research Program, funded by the Australian Commonwealth Scientific and Industrial Research Organisation (CSIRO) is the first to propose a comprehensive modelling framework for FG scenario analysis that also includes *stability assessment*. The project aim is to explore potential future pathways for the evolution of the Australian grid out to 2050 by looking beyond simple balancing. To this end, a simulation platform has been proposed in [42] that consists of a market model, power flow analysis, and stability assessment, as illustrated in Fig. 1.1. The platform has been used, with additional improvements, to study fast stability scanning [43] and impact of DSM heuristically on voltage stability [44]. Also in [44] CST is treated in an ad-hoc manner and a constant dispatch is considered for some particular hours of the day.

In order to capture the inter-seasonal variations in the renewable generation portfolios, computationally intensive time-series analysis needs to be used. A significant computation bottleneck of the framework is the market simulation. As evident from the current literature,

there is a gap for a comprehensive and computationally efficient market model for FG scenario analysis. The market model should be capable of providing UC and economic dispatch decision considering network coupling constraints, while having the flexibility to integrate emerging technologies such as, but not limited, to DSM, CST, prosumers, shiftable loads, storage, etc. in the optimisation framework. These requirements are systematically provided by the work contained in this thesis.

1.4 Research Contributions

The aim of this thesis is to develop a generic market model capable of generating commitment and dispatch decisions while considering power flow constraints and emerging future technologies. To provide the necessary inputs for starting point for extensive stability analysis. In contrast to the studies presented in Section 1.3.1, this thesis takes into account DC power flow constraints to explore network related issues, and integrates utility scale storage, prosumers and CST model into the optimisation framework.

Against this backdrop, first, in Chapter 2 a generic demand model is proposed to captures the **aggregated effect of a large population of price-responsive users** equipped with small-scale PV-battery systems, called prosumers. The challenge is how to incorporate the price anticipatory behaviour of prosumers. A simple iterative solution of cycling between market and prosumers will not converge due to the significant share of prosumers and their power to significantly alter the demand profile. Thus, in contrast to previous works, that either include prosumers' impact in an ad-hoc fashion or heuristically, the problem is approached in a systematically and prosumers' optimisation problem (objective and constraints) is included as a constraint. This gives rise to an optimisation problem constrained by another optimisation problem. In game theory, these types of problems are known as Stackelberg games. Here, the upper-level problem (ISO) minimises the total generation cost, and the lower-level problem (prosumers) maximises prosumers' self-consumption. The other salient feature of the proposed model is, the coupling between prosumers and the ISO is through the prosumers' demand, not through the electricity price. This renders the proposed model market structure agnostic, making it suitable for FG studies where the market structure is potentially unknown. For modelling simplicity, this chapter ignores network coupling constraints. Also, flexibility options through utility-scale storage (USS) and prosumers are explored and compared.

Chapter 3 builds on the optimisation framework proposed in Chapter 2 and includes **DC power flow constraints** as the network is a critical part for reliable FG stability studies (ignored in most of FG studies mention in Section 1.3). The addition of network constraints complicates not only the dispatch of generators but also presents additional complication

Table 1.1 Salient features of dispatch model proposed in different Chapters.

Constraints	Chapter 2	Chapter 3	Chapter 4	Chapter 5
Power Flow		DC		DC
Utility-scale storage	✓			✓
Prosumers	✓	✓		✓
CST Dispatch			✓	✓
Min. Inertia				✓
Variables	Binary	Binary	Binary	Integer
Rolling Horizon		✓	✓	✓
Constraint Clipping				✓

regarding prosumer aggregation. This action limits the system level aggregation of prosumers and provides additional challenges regarding the interaction of multiple aggregators, not to mention the exponential increase in computation time associated with each aggregator. To this end, two strategies are explored: i) aggregators can exchange power among themselves and the grid, ii) aggregators are restricted to maximise self consumption at a particular node and cannot send power back to the grid. Steady-state voltage stability analysis of a simplified model of the NEM with significant penetration of renewable generation and prosumers is then performed to understand the RES integration using the flexibility provided by prosumers.

In contrast to Chapter 3 (exploring flexibility from demand side), Chapter 4 explores FG flexibility option from the generation side. CST presents an excellent RES with inherent flexibility. This chapter proposes **aggregation of inflexible non-synchronous RES with CST** to achieve the required flexibility. The challenge with the integration of WGs and PVs is the design of existing power systems. Currently installed conventional generators (CG) are not designed to cope up with the addition ramp stress caused by these non-synchronous RES. Thus, a solution is formulated to keep in check the ramping stress imposed on CG due to the integration of non-synchronous RES. For this purpose, an RES aggregation is proposed, primarily responsible for absorbing the additional ramp rate stress of non-synchronous RES by utilising flexibility from thermal energy storage of CST. Again, a Stackelberg game is used to capture the interaction between an ISO and the REA. In cost minimisation analysis, the ISO tries to minimise generation cost, while REA seeks to maximise revenue. In this setting optimising power dispatch from REA considering total energy and ramp rate limitations is a challenging task. Case studies benchmark the effect of purposed REA against the business as usual (BAU) scenario for the Australian NEM.

Chapter 5 combines all approaches developed in the previous chapters and proposes a **market model considering DC power flow, prosumers, utility storage, CST dispatch and minimum inertia** as presented in Table 1.1. The inclusion of all these details signif-

icantly increases the computation time of the model. To reduce the computation burden, modifications are made to improve the run time performance of the model. To achieve that, the accuracy of the model is also improved significantly. In overcoming these challenges, a computationally efficient market simulation tool (MST) suitable for FG scenario analysis is proposed and its performance is benchmarked against slower, more accurate approaches and models used in the previous chapters.

With the higher penetration of power electronic interfaced RES, the rotational kinetic energy in a power system decreases. This causes detrimental effects on the system's frequency behaviour. The existing literature deals with this effect in an ad hoc way and lacks a systematic approach to deal with this issue. Chapter 6 utilises MST proposed in Chapter 5 for a **comprehensive frequency performance assessment of the NEM considering various penetration levels of non-synchronous RES**. Also, Chapter 6 explores the impact of dynamic inertia constraint and prosumers on system frequency. A summary of the contribution is shown in Fig. 1.2. In summary, Chapters 2, 3 and 4 build toward the formulation of MST presented in Chapter 5 that is then used in Chapter 6 for a comprehensive frequency assessment of the NEM.

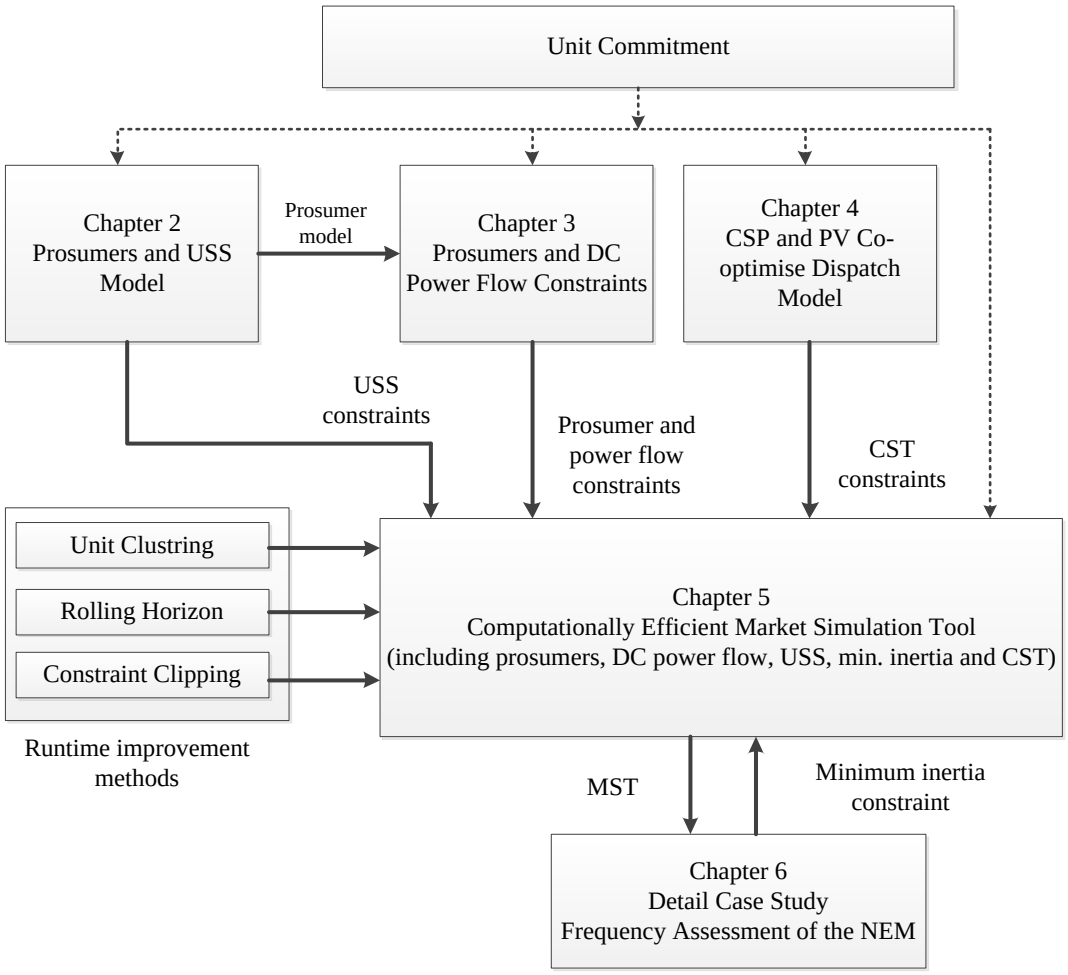

Fig. 1.2 Summary of the thesis' contribution.

Chapter 2

Generic Demand Model Considering the Impact of Prosumers

Demand response (DR) is expected to be an important feature of future grids (FGs) with high penetration of renewable energy sources (RES). The increasing penetration of utility and distributed RES challenges the balancing, stability and security of power systems in new ways. Existing FG studies have shown that a high penetration of RES is feasible with combinations of flexible resources, geographically and technologically diverse RES, utility storage and flexible generation [33, 34, 38, 39, 45]. However, they have relied upon conventional demand models and ignored the effect of the emerging demand-side technologies.

Conventional demand models are no longer valid for modelling net demand in FGs, as the increased penetration of distributed generation and residential battery storage have started to alter the demand profile. Notably, the installed capacity of rooftop-PV has increased globally from approximately 4 GW in 2003 to nearly 128 GW in 2013 [44]. This phenomenon has been driven mainly by increasing electricity tariffs, decreasing technology cost and governmental incentives. At present in Australia, the penetration of rooftop-PV in the NEM is around 6 GW[1] and is projected to rise to 12.8 GW by 2025 [46].

Increasing penetration of rooftop-PV has created new problems in distribution networks [47, 48], voltage rise being the most troublesome. This effect has forced network operators to discourage the uptake of rooftop-PV either by imposing a maximum capacity limit that can be installed per household or feeder, and has also resulted in governments and regulators reducing generous feed-in tariffs. In Australia, feed-in tariffs have been reduced from 0.60 \$/kWh to 0.05 \$/kWh, or even less in some cases.

[1] http://pv-map.apvi.org.au/analyses

Due to the lack of incentives for prosumers to send power back to the grid, they will look for new ways to maximise self-consumption, battery storage being the most likely option [49]. Currently, residential battery storage is still expensive; however, some studies have suggested that they will reach retail price parity in the NEM and the USA grid by 2020-2030 [49–53]. Battery storage provides two-fold advantage. First, it enables prosumers to store excess energy from rooftop-PV. Second, it assist them in avoiding peak hour prices through energy time-shifting. So, the future grids needs to be remodelled to handle flexibility added to it either be because DR or utility storage [1, 54, 55].

2.1 Literature Review of DR Models

The literature below reviews new modelling approaches for incorporating DR into conventional demand models. Few new studies have attempted to consider the effect of DR by incorporating emerging demand-side technologies [1, 44, 56–61]. These studies can be classified into three categories.

The first group of studies is based on *supply-side* models, which use simplified demand-side representation [1, 56, 57]. In these studies, a price elasticity or virtual generator approach is usually used to represent the demand-side. A cross-price elasticity approach is employed in [1] to investigate the interaction of price-responsive users in a microgrid. In [56], a unified system level model is utilised to enable the integration of RESs and energy storage in power systems. Load-shifting behaviour of consumers submitting price-sensitive bids is studied in [57].

The second group is based on detailed demand-side modelling that uses a simplified market structure [58–60]. These studies mostly use a price profile to represent the supply-side. A simple control strategy for management of demand-side devices is proposed in [60], aiming to show that it is possible to aggregate demand-side devices that provide primary reserves in the electricity market. An effort is made in [58] to coordinate different devices indirectly to flatten the total demand. This study shows the existence of a time-varying price to align individual optimality with the social welfare. An optimal bidding strategy for electric vehicles for the day-ahead market is proposed using a bi-level optimisation framework in [59].

The third group has suggested the need for integrated demand and supply-side models to obtain an accurate picture of the impact of demand-side technologies [44, 61]. In [61], it has been shown that a heating system is constrained by user behaviour, weather conditions, occupants and electric supply, which requires a more realistic integrated approach. In the

same direction, the researchers have integrated the aggregated effect of DR into conventional demand models using a heuristic search in [44].

Although the above models have shown their merits, they are dependent on specific practical details such as the electricity price or the implementation of a mechanism for DR aggregation, which limits their usefulness for FG scenario analysis where the detailed market structure is potentially unknown. Therefore, a *generic* modelling framework is required that it properly captures the aggregated effect of prosumers on the demand profile. A key feature of such generic models is that they do not depend on specific practical details that will vary in the long-run. This concept is already well-known in power systems, such as in conventional load modelling, where the aggregated effect of millions of devices is captured by simple analytical expressions [62, 63]. In FG scenario analysis, the purpose of generic demand models in market simulation is to capture accurate dispatch decisions, used as the initial point for balancing and stability analysis.

2.2 Conceptual Framework for Prosumer Integration

As evident from the discussion in Section 2.1, existing literature fails to incorporate prosumers into the optimisation framework. Against this backdrop, Chapter 2 proposes a principled method for generic demand modelling including the aggregated effect of prosumers.

The problem is motivated by the emerging situation in Australia, where rooftop-PV owners are increasingly discouraged from sending power back to the grid due to very low PV feed-in-tariffs versus increasing retail electricity prices. In this setting, an obvious cost-minimizing strategy is to install small-scale battery storage, to maximise self-consumption of local generated energy and offset energy used in peak pricing periods. Similar tariff settings appear likely to occur globally in the near future, as acknowledged in [38].

From modelling point of view, ISO is responsible for maintaining balance between generation and demand, and setting of clearance price. In price anticipatory environment, prosumers will have the ability to shift their grid power requirement[2]demand to low pricing periods, if prosumer penetration is large enough they will alter the generation dispatch and affect the clearance price. Also, because of the anticipatory behaviour any change in clearance price will alter grid power intake pattern of prosumers and so on. This means that clearance price depends upon the prosumers grid power intake and prosumer grid power intake depends upon the market clearance price. In theory, dependency of these two can be

[2]Prosumer demand is first met by rooftop-PV and/or household batteries, remaining power demand will be met by power intake from grid, also prosumers will charge batteries from grid power during cheaper time slots to save electricity cost.

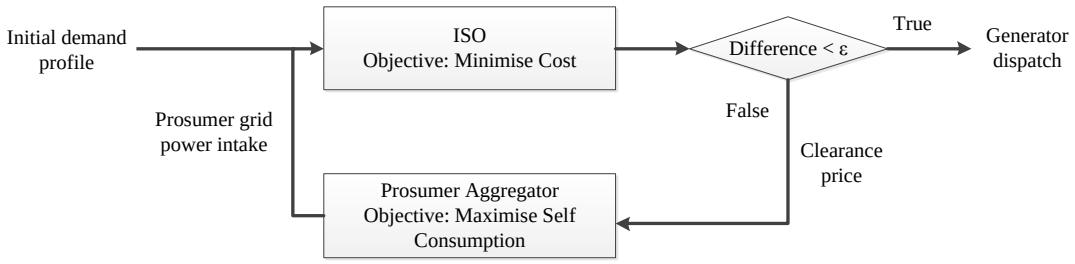

Fig. 2.1 Structure of the iterative problem.

dealt in a iterative manner, i.e running the market problem with the objective to minimise cost and plugging clearance price to prosumer problem to get new prosumer grid intake profile as shown in Fig. 2.1. Given a large prosumer penetration as predicted in [53], an iterative solution is likely to result in oscillations between two states rather than converging to an equilibrium state.

The problem is approached by constricting the ISO dispatch with the prosumers' optimisation problem. This presents a scenario where an optimisation problem is constrained by or nested within another optimisation problem. In game theory, such bi-level optimisation problems are known as *Stackelberg games*. The upper-level optimisation problem is known as the *leader* and lower-level problem is known as the *follower*. The Model presented here uses this approach, and is formulated as a bi-level program in which the leader (ISO) minimises the total generation cost, and the follower (*aggregator*) maximises prosumers' self-consumption. Moreover, self-consumption within an aggregated block of prosumers is a good approximation of many likely behaviours and responses to other future incentives and market structures, such as (peak power-based) demand charges, capacity constrained connections, virtual net metering across connection points, transactive energy and local energy trading, and a (somewhat irrational) desire for self-reliance.

Fig. 2.2 shows the structure of the proposed modelling framework. The demand model consists of two parts: (i) consumer demand, p_{c}, with a fixed demand profile, representing large industrial loads and loads without flexible resources; and (ii) prosumer demand, p_{p}, comprising a large population of prosumers who collectively maximise self-consumption.

A key difference from existing bi-level optimisation frameworks is that in our formulation, the levels are coupled through the prosumers' demand, not through the electricity price. In contrast, other models, which focus on the interaction between an aggregator and the prosumers [64] or the aggregator and the wholesale market [59], couple the levels through prices. These approaches essentially define a market structure, that is, a pricing rule to

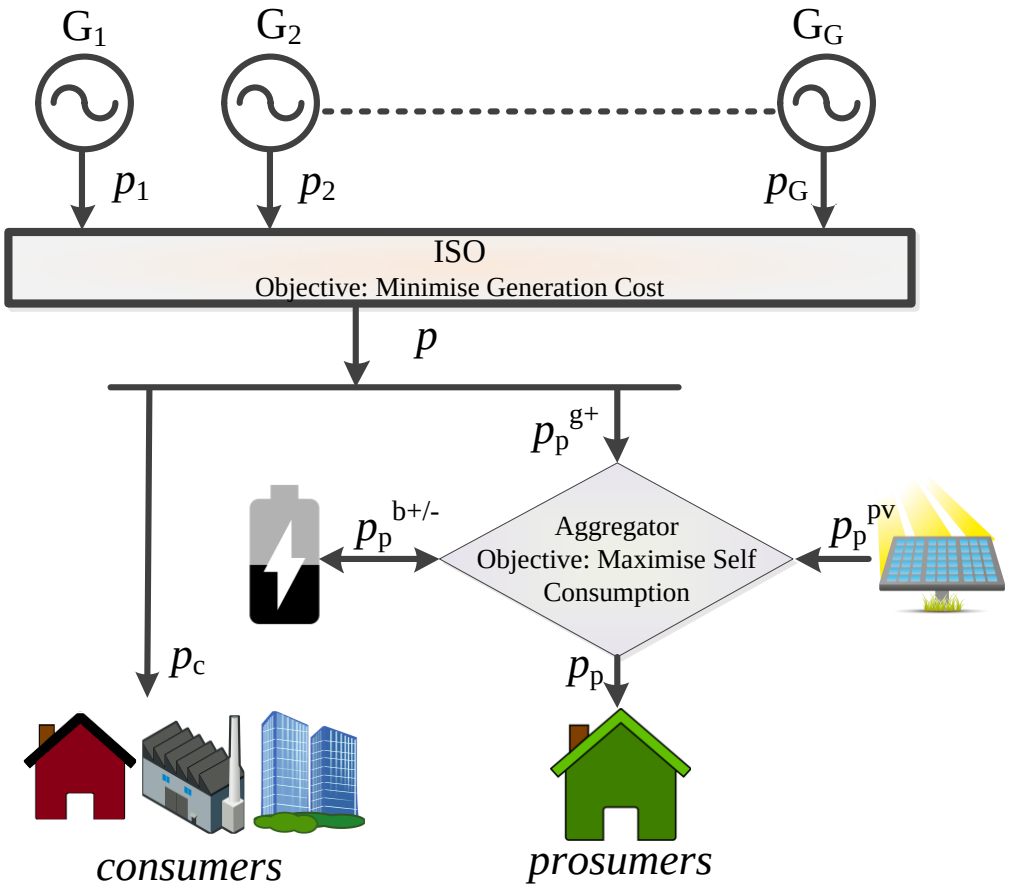

Fig. 2.2 Structure of the proposed modeling framework.

support an outcome. In contradistinction, our proposed model is market structure agnostic. That is, it implicitly assumes that an efficient mechanism for demand response aggregation is adopted, with prices determined by that unspecified mechanism, which support the outcomes computed by our optimisation framework.

2.2.1 Bi-level optimisation

In the model, we are specifically interested in the aggregated effect of a large prosumer population on the demand profile, assuming that the prosumers collectively maximise their self-consumption. Given that the objective of the ISO is to minimise the generation cost, the problem exhibits a bi-level structure. They can be formulated as bi-level mathematical

programs of the form [64]:

$$\begin{aligned} \underset{\mathbf{x},\mathbf{y}}{\text{minimise}} \quad & \Phi(\mathbf{x},\mathbf{y}) \\ \text{subject to} \quad & (\mathbf{x},\mathbf{y}) \in \mathcal{Z} \\ & \mathbf{y} \in \mathcal{S} = \arg\min_{\mathbf{y}} \{\Omega(\mathbf{x},\mathbf{y}) : \mathbf{y} \in \mathcal{C}(\mathbf{x})\} \end{aligned}$$

where $\mathbf{x} \in \mathbb{R}^n$, $\mathbf{y} \in \mathbb{R}^m$, are decisions vectors, and $\Phi(\mathbf{x},\mathbf{y}) : \mathbb{R}^{n+m} \to \mathbb{R}$ and $\Omega(\mathbf{x},\mathbf{y}) : \mathbb{R}^{n+m} \to \mathbb{R}$ are the objective functions of the upper- and the lower-level problems, respectively. $\mathcal{Z}$ is the joint feasible region of the upper-level problem and $\mathcal{C}(\mathbf{x})$ the feasible region of the lower-level problem induced by $\mathbf{x}$.

In the existing market models that adopt a hierarchical approach, the coupling variable $\mathbf{y}$ is the electricity price (e.g. [59, 64]). That is, the upper level (the ISO in our case) determines the price schedule, while the lower level (the aggregator acting on behalf of the prosumers), optimises its consumption based on this price schedule.

2.3 Modeling Assumptions

Given the uncertainty associated with future grid studies, the modelling framework should be market structure agnostic, and capable of easy integration of various types and penetrations of emerging demand-side technologies. To this effect, we make the following assumptions:

1. The load is modelled as price anticipator. In studies [42, 65], researchers have modelled the loads as price-takers, inspired by the smart home concept [66], in which the loads respond to the electricity price to minimise energy expenditure. The study has shown that with large penetration of price-taking prosumers, the marginal benefit might become negative when secondary peaks are created due to the load synchronization (see Fig. 2.3 showing the operational demand with different penetrations of prosumers). Therefore, prosumer aggregators (henceforth simply called aggregators) have started to emerge to fully exploit the demand-side flexibility. To that effect, the model implicitly assumes an efficient mechanism for aggregation (an interested reader might refer to [67] for a discussion on practical implementation issues). However, specific implementation details, like price structure or the division of the profit earning by the aggregated collection of prosumers, are not of explicit interest in the proposed model.

2. The demand model representing an aggregator consists of a large population of prosumers connected who collectively maximise self-consumption (made possible by an efficient internal trading and balancing mechanism).

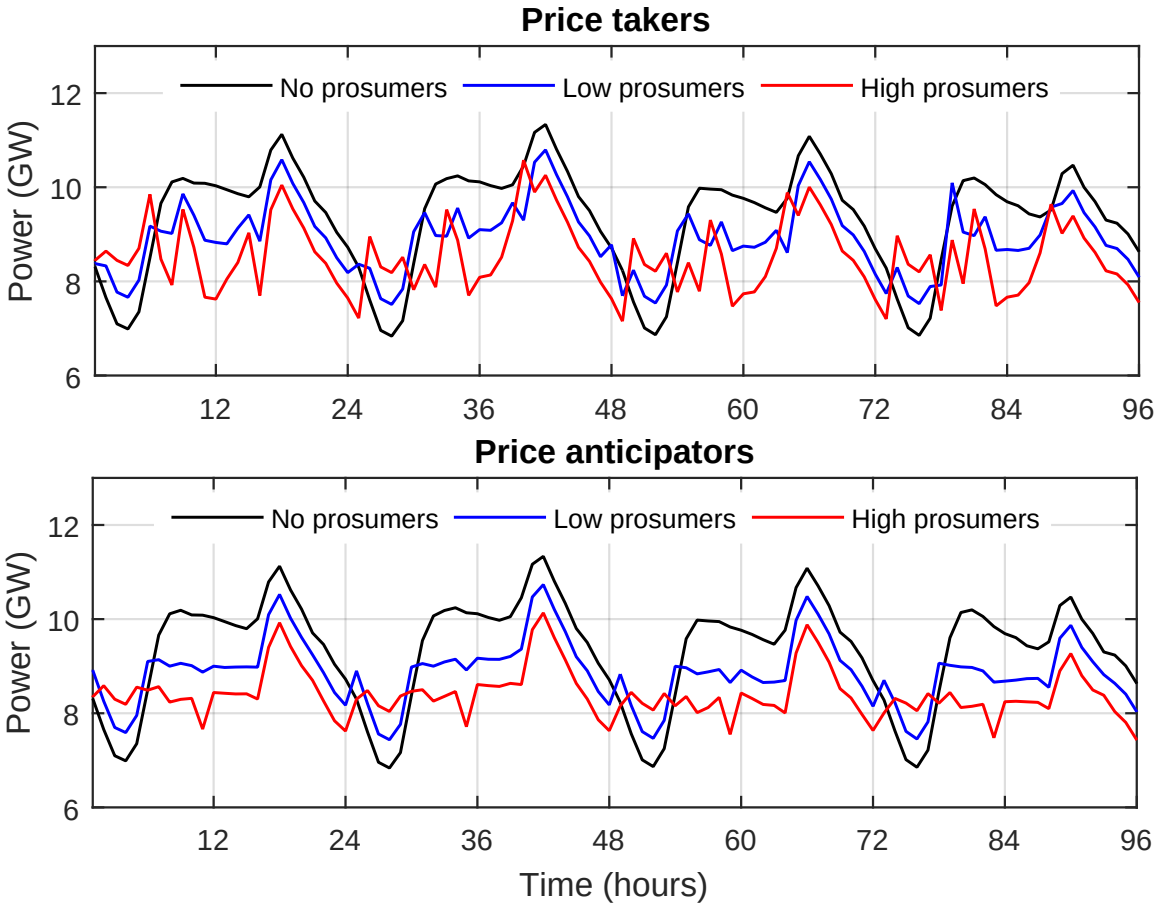

Fig. 2.3 Operational demand with different penetrations of price-taking (top) and price-anticipating prosumers (bottom).

3. Aggregator do not alter the underlying power consumption of the prosumers. That is, except for battery losses the total power consumption with and without aggregator remain the same; however, the power grid power intake profile does change, by employing storage technologies.

4. Prosumers have smart meters equipped with home energy management systems for scheduling of the PV-battery systems. Also, a communication infrastructure is assumed that allows a two-way communication between the grid, the aggregator and the prosumers, facilitating energy trading between prosumers in the aggregation.

These assumptions appear to be appropriate for scenarios arising in time frame of several decades into the future.

2.4 Market Model

The market model is based on the modified UC problem, where power from the cheapest generator will be dispatched first while taking into account their minimum stable limits, ramp rates and minimum up/down time considerations. Hence, RES that have the lowest short run marginal cost (SRMC) will be prioritised for dispatch. The inclusion of a large amount of non-synchronous RES necessitates the need for flexible resources such as DR and energy storage. In this work, such flexibility is explored by utility storage and residential batteries, which can shift the power requirement from peak hours to cheaper time-slots.

Given that there are about a hundred units installed in the systems; it is computationally infeasible to keep track of indvidual unit for long horizons as acknowledged in [5, 31]. Hence, identical units at each generation station are aggregated and their status is tracked by one binary variable as used in previous literature [42, 44, 68]. This means that all of them are either on or off at any given time.

The mathematical model adopted in this work is a two level optimisation problem cast as a Mathematical Program with Equilibrium Constraints (MPEC). The upper-level problem is a standard unit commitment (UC) problem, which, if it wasn't for the prosumers, would be solved in a standard way. Due to the price-anticipatory prosumer behavior, their demand profile is not known in advance, which requires a different approach. The optimum is achieved when the prosumers cannot shift their demand further (no additional price reduction is possible), which results in an equilibrium. The Karush-Kuhn-Tucker (KKT) optimality conditions of the lower-level problem are then added to the upper-level problem, resulting in an MPEC. The resulting optimisation problem is nonlinear, for which no efficient solvers exist. Therefore the optimisation problem needs to be reformulated further. The reformulation is an inner product reformulation with positive slack variables and constraint equalities set to zero, which results in an Mixed Integer Linear Program (MILP) that can be solved using off-the-shelf solvers.

For initial verification network is ignored to reduce the computation burden and thus consumers and prosumers can be lumped into one load profile each. All conventional generators and utility RESs submit their respective bids to the ISO, which then sorts the bids and computes the least-cost dispatch schedule that fulfils the demand requirements. This formulation is detailed below.

2.4.1 ISO (leader) problem

The ISO objective is to minimise the generation cost as follows:

$$\underset{\Omega}{\text{minimise}} \quad \sum_{t\in\mathcal{T}}\sum_{g\in\mathcal{G}}\Big(c_g^{\text{fix}}s_{g,t}+c_g^{\text{su}}u_{g,t}+c_g^{\text{sd}}d_{g,t}+c_g^{\text{var}}p_{g,t}\Big), \tag{2.1}$$

where $\Omega=\{s_{g,t},u_{g,t},d_{g,t},p_{g,t},p_{s,t}\}$ are the decision variables of the problem, and c_g^{fix}, c_g^{su}, c_g^{sd}, and c_g^{var} are fixed, startup, shutdown and variable cost, respectively.

Note that as we have ignored the network. The system can be represented as a single bus to which all the generators, utility storage, consumers and prosumers are connected. Hence, only one aggregated load profile can capture power requirement of consumers and one prosumer aggregator is sufficient to maximise self consumption of all prosumers in the system. Furthermore, dispatch is restricted by the constraints (2.2)-(2.13):

Power balance: Generator dispatch must be equal to system demand requirement:

$$\sum_{g\in\mathcal{G}}p_{g,t}=p_{c,t}+p_{p,t}^{\text{g+}} \qquad \forall t, \tag{2.2}$$

where $p_{c,t}$ and $p_{p,t}^{\text{g+}}$ represent consumers and prosumers grid power demand.

Active power reserves: Reserve margins from synchronous generators G^{Synch}, are considered to overcome demand and RES prediction errors.

$$\sum_{g\in\mathcal{G}^{\text{syn}}}(\overline{p}_g-p_{g,t})s_{g,t}\geq p_t^{\text{r}} \qquad \forall t, \tag{2.3}$$

where $\overline{p}_g$ represents the maximum stable limit and p_t^{r} represents the system reserve requirement[3].

On/off restriction: Generator can only be turned on if it is off and vice versa:

$$u_{g,t}-d_{g,t}=s_{g,t}-s_{g,t-1} \qquad \forall g,t, \tag{2.4}$$

where $s_{g,t-1}=0$ for $t=1$.

Generation limits: Generators should always operate between their respective minimum and maximum stable limits:

$$\underline{p}_g s_{g,t}\leq p_{g,t}\leq\overline{p}_g s_{g,t} \qquad \forall g,t, \tag{2.5}$$

[3]Usually 10 % reserves are maintained from synchronous sources to overcome unforeseen variation.

where $\underline{p}_g$ represents the minimum stable limit of generators g.

Ramp rate limitation: The change in generator dispatch level should not be more than its allowed ramp rate:

$$-r_g^- \leq p_{g,t} - p_{g,t-1} \leq r_g^+ \qquad \forall g,t, \tag{2.6}$$

where r^- and r^+ represent ramp-down and ramp-up rates of generator g, respectively.Also, $p_{g,t-1} = 0$ at $t = 1$.

Generator minimum up time: If generator is turned on it has to remain on for time τ_g^{u}:

$$u_{g,t} - \sum_{\tilde{t}=0}^{\tau_g^{\mathrm{u}}-1} d_{g,t+\tilde{t}} \leq 1 \qquad \forall g,t, \tag{2.7}$$

it is assumed that there is no minimum up time (MUT) limitation after $\bar{t}$.

Generator minimum down time: If generator is turned off it has to remain on for time τ_g^{d}:

$$d_{g,t} - \sum_{\tilde{t}=0}^{\tau_g^{\mathrm{d}}-1} u_{g,t+\tilde{t}} \leq 1 \qquad \forall g,t, \tag{2.8}$$

again, it is assumed that there is no minimum down time (MDT) limitation after $\bar{t}$.

Utility storage energy balance: State of charge (SOC) of utility storage tracks the amount of energy available in storage.

$$e_{s,t} = \eta_s e_{s,t-1} + p_{s,t} \qquad \forall s,t, \tag{2.9}$$

where $e_{s,t}$ and $p_{s,t}$ represents energy and power of storage s, respectively.

Utility storage capacity limits: Energy stored capacity of storage plant s is restricted as:

$$\underline{e}_s \leq e_{s,t} \leq \overline{e}_s \qquad \forall s,t. \tag{2.10}$$

Utility storage power flow: Power flow of utility storage is restricted by its charge and discharge rate:

$$\overline{p}_s^- \leq p_{s,t} \leq \overline{p}_s^+ \qquad \forall s,t, \tag{2.11}$$

where $\overline{p}_s^-$ and $\overline{p}_s^+$ represent the maximum power discharge and charge rates of a storage plant, respectively.

Prosumers: ISO optimal dispatch decision are also bounded by prosumers optimisation problem:

$$\arg\min_{p^{\mathrm{g+}},e^{\mathrm{b}}}\{\sum_{t\in\mathcal{T}} p^{\mathrm{g+}}_{p,t} \text{ subject to (2.13b)} - \text{(2.13c)}\}, \tag{2.12}$$

2.4.2 Prosumer (follower) problem

Prosumers aim to maximise their self-consumption, as the under line prosumer demand is unchanged hence minimising grid power intake is identical to maximising self consumption:

$$\underset{p^{\mathrm{g+}}_{p,t},e^{\mathrm{b}}_{p,t}}{\text{minimise}} \quad \sum_{t\in\mathcal{T}} p^{\mathrm{g+}}_{p,t} \qquad \forall t. \tag{2.13a}$$

In the follower optimisation, the decision variables are $p^{\mathrm{g+}}_{p,t}$, and $e^{\mathrm{b}}_{p,t}$ representing prosumers grid power requirement and battery SOC, respectively. Prosumer problem is constrained by:

Power balance: Sum of prosumers grid power requirement and rooftop-PV generation is equal to their load demand and power flow to battery:

$$p^{\mathrm{g+}}_{p,t} + p^{\mathrm{pv}}_{p,t} = p_{p,t} + p^{\mathrm{b}}_{p,t} \qquad \forall p,t, \tag{2.13b}$$

where $p_{p,t}$,$p^{\mathrm{pv}}_{p,t}$and$p^{\mathrm{b}}_{p,t}$ represent prosumer power demand, rooftop-PV generation and battery power, respectively.

State of charge: Battery SOC is sum of remaining energy times efficiency and power in flow at current hour, as given:

$$e^{\mathrm{b}}_{p,t} = \eta^{\mathrm{b}}_{p} e^{\mathrm{b}}_{p,t-1} + p^{\mathrm{b}}_{p,t} \qquad \forall p,t, \tag{2.13c}$$

where, η^{b}_{p} represents battery efficiency[4] and $e^{\mathrm{b}}_{p,t-1}$ is assumed to be at its lowest limit at $t = 1$.

Battery charge/discharge rate: Battery power should not exceed charge/discharge rate:

$$\overline{p}^{\mathrm{b\text{-}}}_{p,t} \leq p^{\mathrm{b}}_{p,t} \leq \overline{p}^{\mathrm{b+}}_{p,t} \qquad \forall p,t, \tag{2.13d}$$

where $\overline{p}^{\mathrm{b\text{-}}}_{p,t}$ and $\overline{p}^{\mathrm{b+}}_{p,t}$ are maximum battery discharge and charge rate, respectively.

[4] In simulation self-discharge is neglected.

Battery storage limits: Energy stored in the battery should always be less than its capacity:

$$\underline{e}^{\mathrm{b}}_{p,t} \leq e^{\mathrm{b}}_{p,t} \leq \overline{e}^{\mathrm{b}}_{p,t} \qquad \forall p,t, \tag{2.13e}$$

where $\underline{e}^{\mathrm{b}}_{p,t}$ and $\overline{e}^{\mathrm{b}}_{p,t}$ are the battery minimum and maximum energy limit, respectively.

2.4.3 Resultant MILP model

Optimisation problem presented in Section 2.4.1 is not computationally tractable owing to the fact that it is constrained by prosumer optimisation 2.4.2, Fortunately, the prosumer problem is convex, it can be translated in to a computationally retractable model by incorporating its KKT conditions along with the slackness variables in the upper level optimisation to form a MILP as explained in Appendix A.

The resultant MILP model is as follows:

$$\underset{\Omega}{\text{minimise}} \quad \sum_{t\in\mathcal{T}}\sum_{g\in\mathcal{G}}\Big(c^{\mathrm{fix}}_{g}s_{g,t} + c^{\mathrm{su}}_{g}u_{g,t} + c^{\mathrm{sd}}_{g}d_{g,t} + c^{\mathrm{var}}_{g}p_{g,t}\Big), \tag{2.14}$$

there are no changes to the ISO optimisation objective, ISO is still minimising dispatch cost considering fix, startup, shutdown and variable cost of generators. The decision variables of problem are as follows:

$$s_{g,t}, u_{g,t}, d_{g,t}, b^{\mathrm{g+}}_{p,t}, b^{\mathrm{p}}_{p,t}, b^{\overline{\mathrm{p}}}_{p,t}, b^{\mathrm{e}}_{p,t}, b^{\overline{\mathrm{e}}}_{p,t} \in \{0,1\},$$

$$p_{g,t}, p^{\mathrm{g+}}_{p,t}, e^{\mathrm{b}}_{p,t}, \mu^{\mathrm{g+}}_{p,t}, \mu^{\mathrm{p}}_{p,t}, \mu^{\overline{\mathrm{p}}}_{p,t}, \mu^{\mathrm{e}}_{p,t}, \mu^{\overline{\mathrm{e}}}_{p,t} \in \mathbb{R}^{+},$$

$$p_{s,t}, p^{\mathrm{b}}_{p,t}, \lambda^{\mathrm{p}}_{p,t}, \lambda^{\mathrm{e}}_{p,t} \in \mathbb{R},$$

where, $s_{g,t}, u_{g,t}, d_{g,t}, p_{g,t}, p_{s,t}$ are the original decision variables of ISO, $p^{\mathrm{g+}}_{p,t}, e^{\mathrm{b}}_{p,t}, p^{\mathrm{b}}_{p,t}$ are the decision variables of prosumers now transferred to ISO, $\lambda^{\mathrm{p}}_{p,t}, \lambda^{\mathrm{b}}_{p,t}, \mu^{\mathrm{g+}}_{p,t}, \mu^{\mathrm{p}}_{p,t}, \mu^{\overline{\mathrm{p}}}_{p,t}, \mu^{\mathrm{e}}_{p,t}, \mu^{\overline{\mathrm{e}}}_{p,t}$ are the dual variables associated with prosumers constraints and $b^{\mathrm{g+}}_{p,t}, b^{\mathrm{p}}_{p,t}, b^{\overline{\mathrm{p}}}_{p,t}, b^{\mathrm{e}}_{p,t}, b^{\overline{\mathrm{e}}}_{p,t}$ are binary variables used to maintain orthogonality between the prosumers' inequality constraints and the associated dual variables. The optimal solution of the resultant problem is constrained by:

$$\sum_{g\in\mathcal{G}} p_{g,t} = p_{c,t} + p^{\mathrm{g+}}_{p,t} \qquad \forall t, \tag{2.15}$$

$$\sum_{g\in\mathcal{G}^{\mathrm{syn}}} (\overline{p}_{g} - p_{g,t})s_{g,t} \geq p^{\mathrm{r}}_{t} \qquad \forall t, \tag{2.16}$$

$$u_{g,t} - d_{g,t} = s_{g,t} - s_{g,t-1} \qquad \forall g,t, \tag{2.17}$$

$$\underline{p}_g s_{g,t} \leq p_{g,t} \leq \overline{p}_g s_{g,t} \qquad \forall g,t, \tag{2.18}$$

$$-r_g^- \leq p_{g,t} - p_{g,t-1} \leq r_g^+ \qquad \forall g,t, \tag{2.19}$$

$$u_{g,t} - \sum_{\tilde{t}=0}^{\tau_g^{\mathrm{u}}-1} d_{g,t+\tilde{t}} \leq 1 \qquad \forall g,t, \tag{2.20}$$

$$d_{g,t} - \sum_{\tilde{t}=0}^{\tau_g^{\mathrm{d}}-1} u_{g,t+\tilde{t}} \leq 1 \qquad \forall g,t, \tag{2.21}$$

$$e_{s,t} = \eta_s e_{s,t-1} + p_{s,t} \qquad \forall s,t, \tag{2.22}$$

$$\underline{e}_s \leq e_{s,t} \leq \overline{e}_s \qquad \forall s,t. \tag{2.23}$$

$$\overline{p}_s^- \leq p_{s,t} \leq \overline{p}_s^+ \qquad \forall s,t, \tag{2.24}$$

$$1 - \mu_{p,t}^{\mathrm{g+}} + \lambda_{p,t}^{\mathrm{p}} = 0 \qquad \forall p,t, \tag{2.25a}$$

$$-\lambda_{p,t}^{\mathrm{p}} - \lambda_{p,t}^{\mathrm{e}} - \mu_{\underline{p},t}^{\mathrm{p}} + \mu_{p,t}^{\overline{\mathrm{p}}} = 0 \qquad \forall p,t, \tag{2.25b}$$

$$\lambda_{p,t}^{\mathrm{e}} - \eta_p^{\mathrm{b}} \lambda_{p,t+1}^{\mathrm{e}} - \mu_{\underline{p},t}^{\mathrm{e}} + \mu_{p,t}^{\overline{\mathrm{e}}} = 0 \qquad \forall p,t, \tag{2.25c}$$

$$p_{p,t}^{\mathrm{g+}} + p_{p,t}^{\mathrm{pv}} - p_{p,t} - p_{p,t}^{\mathrm{b}} = 0 \qquad \forall p,t, \tag{2.25d}$$

$$e_{p,t}^{\mathrm{b}} - \eta_p^{\mathrm{b}} e_{p,t-1}^{\mathrm{b}} - p_{p,t}^{\mathrm{b}} = 0 \qquad \forall p,t. \tag{2.25e}$$

$$p_{p,t}^{\mathrm{g+}} \leq M^{\mathrm{a\text{-}}} b_{p,t}^{\mathrm{g+}} \qquad \forall p,t, \tag{2.25f}$$

$$\mu_{p,t}^{\mathrm{g+}} \leq M^{\mathrm{a\text{-}}} (1 - b_{p,t}^{\mathrm{g+}}) \qquad \forall p,t, \tag{2.25g}$$

$$\overline{p}_{p,t}^{\mathrm{b\text{-}}} \leq p_{p,t}^{\mathrm{b}} \qquad \forall p,t, \tag{2.25h}$$

$$p_{p,t}^{\mathrm{b}} \leq M^{\mathrm{b\text{-}}} b_{\underline{p},t}^{\mathrm{p}} \qquad \forall p,t, \tag{2.25i}$$

$$\mu_{\underline{p},t}^{\mathrm{p}} \leq M^{\mathrm{b\text{-}}} (1 - b_{\underline{p},t}^{\mathrm{p}}) \qquad \forall p,t, \tag{2.25j}$$

$$p_{p,t}^{\mathrm{b}} \leq \overline{p}_{p,t}^{\mathrm{b+}} \qquad \forall p,t, \tag{2.25k}$$

$$-M^{\mathrm{b+}} b_{p,t}^{\overline{\mathrm{p}}} \leq p_{p,t}^{\mathrm{b}} \qquad \forall p,t, \tag{2.25l}$$

$$\mu_{p,t}^{\overline{\mathrm{p}}} \leq M^{\mathrm{b+}} (1 - b_{p,t}^{\overline{\mathrm{p}}}) \qquad \forall p,t, \tag{2.25m}$$

$$\underline{e}_{p,t}^{\mathrm{b}} \leq e_{p,t}^{\mathrm{b}} \qquad \forall p,t, \tag{2.25n}$$

$$e_{p,t}^{\mathrm{b}} \leq M^{\mathrm{c\text{-}}} b_{\underline{p},t}^{\mathrm{e}} \qquad \forall p,t, \tag{2.25o}$$

$$\mu_{\underline{p},t}^{\mathrm{e}} \leq M^{\mathrm{c\text{-}}} (1 - b_{\underline{p},t}^{\mathrm{e}}) \qquad \forall p,t, \tag{2.25p}$$

$$e_{p,t}^{\mathrm{b}} \leq \overline{e}_{p,t}^{\mathrm{b}} \qquad \forall p,t, \tag{2.25q}$$

$$-M^{c+}b^{\bar{e}}_{p,t} \quad \leq \quad e^{b}_{p,t} \qquad \forall p,t, \tag{2.25r}$$

$$\mu^{\bar{e}}_{p,t} \quad \leq \quad M^{c+}(1-b^{\bar{e}}_{p,t}) \qquad \forall p,t, \tag{2.25s}$$

where upper level optimisation constraints (2.15) to (2.24) remain unchanged, while non-linear constraint (2.13) is replaced with a set of linear constraints (2.25a)-(2.25e) (prosumers' KKT conditions along with additional slackness variables required for orthogonality) ensuring prosumers' optimal grid power intake while generating dispatch decision.

2.5 Case Study

The NEM 14-generator model developed for small signal stability studies [69] is used in the case study[5]. The generation portfolio assumed for this case study consist of CGs such as, hydro, black coal, brown coal, open cycle gas turbine (OCGT) and combine cycle gas turbine (CCGT). It is assumed that the conventional generators bid at SRMC. Furthermore, cost of generating electricity from utility RES is lower than conventional generators. Generators bids are based on the respective fix and variable operation and maintenance cost (O&M) costs. Predicted fuel prices are derived from [70, 71]. Hourly demand and RES generation traces are taken from the AEMO published National Transmission Network Development Plan (NTNDP) [72]. The simulation scenarios and discussion in the following section are not presented in any previously published work.

2.5.1 Simulation scenarios

The case studies are designed to compare the impact of Utility PV and utility storage with distributed behind the meter PV-battery system, using power dispatch from conventional generators as a benchmark. The aim is to highlight the efficacy of the proposed model and to ascertain that the same effect cannot be captured by utility PV and utility storage models. First in **Scenario I**, the NEM is powered by the combination of conventional generators including hydro, black-coal, brown-coal, CCGT and OGCT. Second, in **Scenario II-a** 4 GW of utility PV is installed on top of generation mix considered in scenario I and in **Scenario II-b** the same amount i.e. 4 GW of PV is installed as rooftop-PV to compare the effects on the dispatch. Then, in **Scenario III-a**, demand profile alteration is studied in the presence of 4 GW of utility PV and 12 GW h of utility storage and compared to **Scenario III-b**. In Scenario III-b, 4 GW of utility PV and 12 GW h of house hold battery capacity is considered at the household level. A summary of these scenarios is also represented in Table 2.1.

[5] Tasmania is not included in 14-generator model as it is connected through HVDC link.

Table 2.1 Summary of scenarios.

	Utility-PV	Utility Storage	Rooftop-PV	Household Batteries
Scenario I	-	-	-	-
Scenario II-a	4 GW	-	-	-
Scenario II-b	-	4 GW	-	-
Scenario III-a	4 GW	-	12 GWh	-
Scenario III-b	-	4 GW	-	12 GWh

2.5.2 Discussion

Simulations are run for typical summer and winter weeks to test model accuracy for different demand and PV generation scenarios. In the NEM, the summer demand peak occurs during mid-day due to the air-conditioning load. In contrast, the winter peak occurs in the morning and evening due to heating load. A weekly average demand profile of the NEM for a year is shown in Fig. 2.4.

In the Scenario I, most of the power demand is met by cheaper coal generators, while the contribution of expensive gas power plants, is limited to peak demand conditions. The addition of utility and rooftop-PV has profoundly different results. From as system point of view, the addition of utility PV puts additional ramp stress on conventional generator especially during winter evenings, when the demand requirement is increasing and PV output is decreasing. An identical behaviour is observed for rooftop-PV, most of the rooftop-PV power is consumed by the prosumers itself resulting in reduction of mid-day demand and remaining power is spilled due to the lack of incentive to send it back to the grid. Fig. 2.5 (top) and Fig. 2.6 (top) shows the power dispatch from conventional generators for Scenario II-a and II-b compared to Scenario I, for typical summer and winter weeks. In the absence of storage where prosumers are expected to utilise power from rooftop-PV and get the remaining power from the grid, model accurately captures this effect as shown in the prosumers' power consumption mix in Fig. 2.5 (bottom) and Fig. 2.6 (bottom). Although this is not the case in the current study, it is worth mentioning that if rooftop-PV generation capacity is less than the underlying prosumer demand then the power dispatch from conventional generators in Scenario II-a and Scenario II-b will be identical.

In the absence of feed-in tariffs, economic viability of residential storage improves significantly. Fig. 2.7 and Fig. 2.8 shows power dispatch from conventional generators (top), prosumers power flows (middle) and battery charging profile (bottom) for a typical summer and a winter week, respectively. In Scenario III-a utility storage helps mitigate the additional ramp stress of conventional generators induced by PV, which results in the reduction of the peak to average demand ratio. Utility storage helps shifting the energy from cheaper time

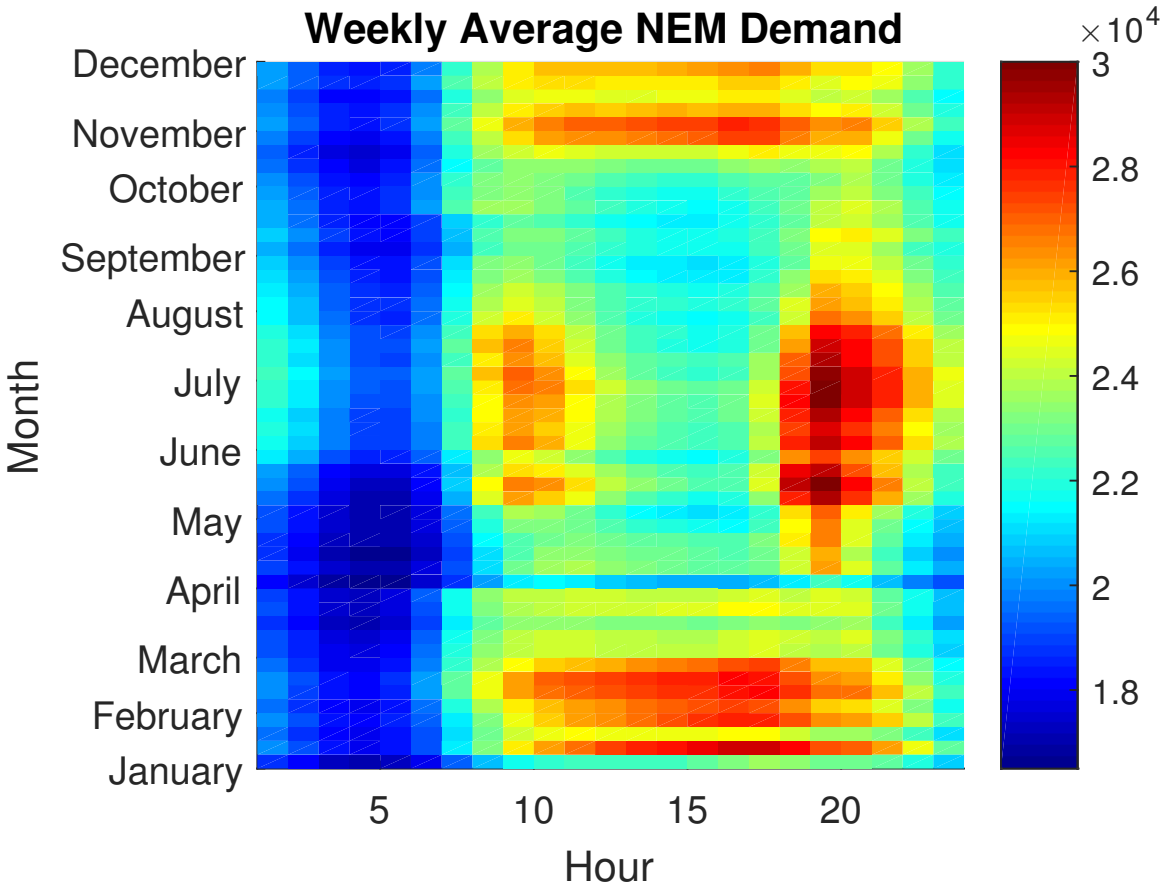

Fig. 2.4 NEM demand profile variation over the year.

slots to the peak, which results in a notable decrease in peak demand. Furthermore, proposed model behaves as anticipated, it accurately mimics prosumers behaviour as represented in Fig. 2.7 and Fig. 2.8. Observe that the power from rooftop-PV is first used to meet the prosumers' demand, with the rest stored for latter use. The model also successfully predicts the prosumers behaviour to charge batteries during the off peak hours and utilising that energy during peak hours to reduce the electricity cost. The efficacy of the model can be ascertained by the fact that, during summer, prosumer battery is only charged during night time from the grid. However, in winter, the batteries are charged not only during the night but also during the day. This is due to the fact that in winter the peak load occurs during the morning and evening, hence the optimal solution for prosumers is to charge batteries during the night and consume that power to cover the morning peak, then utilise a combination of excess PV generation and the cheap electricity generated at midday to charge the batteries again and use that to cover the evening peak.

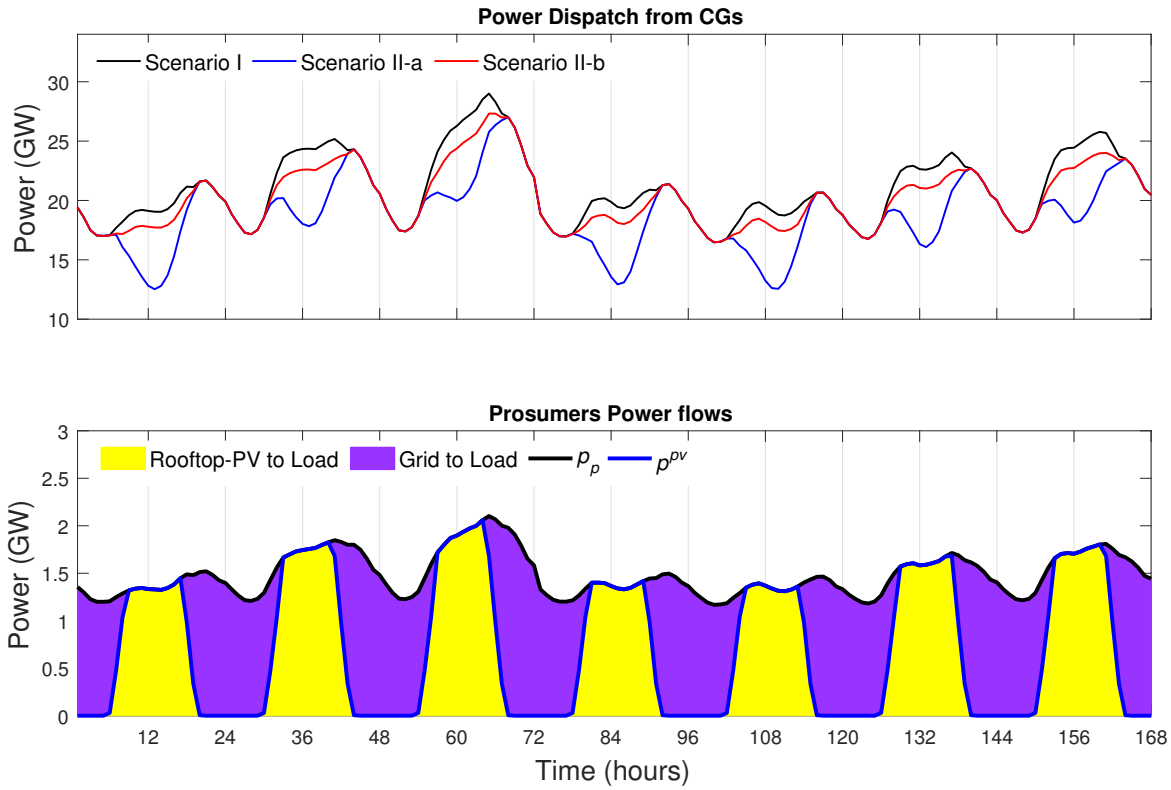

Fig. 2.5 Aggregated power dispatch in summer from conventional generators for Scenario II (top) and prosumers consumption mix for Scenario II-b (bottom).

The computation burden of the proposed model is significantly higher compared to the standard UC problem, mainly due to the high number of linear constraints and a significant increase in the number of integer variables required to deal with the bi-level structure and the non linearities of the proposed model. In this Chapter the network is ignored altogether, which limits the applicability of the proposed model to simple balancing. The case studies are designed to bring out the most salient features of the model and to ascertain it efficacy. Also, prosumers are not allowed to send power back to the grid, which requires further research. In Chapter 3 this model is developed further to include the network constraints, thus making it suitable for stability studies.

2.6 Summary

This chapter proposed a generic demand model that captures the aggregate effect of a large number of prosumers equipped with rooftop-PV battery system. In recent years high rooftop-PV uptake has caused reverse power flows resulting into voltage issues at the distribution level. In response to that, feed-in-tariffs have been significantly reduced. In the absence of

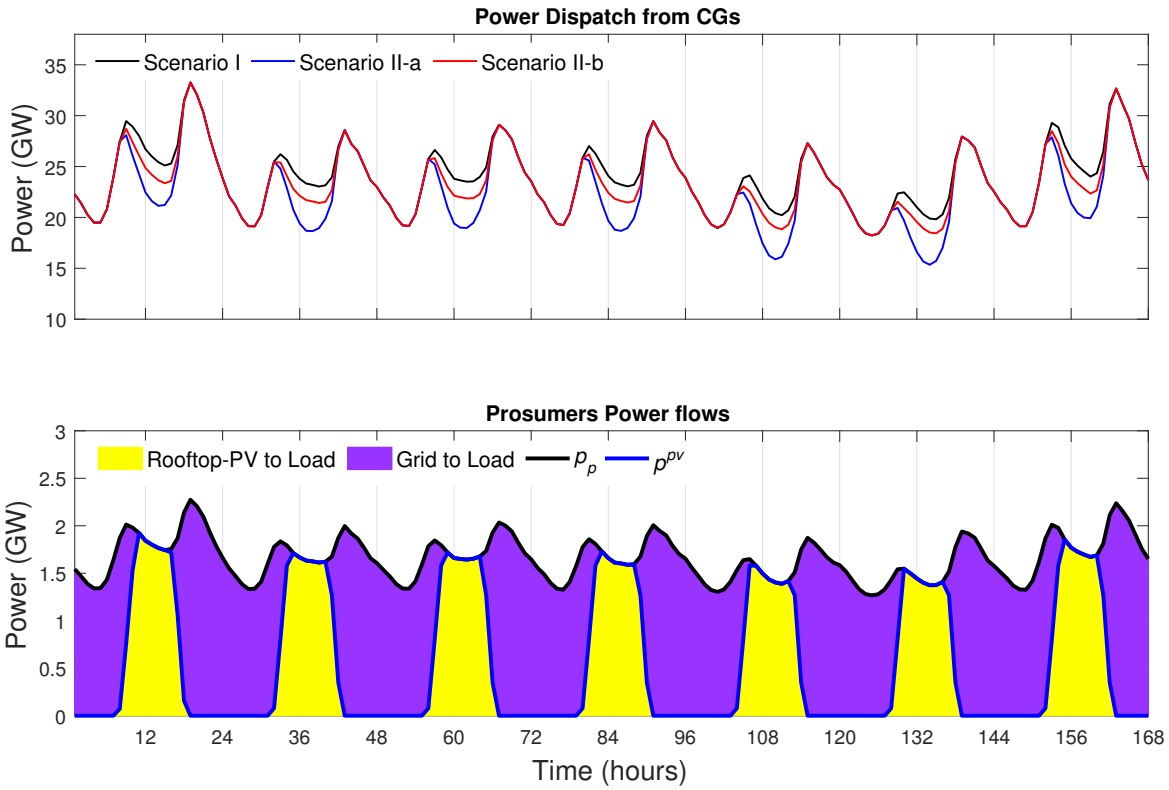

Fig. 2.6 Aggregated power dispatch in winter from conventional generators for Scenario II(top) and prosumers consumption mix for Scenario II-b(bottom).

such incentives, existing rooftop-PV owners (previously enjoying generous feed in tariffs) are prompted deploy household batteries to maximise the self-consumption of the power generated by the PV. The proposed model is generic in that it does not depend on specific practical implementation details that will vary in the long-run.

Results verified the efficacy of the model as it is able to capture the prosumers' behaviour. The results show that the prosumer penetration flattens the demand profile and their impact is vastly different from the results of utility storage and utility PV. It is also shown that utility PV can potentially reduce daytime peak demand at a cost of additional ramp stress imposed on conventional generators. This drawback can be overcome by utility storage. Although utility storage cost is quite high, however decreasing technology cost might make this option feasible. Storage also introduces flexibility without requiring consumers to change their consumption patterns.

The prosumer model presented in this chapter is further extended in Chapter 3 and is modified such that it is suitable for stability studies spanning over longer horizons. Also, the model is modified such that instead of spilling prosumers can send excess power back to grid.

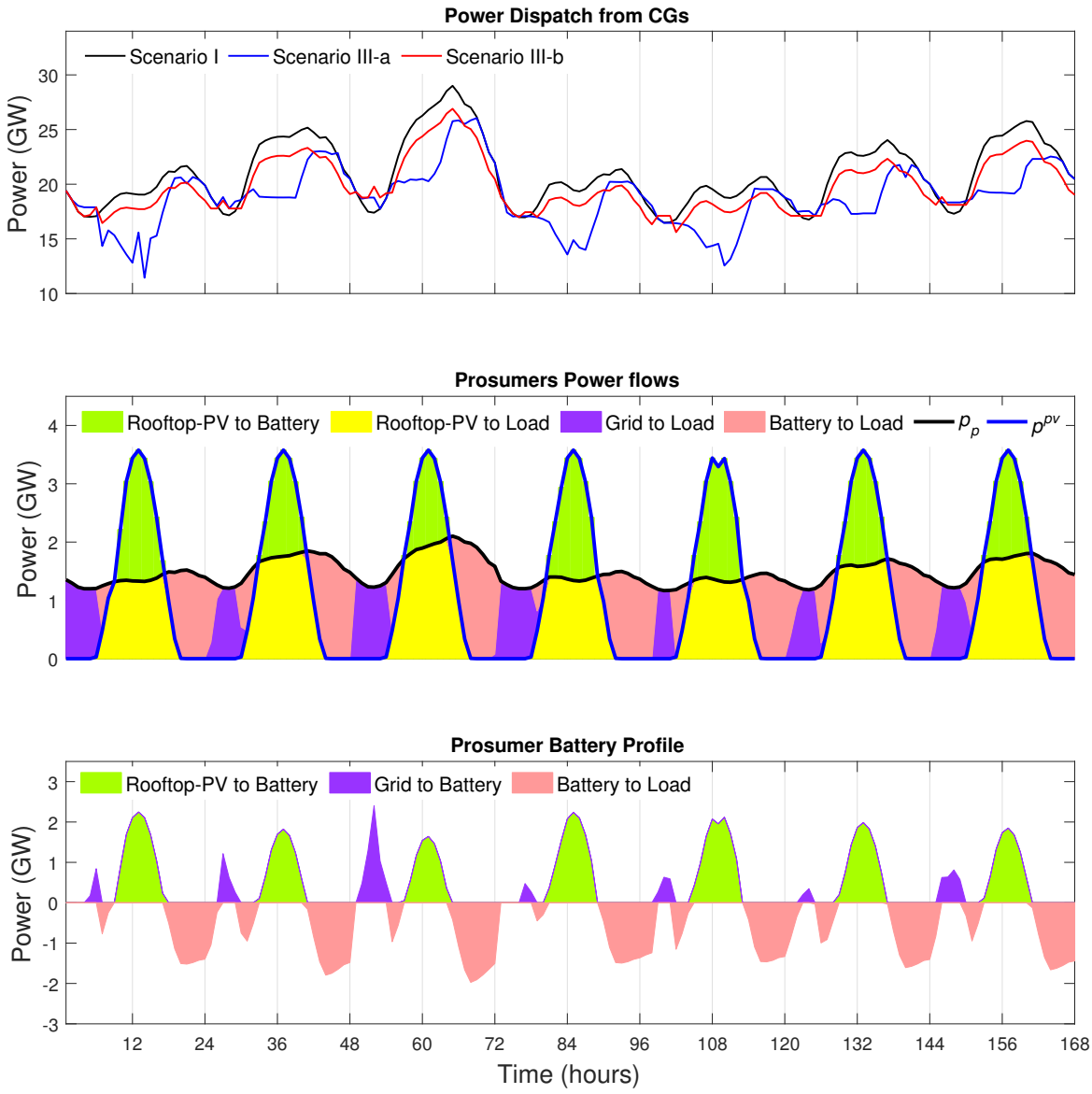

Fig. 2.7 Aggregated power dispatch in summer from conventional generators for Scenario III (top) and prosumers power flows (middle) and prosumer battery charging profile (bottom).

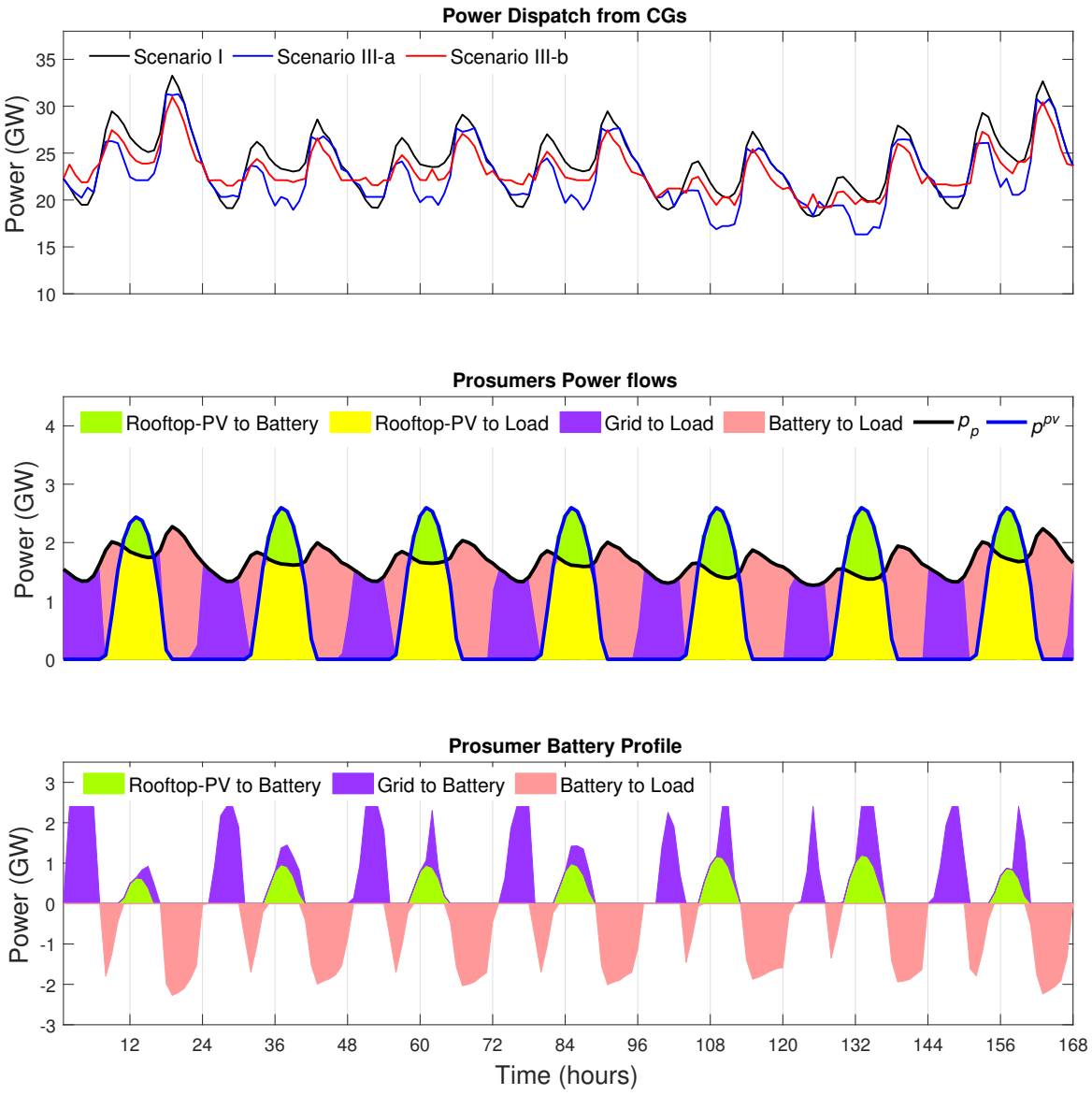

Fig. 2.8 Aggregated power dispatch in winter from conventional generators for Scenario III (top) and prosumers power flows (middle) and prosumer battery charging profile (bottom).

Chapter 3

Impact Study of Prosumers on Loadability and Voltage Stability of Future Grids

The work presented here builds on Chapter 2 that presents a simplified prosumer model based on bi-level optimisation. In Chapter 2, it is assumed that a prosumer aggregation represents a homogeneous group of loads; that is, we have assumed that they all behave in the same way and have the same capacity. However, the model lacks network constraints, thereby, limiting its usage to balancing studies only. As power system stability depends on network constraints, here, we take a step further and include DC power flow constraints. As a result, consumers and prosumers can no longer be lumped into one profile, rather they have to be represented by one entity at each node. This results in $|\mathcal{N}|$ prosumers and consumer aggregators, which result in $|\mathcal{N}|$ prosumers sub-problems and an increase in the search space of the problem.

Specifically, In Case Study I presented in Section 3.4, the model is also modified so that if the uptake of household battery is low, the prosumers can send the excess rooftop-PV power back to the grid. In addition to the assumption stated in Section 2.3, the following additional assumptions were made:

1. By treating feed-in tariffs as negligible, the prosumers' objective can be cast as maximising self-consumption by storing the excess PV power in the battery. In other words, they only send power back to the grid if rooftop-PV generation exceeds their consumption and storage capability. To minimise cost, prosumers can also use cheap grid power to charge the battery. However, this option is more dependent on the market rather than choice of prosumers. From ISO perspective, the cost of feed-in power is the lowest in the system, it will be always prioritised in the dispatch.

2. Prosumer aggregation can assist the market by shifting energy produced cheaply to times of peak prices, thereby reducing the electricity procured from expensive gas power plants, which specifically operate during these peak hours. However, prosumers do not allow an ISO to have a direct control of their batteries, due to life cycle reduction of battery and lack of proper incentive (e.g. feed-in tariffs).

3. We assume that the demand model representing an aggregator consists of a large population of prosumers connected to an unconstrained distribution network who collectively maximise self-consumption (made possible by an efficient internal trading and balancing mechanism).

Work done in this chapter is part of the FG Research Program funded by the CSIRO, whose aim is to explore possible future pathways for the evolution of the Australian grid out to 2050 by looking beyond simple balancing. To this end, a comprehensive modelling framework for future grid scenario analysis has been proposed in [42], which includes a market model, power flow analysis, and stability analysis. The demand model, however, assumes that the users are price-takers, which doesn't properly capture the aggregated effect of prosumers on the demand profile, as discussed later.

Remark on the author's contribution: the work presented in this Chapter resulted from the collaborative work with former PhD student Hesamoddin Marzooghi. The author's contribution is an extension of the prosumers integration into dispatch model presented in Chapter 2 and the inclusion of the network constraints, thus making it suitable for stability studies, whereas Hesamoddin Marzooghi carried out the stability assessment.

3.1 Background and Literature Regarding Prosumers

As described in Chapter 1, power systems worldwide are undergoing a major transformation driven by the increasing uptake of variable RES. At the demand side, the emergence of cost-effective "behind-the-meter" distributed energy resources, including on-site generation, energy storage, electric vehicles, and flexible loads, and the advancement of sensor, computer, communication and energy management technologies are changing the way electricity consumers source and consume electric power.

Indeed, recent studies suggest that rooftop-PV battery systems will reach retail price parity from 2020 in the USA grids and the NEM [50]. A recent forecast by Morgan Stanley has suggested that the uptake can be even faster, by boldly predicting that up to 2 million Australian households could install battery storage by 2020 [73]. This has been confirmed by the Energy Networks Australia and the CSIRO who have estimated the projected uptake of

solar PV and battery storage in 2050 to be 80 GW and 100 GWh [74], which will represent between 30%–50% of total demand, a scenario called "Rise of the Prosumer" [49]. Here, the *prosumer* they refer to is a small-scale (residential, commercial and small industrial) electricity consumer with on-site generation. A similar trend has been observed in Europe as well [75]. Given this, it is expected that a large uptake of demand-side technologies will significantly change demand patterns in future grids, which will in turn affect their dynamic performance.

Existing future grid feasibility studies [33–37] typically use conventional demand models, possibly using some heuristics to account for the effect of emerging demand-side technologies, and the synergies that may arise between them. They also assume specific market arrangements by which RES are integrated into grid operations. Most importantly, they rely on simple balancing and ignored network constraints, line congestion and stability, The challenge associated with future grid planning is that the grid structure and the regulatory framework, including the market structure, cannot be simply assumed from the details of an existing one. Instead, several possible evolution paths need to be accounted for.

Due to the influence of a demand profile on power systems performance and stability, recent studies have attempted to integrate the aggregated impact of prosumers into the demand models [1, 59, 61, 64, 76, 77]. The focus, however, is usually on scheduling of particular emerging demand-side technologies, e.g. HVAC [1, 61, 64], flexible loads [76], PV-battery systems [77], and electrical vehicles [59]. Most of these modelling approaches assume an existing market structure, with the impact of prosumers incorporated by allowing demand and supply to interact in some limited or predefined ways. Specifically, this is mainly done via three different approaches:

1. Only the supply-side is modelled physically while prosumers are considered by a simplified representation of demand-side technologies. In [76], flexible loads' effects on reserve markets are analysed by modelling prosumers with a tank model; however, the reserve market is greatly simplified. In [1], prosumers are represented by a price-elasticity matrix, which is used to model changes in the aggregate demand in response to a change in the electricity price, and are acquired from the analysis of historical data.

2. Demand-side technologies are physically modelled while a simplified representation of supply-side is employed. For instance, in [77], the supply-side is represented by an electricity price profile.

3. Both supply and demand sides can be modelled physically and optimised jointly, as in [61, 59], which can produce more realistic results. For example, the study in [59]

integrates the aggregated charging management approaches for electric vehicles into the market clearing process, with a simplified representation of the latter.

Although the above models have shown their merits, they are dependent on specific practical details such as the electricity price or the implementation of a mechanism for DR aggregation, which limits their usefulness for future grid scenario analysis where the detailed market structure is potentially unknown. Therefore, a *generic* modelling framework is required that properly captures the aggregated effect of prosumers on the demand profile. A key feature of such generic models is that they do not depend on specific practical details that will vary in the long-run. This concept is already well-known in power systems, such as in conventional load modelling, where the aggregated effect of millions of devices is captured by simple analytical expressions [62, 63]. In future grid scenario analysis, the purpose of generic demand models in market simulation is to capture accurate dispatch decisions, used as the initial point for balancing and stability analysis.

3.2 Voltage Stability

Voltage stability deals with the ability of the power system to keep voltages near their nominal values after a disturbance, typically characterised as the levels being within specified range [62]. This can be assessed by simulating or monitoring so called voltage collapse proximity indicators. The loadability and voltage stability has been assessed in this study using the following methods:

Contingency screening

As the first step, all the credible contingencies are screened to determine the most severe ones based on the maximum power transfer level. Among all the N-1 contingencies, the twenty most severe ones are selected.

Loadability calculation

To calculate the system loadability, first, the power flow is solved for the base case (i.e. market dispatch) and for each of the chosen contingencies in the previous step. We assume the following strategy for loadability calculation: the power of all the loads increases uniformly in small steps with constant power factor, and all the associated generators are scheduled with the same participation factor to pick up the system load. The loadability is computed as the step before power flow divergence.

Modal analysis

This analysis is employed at the base case (market dispatch result) for computing the smallest eigenvalues and the associated eigenvectors. For such a calculation, we compute the Jacobian matrix and reduce it to the V-Q sub-matrix. Such analysis can provide a relative measure of the proximity to instability. Also, it provides information on critical voltage modes and weak points in the grid (i.e. areas prone to voltage instability).

3.3 Optimisation Framework

The presented framework is specifically developed to model future net demand by incorporating prosumers. The model is based on a UC problem aiming to minimise the generation cost. The prosumer aggregation is used to represent a homogeneous group of loads, aiming to maximise their self-consumption by reducing their feed-in power. That is, we assumed that they all behave in the same way and have the same capacity. As such, they are represented by one single load per node. Moreover, we also assume that the aggregator uses an economic mechanism that elicits price-anticipating behaviour from the prosumers. Given this, a Stackelberg game can be used to model the interaction between the ISO and prosumers, as illustrated in Fig. 3.1.

3.3.1 Upper-level problem (ISO)

To emulate the market outcome, the upper-level problem is cast as a UC problem aiming to minimise the generation cost:

$$\underset{s,u,d,p,\theta}{\text{minimise}} \sum_{t\in\mathcal{T}} \sum_{g\in\mathcal{G}} \left(c_g^{\text{fix}} s_{g,t} + c_g^{\text{su}} u_{g,t} + c_g^{\text{sd}} d_{g,t} + c_g^{\text{var}} p_{g,t} \right), \tag{3.1}$$

where $s_{g,t}, u_{g,t}, d_{g,t} \in \{0,1\}$, $p_{g,t} \in \mathbb{R}^+$, $\theta_{i,t} \in \mathbb{R}$ are the decision variables of the problem.

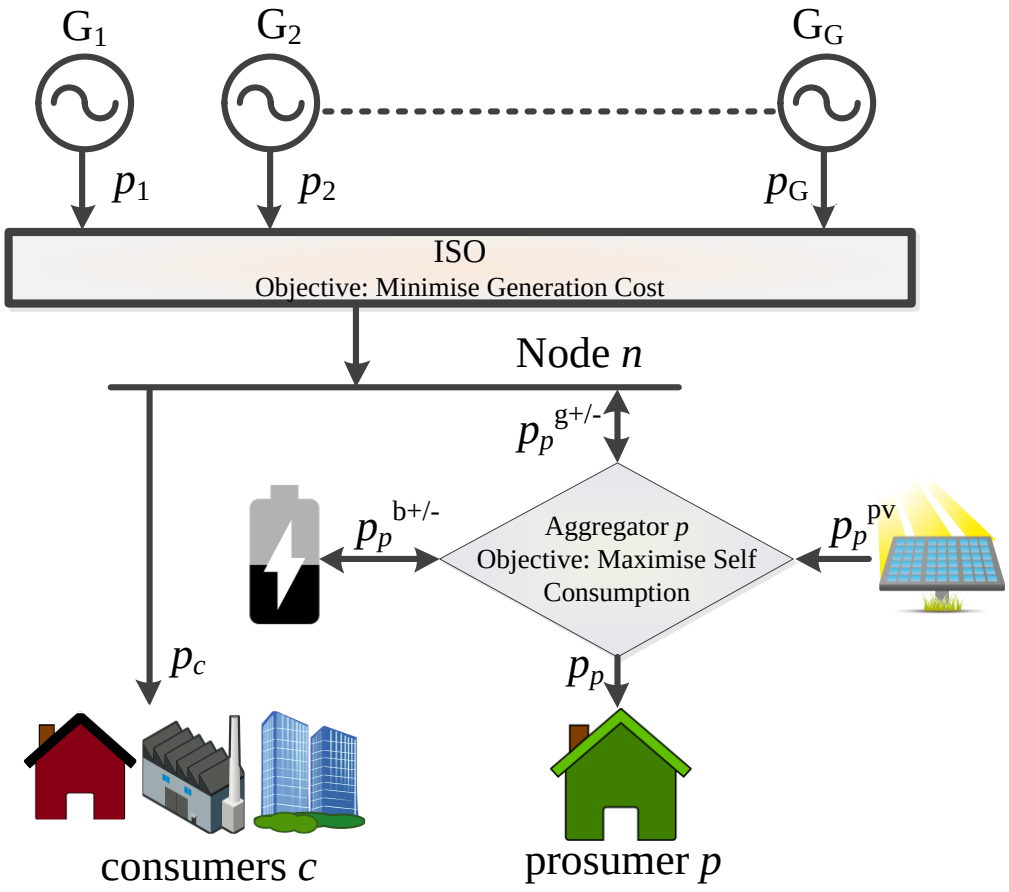

Fig. 3.1 Structure of the proposed modelling framework.

The problem is subject to the following constraints[1]:

$$\sum_{g\in\mathcal{G}_n} p_{g,t} = \sum_{c\in\mathcal{C}_n} p_{c,t} + \sum_{p\in\mathcal{P}_n} (p^{\text{g+}}_{p,t} - p^{\text{g-}}_{p,t}) + \sum_{l\in\mathcal{L}_n} (p_{l,t} + \Delta p_{l,t}), \tag{3.2}$$

$$|B_{i,j}(\delta_{i,t} - \delta_{j,t})| \leq \overline{p}_l, \tag{3.3}$$

$$\underline{p}_g s_{g,t} \leq p_{g,t} \leq \overline{p}_g s_{g,t}, \tag{3.4}$$

$$u_{g,t} - d_{g,t} = s_{g,t} - s_{g,t-1}, \tag{3.5}$$

$$\sum_{g\in\{\mathcal{G}_r\cap\mathcal{G}^{\text{syn}}\}} \overline{p}_g s_{g,t} - p_{g,t} \geq \sum_{n\in\mathcal{N}_r} p^{\text{r}}_{n,t}, \tag{3.6}$$

$$u_{g,t} + \sum_{\tilde{t}=0}^{\tau^{\text{u}}_g - 1} d_{g,t+\tilde{t}} \leq 1, \tag{3.7}$$

$$d_{g,t} + \sum_{\tilde{t}=0}^{\tau^{\text{d}}_g - 1} u_{g,t+\tilde{t}} \leq 1, \tag{3.8}$$

$$-r^-_g \leq p_{g,t} - p_{g,t-1} \leq r^+_g, \tag{3.9}$$

$$\underset{p^{\text{g-}},p^{\text{g+}},p^{\text{b}}}{\arg\min} \{ \sum_{t\in\mathcal{T}} p^{\text{g-}}_{p,t} \text{ s.t. equation (3.12)} - \text{(3.15)} \}, \tag{3.10}$$

[1] All the constraints must be satisfied in all time slots t, however, for sake of notational brevity, this is not explicitly mentioned.

where (3.2) is the power balance equation at each node n in the system[2], with $\mathcal{G}_n$, $\mathcal{C}_n$, $\mathcal{P}_n$, $\mathcal{L}_n$ representing respectively the sets of generators, consumers, prosumers and lines connected to node n, and $p_{c,t}$, $p^{\text{g+}}_{p,t}$, $p^{\text{g-}}_{p,t}$, $p^{i,j}_{l,t}$ and $\Delta p^{i,j}_{l,t}$ representing respectively the consumer demand, prosumer demand, prosumer feed-in of aggregator n, line power and line power loss (assumed to be 10% of the line flow) on each line connected to node n; (3.3) represents line power limits; (3.4) limits the dispatch level of a generating unit between its respective minimum and maximum limits; (3.5) links the status of a generator unit to the up and down binary decision variables; (3.6) ensures spinning reserves for system stability are provided by synchronous generation in reach region of the grid, with $\mathcal{N}_r$ and $\mathcal{G}_r$ being the set of aggregators and generators in region r; (3.7) and (3.8) ensure minimum up and minimum down times of the generators; (3.9) are the generator ramping constraints; and (3.10) is the prosumers aggregator optimisation constraint as detailed out in Section 3.3.2.

3.3.2 Lower-level problem (prosumer aggregators)

Prosumer aggregation is formulated in the lower-level problem. The loads within an aggregator's domain are assumed homogeneous, which allows us to represent the total aggregator's demand with a single load model. The electricity price is not explicitly shown in the optimisation problem[3] (see Assumptions 1 and 2 in Section 2.3). Note that in a home energy management problem [66], the electricity price is known ahead of time, resulting in a price-anticipating behaviour. In our framework, the electricity price is a by-product of the specific mechanism adopted for prosumer aggregation and is dynamic. In a practical implementation, a home energy management system is an agent acting on behalf of the prosumer. Given a sufficient battery capacity, the end-users' comfort is not jeopardised.

The lower-level problem is formulated as follows:

$$\underset{p^{\text{b}}_{p,t}, p^{\text{g+}}_{p,t}, p^{\text{g-}}_{p,t}}{\text{minimise}} \sum_{t \in \mathcal{T}} p^{\text{g-}}_{p,t}, \tag{3.11}$$

[2]Note that the prosumer demand and feed-in of each aggregator, $p^{\text{g+/-}}_{p,t}$, couples the upper-level (ISO) problem with each of the n lower-level (aggregator) problems.

[3]In a practical implementation, the electricity price could consist of the dual variables associated with the power balance constraint (3.2) and power flow constraints (3.3) of the upper-level problem, plus retail and network charges.

where the battery power $p^{\mathrm{b}}_{p,t} \in \mathbb{R}$ and $p^{\mathrm{g+/-}}_{p} \in \mathbb{R}^{+}$ are the decision variable. The problem is subject to the following constraints:

$$p^{\mathrm{g+}}_{p} = p_{p,t} + p^{\mathrm{g-}}_{p} - p^{\mathrm{pv}}_{p,t} + p^{\mathrm{b}}_{p,t}, \tag{3.12}$$

$$e^{\mathrm{b}}_{p,t} = \eta^{\mathrm{b}}_{p} e^{\mathrm{b}}_{p,t-1} + p^{\mathrm{b}}_{p,t}, \tag{3.13}$$

$$\underline{p}^{\mathrm{b}}_{p} \leq p^{\mathrm{b}}_{p,t} \leq \overline{p}^{\mathrm{b}}_{p}, \tag{3.14}$$

$$\underline{e}^{\mathrm{b}}_{p} \leq e^{\mathrm{b}}_{p,t} \leq \overline{e}^{\mathrm{b}}_{p}, \tag{3.15}$$

where (3.12) is the power balance equation; and (3.14)-(3.15) are the battery storage constraints. Power $p_{p,t}$ is the underlying demand of the prosumers. Note that according to the Assumption 3 in Section 2.3, except for battery losses, the underlying power demand doesn't change, however the grid intake power can. Finally, the KKT optimality conditions of the lower-level problem are added as the constraints to the upper-level problem, which reduces the problem to a single MILP that can be solved using of-the-shelf solvers. Note that because the two levels interacts through a power, not through a price, unlike in [64], no linearisation is required.

3.4 Case Study I

This section demonstrates the effect of increased penetration of residential battery system on the balancing, loadability and voltage stability of the NEM in 2020 using model detailed out in Section 3.3. The 14-generator IEEE test system shown in Fig. 3.2 was initially proposed in [69] as a test bed for small-signal analysis. The system is loosely based on the NEM, the interconnection on the Australian eastern seaboard. The network is radial, with large transmission distances and loads concentrated in a few load centers. It consists of 59 buses, 28 loads, and 14 generators. The test system consists of five areas (regions),last four representing the states of New South Wales (NSW), Victoria (VIC), Queensland (QLD) and SA. In our simulations we considered area 1 (Snowy Hydro) as part of NSW.

Simulations scenarios considered a typical winter and summer week of the year 2020 to study the impact of different levels of distributed storage on the performance and voltage stability of the NEM. A combination of coal, gas, hydro, wind and utility-PV are considered to fulfil demand requirements in 2020. Further, all generators bid at their respective SRMC that are based on the variable O&M cost and the predicted regional fuel prices for 2020 [70, 71]. Solar, wind and demand traces with hourly resolution are taken from the AEMO's planning document [78]. The demand model captures the aggregated effect of a large number of prosumers, as explained in Section 3.3.

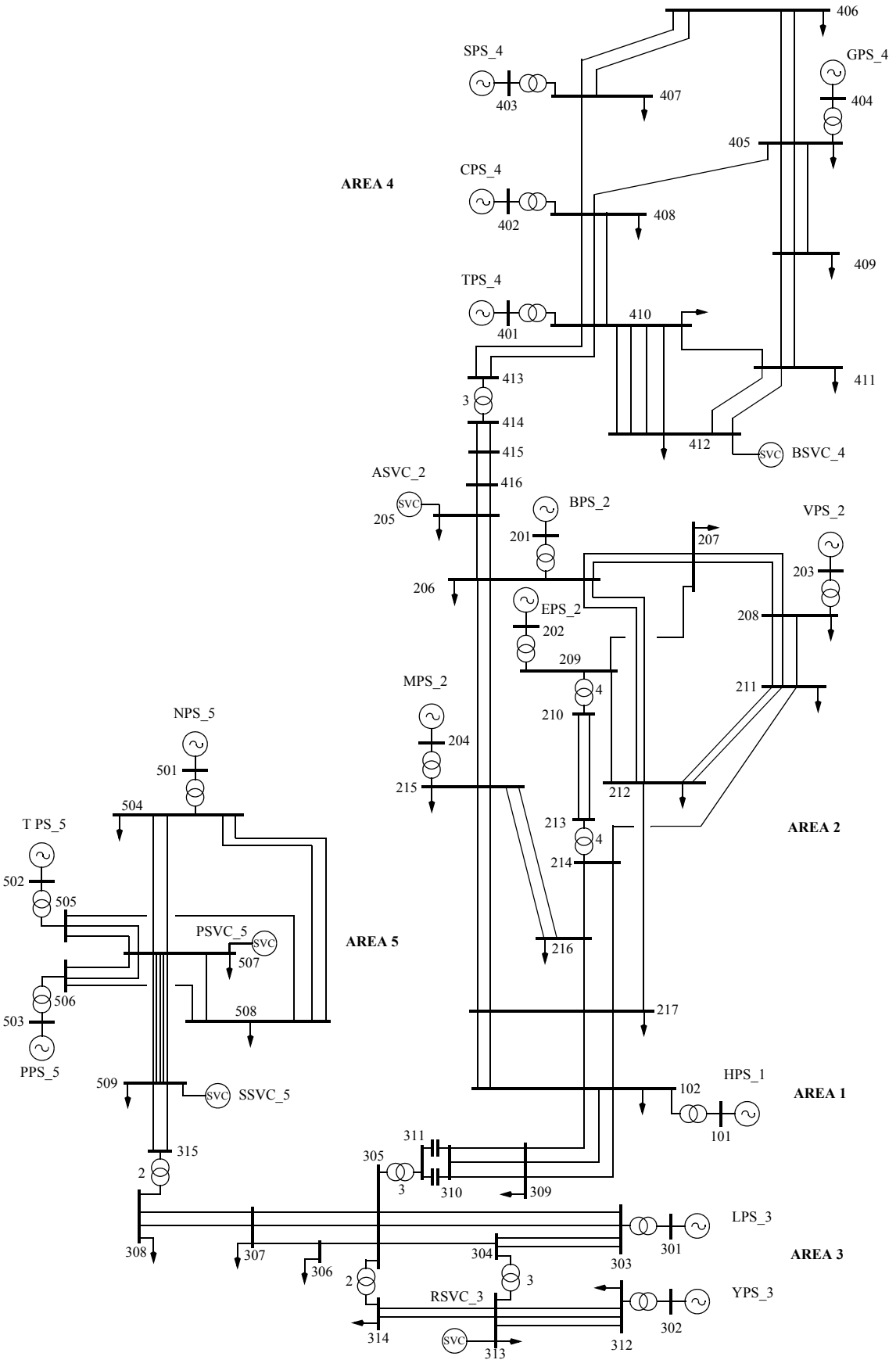

Fig. 3.2 Single-line diagram of the 14-generator model of the NEM.

Table 3.1 Generation mix considered for case study I.

	Hydro (GW)	Coal (GW)	Gas (GW)	Wind (GW)	Utility-PV (GW)	Rooftop-PV (GW)	Battery (GW h)
Case I	4	23.77	15.58	5.16	1.1	8.53	-
Case II	4	23.77	15.58	5.16	1.1	8.53	17.06
Case III	4	23.77	15.58	5.16	1.1	8.53	34.12

The conventional generation mix consists of 2.31 GW hydro, 23.77 GW black coal, 15.58 GW brown coal and 5.16 GW gas. In addition, a further, 10.19 GW of wind and 1.1 GW of utility-PV is added in the system, following the forecast by the AEMO Wind Integration Studies Report [79]. The penetration of rooftop-PV is inspired by the AEMO National Electricity Forecast Report [46], which predicts rooftop-PV capacity to be around 8.53 GW in 2020. Minimum stable limits of 50 % and 40 % are imposed on coal generators and combine cycle gas turbines (CCGT), respectively. The ramp rates of coal-fired generators are set between 50 % to 60 % of rated capacity per hour, while open cycle gas turbines (OCGT) have much higher ramping rates ranging between 80 % to 90 %. Hourly resolution data from different sources is used with perfect foresight (a 10 % reserve margin is assumed to account for uncertainty).

3.4.1 Scenarios

First, **Case I** analyses the scenario where prosumers are equipped with rooftop-PV in the absence of storage. Second, in **Case II** the battery capacity of 2 h of storage capacity per unit of rooftop-PV generation is added on top of Case I, i.e. 2 kW h of battery is installed for every kW of rooftop-PV. Finally, in **Case III**, the installed battery capacity is doubled compared to Case II. Hence for Case III, the ratio of installed battery capacity to rooftop-PV is 4 h. Generation mix considered for different cases is summarised in table 3.1.

3.4.2 Results

The results of our simulations, exploring the impacts of residential batteries on balancing and voltage stability, are discussed below.

Balancing

In Case I, without battery storage, prosumers send their excess rooftop-PV generation back to the grid, which does not earn much in feed-in tariff payments, and may also increase the ramp rate stress on CGs, as shown in Fig. 3.3 (top). Residential batteries benefit prosumers

in two ways. First, it allows them to decrease their energy requirement from the grid by increasing self-consumption. Second, it allows them to utilise the flexibility of battery storage in order to shift their power requirement from expensive time slots to cheaper ones. The shift in prosumers' grid power requirement for Cases I and III along with their consumption patterns and PV generation is shown in Fig. 3.4. From the grid's perspective, in the presence of residential battery storage (Case II and Case III), power flow from the grid to prosumers is reduced during peak hours. This can be seen in Fig. 3.5, which shows the effect of household battery storage on the net demand profile, in contrast to system demand (the sum of consumers' and prosumers' consumption). This phenomenon decreases the peak to average ratio of the demand profile, which reduces the ramp stress on the CG, as shown in Fig. 3.5.

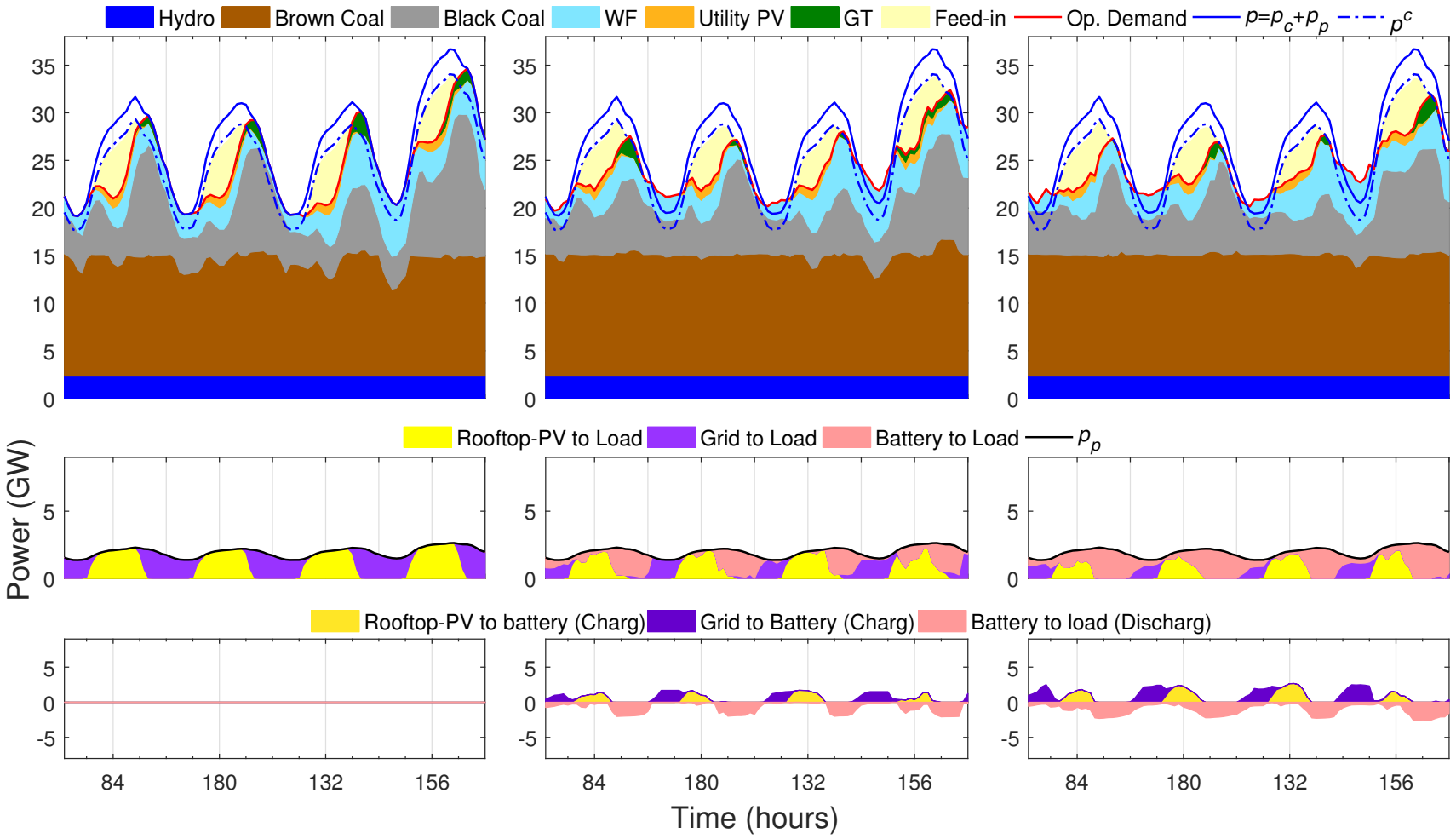

Fig. 3.3 Dispatch results with different amounts of storage: zero (left), 2 h (middle) and 4 h (right).

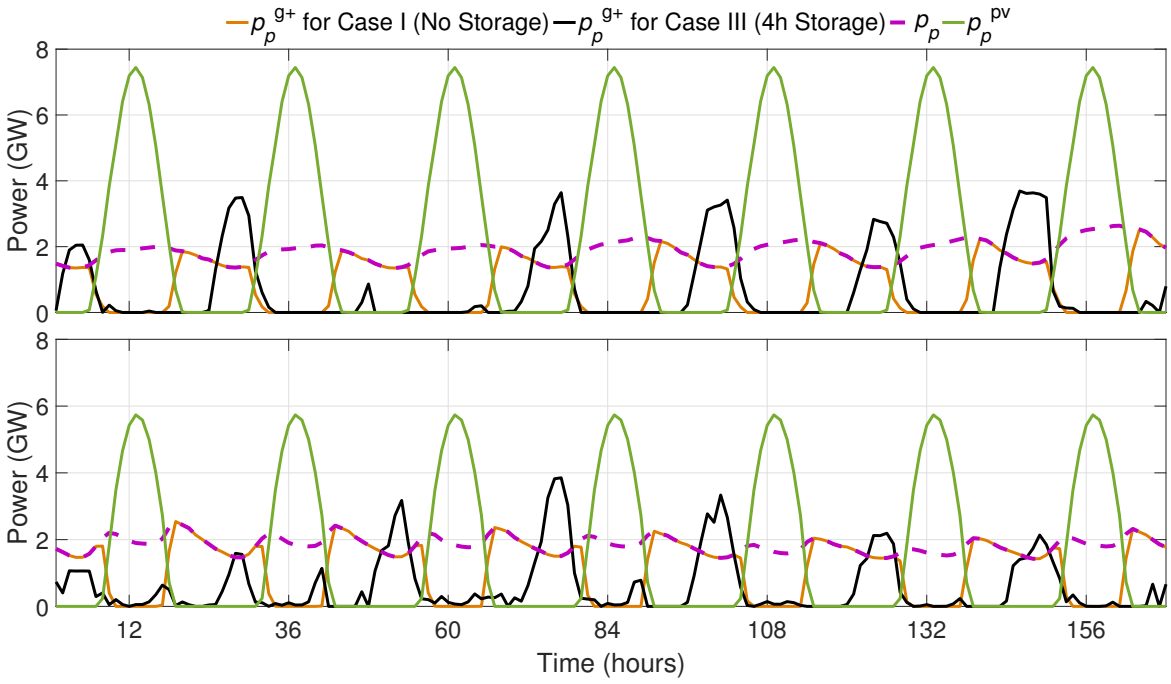

Fig. 3.4 Sum of prosumers grid power ($p^{g+}_{p,t}$) for Case I (No Storage) and Case III (4h Storage) along with their net consumption ($p_{p,t}$) and generation ($p^{pv}_{p,t}$) traces for January (top) and July (bottom).

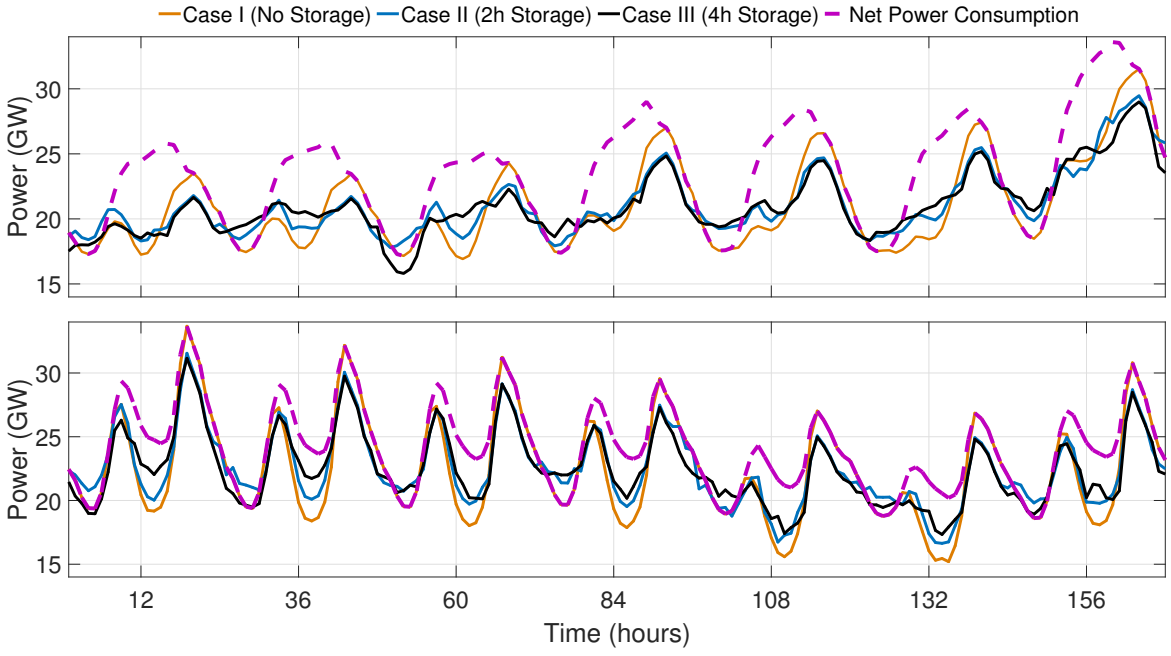

Fig. 3.5 System demand profile for Case I, II and III against sum of consumers and prosumers power consumption; January (top) and July (bottom).

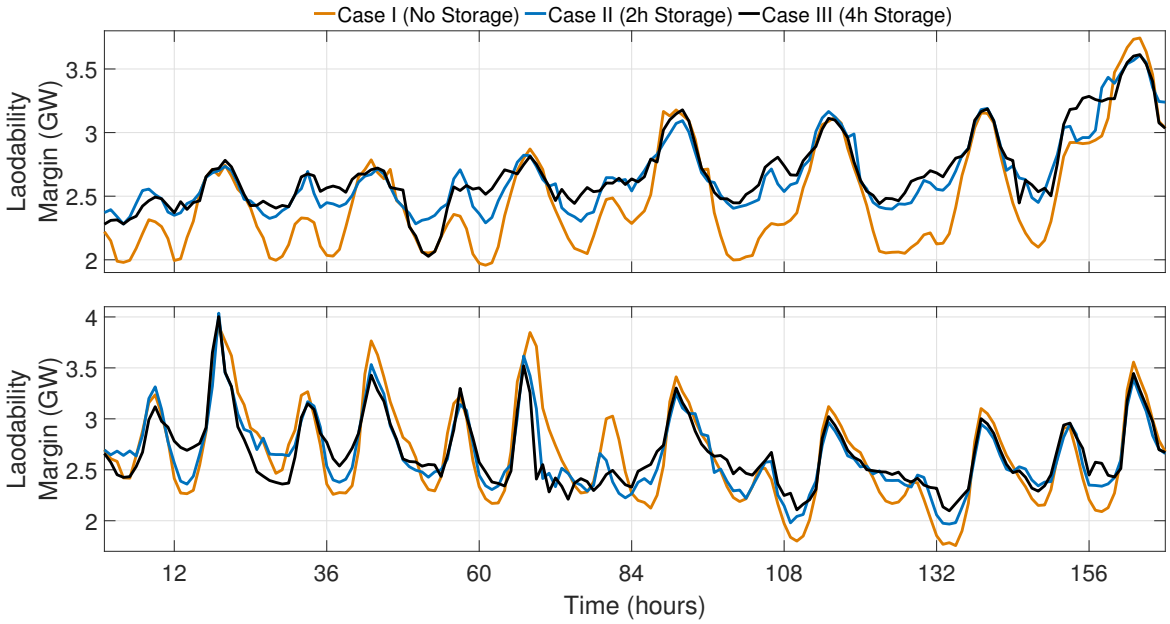

Fig. 3.6 Loadability results of January (top) and July (bottom).

Voltage stability

For voltage stability, it is assumed that all the loads and generators in the NEM have the defined strategy in Section 3.2. Loadability margin results, i.e. the difference between the market dispatch results and the system loadability, for one critical scenario is shown in Fig. 3.6. This shows that the increased residential battery penetration (Case II and Case III) improves the system loadability margin compared to Case I.

Note that the demand reduction in peak hours in Case II and Case III has improved the system loadability. As the generation of the generators which have significant effects on loadability of the grid are mainly reduced allowing them to accept more demands. Further, observe that with the increased penetration of residential batteries, system loadability margin is enhanced during hours where there is excess generation from rooftop-PV compared to Case I. This is due to the flatter net demand curve (see Fig. 3.5) in Case II and Case III compared to Case I, as prosumers use their battery system to store excess PV-generation. It is also interesting to note that the improvement from Case I to Case II for January is greater than for July. This is because of higher rooftop-PV generation levels resulting in more feed-in power as shown in Fig. 3.4. However, the difference between Case II and Case III is not significant for January nor July.

Fig. 3.7 compares the minimum of the real part of all eigenvalues, henceforth called the minimum eigenvalue for the first week of January and July 2020. The observed pattern is the same as the loadability results disscussed above. This implies that the increased penetration

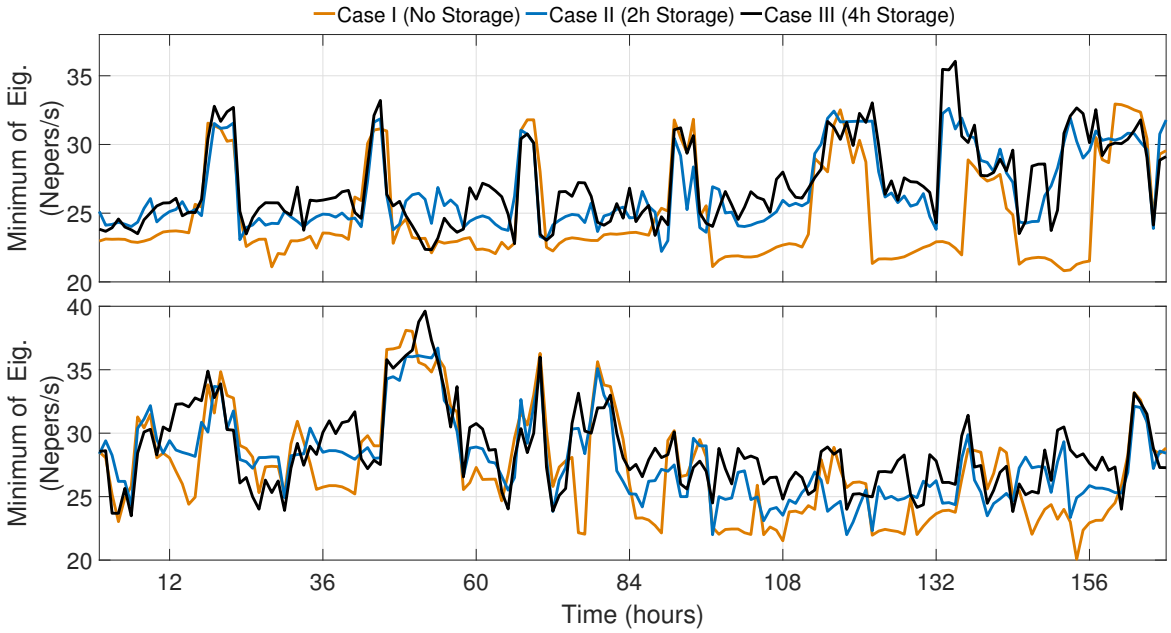

Fig. 3.7 Eigenvalues for January (top) and July (bottom).

of residential batteries improves the voltage stability margin of the network. Also, observe that the voltage stability margin improves significantly when there are more synchronous generators in the grid, especially in SA and QLD (where penetration of utility RES and rooftop-PV is much higher than other regions in the NEM). Examining the participation factor of the busbars in the critical voltage modes revealed that SA and QLD are the voltage constrained regions. The increased penetration of battery system in Case II and Case III, however, has enhanced the voltage stability margins considerably in those region by flattering the demand curve and reducing peak demand.

3.4.3 Discussion

In FGs, decreasing feed-in tariffs and battery installation cost will incentivise prosumers to install residential storage to minimise electricity cost either through energy time-shifting or by maximising self-consumption. In this case study I, it is shown that the installation of residential battery system will not only be beneficial to the prosumers, but will also play a critical role in changing grid operation. Prosumers attempt to utilise as much power as they can from rooftop-PV and send only the excess energy back to the grid. However, due to the lack of proper incentives, they do not allow their battery to be utilised for the benefit of the grid directly.

In particular, case studies show that the increased penetration of residential battery storage improves the system loadability margin for most hours by decreasing peak demand

and flattering the demand curve. Also, it has reduced the peak to average ratio of demand profile. Further, the increased penetration of battery systems can improve the voltage stability margin in voltage constraint areas and weak points. However, a more comprehensive analysis is required before some general trends can be established.

Also, in the absence of an explicit transmission pricing, allowing feeding power from prosumer aggregators can create perverse outcomes, such as power exchange (using transmission network) between aggregators located in different parts of the network. This will complicated the operation of electricity networks. In particular most of the transmission network infrastructure is build on uni direction power flow and installed protection devices interpret reverse power flow as fault. Thus, we assume that the prosumer aggregators should not be allowed to exchange or send power to the grid.

3.5 Case Study II

To restrict the power transfer between aggregators using the transmission network, we remodel the problem in Section 3.3. For this purpose, the aggregators' objective is changed from minimising feed-in power to minimising grid power intake, as explained in Section 2.4.2, and the power balance constraint (3.2) is adjusted to incorporate this change. Although, this look like a minor tweak in the market model, however, it has important implications for stability studies. Case study II uses annual simulation to capture the impact of prosumers on voltage stability of FGs for vast range of demand and RES variation.

The generator technologies and modeling assumptions follow [44]. We consider two RES penetration rates. In the BAU scenario, the generation portfolio includes 39.36 GW coal, 5.22 GW gas, and 2.33 GW hydro. In the high-RES scenario, 40 % of the total demand is covered by variable RES. Inspired by two recent Australian 100% renewables studies [33, 37], part of coal generation is replaced with wind and utility PV using wind and solar traces from the AEMO's planning document [72], which results in 28.94 GW coal, 5.22 GW gas, 2.33 GW hydro, 21 GW wind, and 12 GW utility PV. Fig. 3.8 represents the displaced CGs location and 16 zones proposed by the AEMO. These zones are used to generated PV and wind traces. Given the deterministic nature of the model, we assume 10 % reserves for each region in the system to cater for demand and RES forecast errors. In market simulations, generators are assumed to bid according to their SRMC, while RESs bid at zero cost. Simulations are performed using a rolling horizon approach with hourly resolution assuming a perfect foresight. The optimisation horizon is three days with a two-day overlap. Last, wind and solar generators are assumed to operate in a voltage control mode.

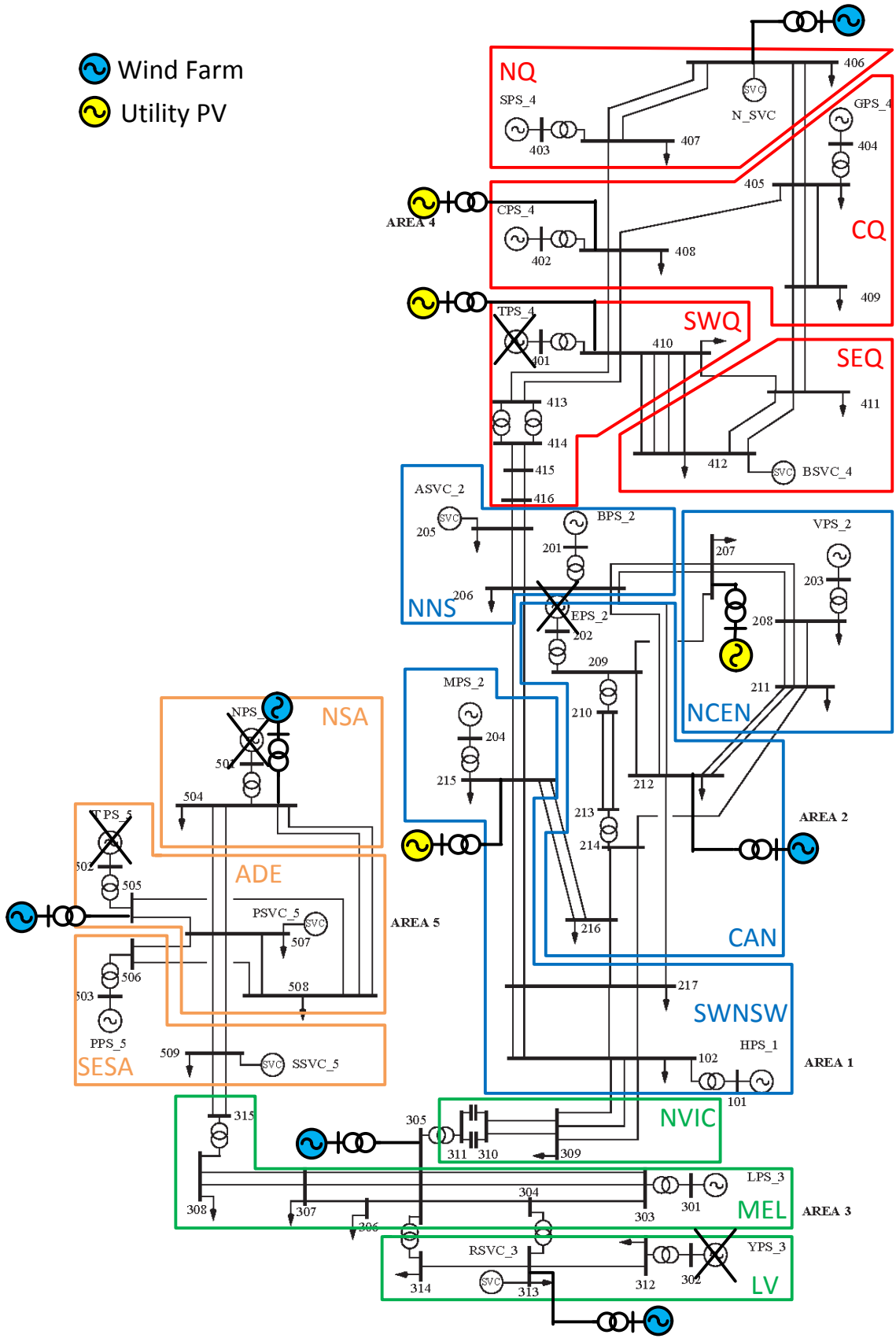

Fig. 3.8 Modified single-line diagram of the 14-generator model of the NEM with the 16 zones as proposed by the AEMO.

3.5.1 Prosumer scenarios

Four different prosumer penetrations: zero, low, medium and high. With no prosumer penetration, the demand is assumed inflexible. For the other three scenarios, we assume that part of the demand is equipped with small-scale (residential and small commercial) PV-battery systems. The uptake of PV loosely follows a recent AEMO study [53]. The PV capacities are respectively 5 GW, 10 GW, and 20 GW for the low, medium and high uptake of prosumers. We consider three different amounts of storage: zero, 2 kW h, and 4 kW h of storage for 1 kW of rooftop-PV.[4] Hourly demand, wind and PV traces are from the AEMO's planning document [72].

3.5.2 Dispatch results

Dispatch results for a typical summer week with high demand (12-15 January) for a few representative scenarios are shown in Fig.s 3.9 and 3.10. The figures show, respectively, generation dispatch results (top row), combined flexible demand of all aggregators (middle row), and a combined battery charging profile of all aggregators (bottom row). Fig. 3.9 shows results for a medium prosumer penetration with, respectively, zero, 2 h and 4 h hours of storage. Fig. 3.10 shows results for different prosumer penetrations (zero, medium, high) with 4 h of storage. Observe that in all six cases peak demand occurs at mid-day due to a high air-conditioning load. After the sunset, however, the demand is still high, so gas generation is needed to cover the gap. In the available generation mix, gas has the highest short-run marginal cost, which increases the electricity price in late afternoon/early evening. The balancing results over the simulated year have revealed that the increased RES penetration in the renewable scenarios requires more energy from gas generation compared to the BAU scenario. This is due to RES intermittency, and the ramp limits of conventional coal-fired generation. An increased penetration of prosumers with higher amounts of storage, however, reduces the usage of gas due to a flatter demand profile.

[4] A typical ratio in the NEM today is 2 h of storage [53], however, in the future, this will likely increase due to the anticipated cost reduction.

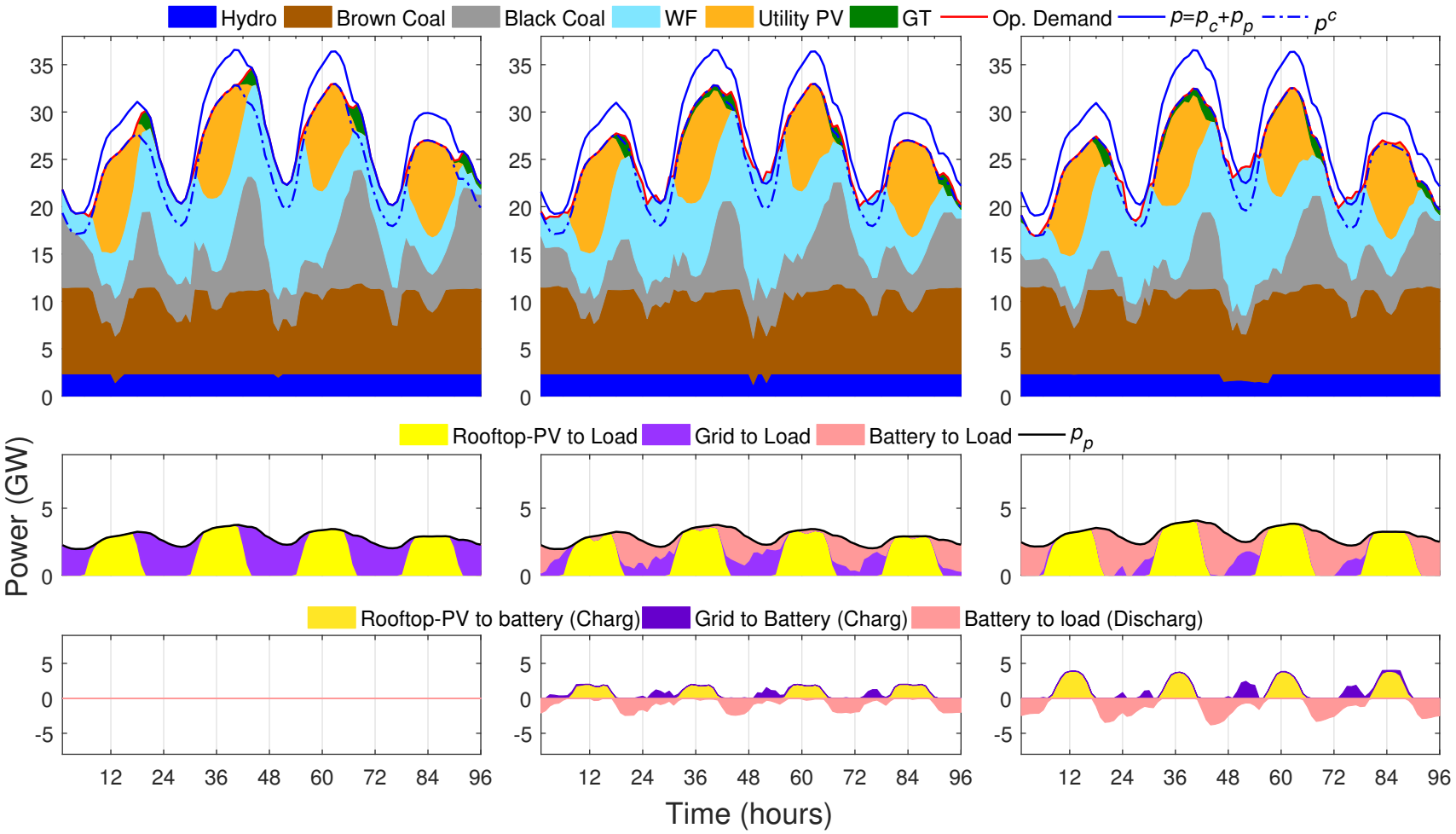

Fig. 3.9 Dispatch results for a typical summer week with high demand (12-15 January) for a medium prosumer penetration with different amounts of storage: zero (left), 2 h (middle) and 4 h (right).

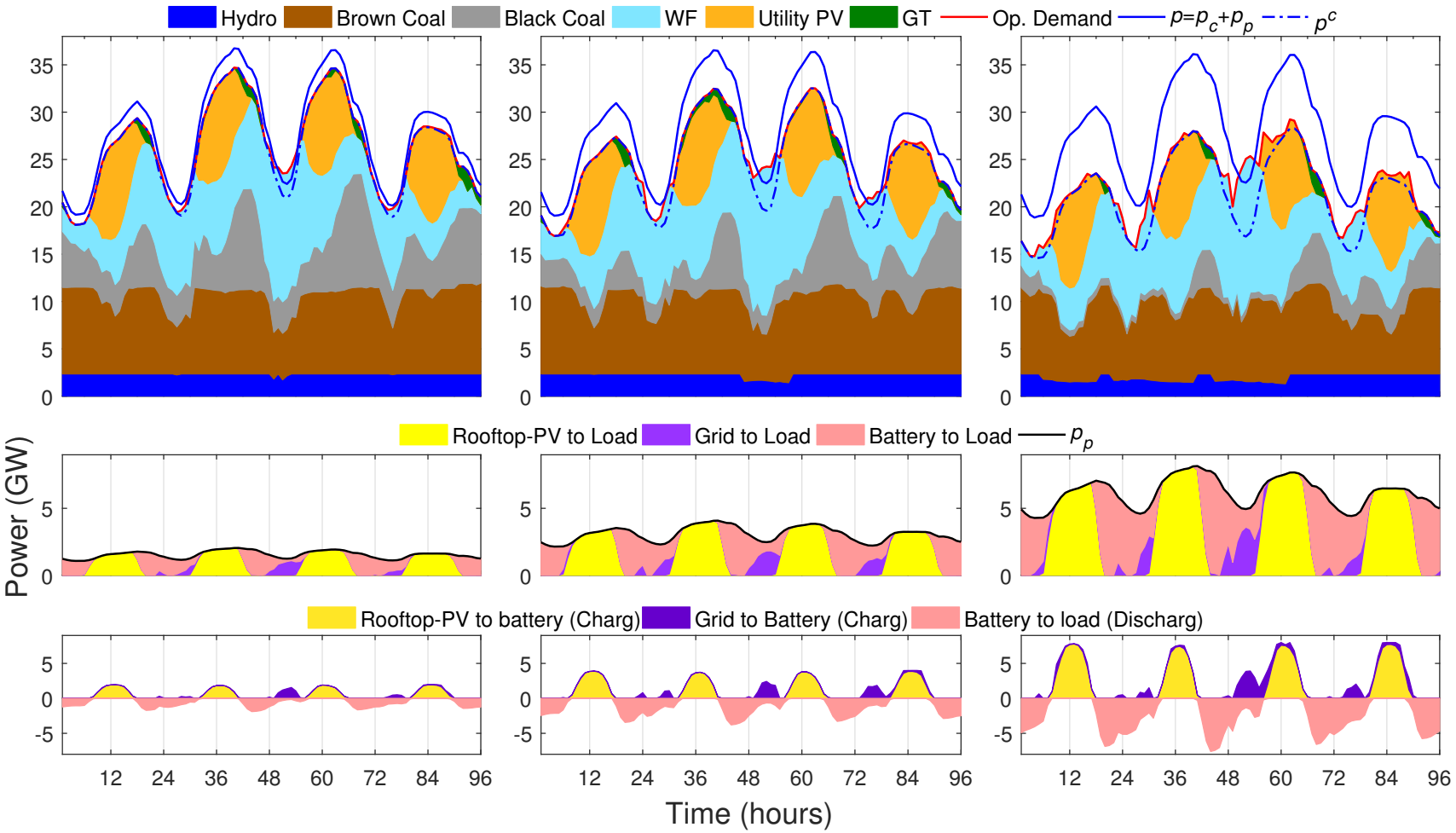

Fig. 3.10 Dispatch results for a typical summer week with high demand (12-15 January) for different penetrations of prosumers with 4 h of storage: zero (left), medium (middle), high (right).

Observe in Fig. 3.9 how an increasing amount of storage increases prosumers' self-sufficiency. Without storage, the load is supplied by PV during the day, and the rest is supplied from the grid. When storage is added to the system, batteries are charged when electricity is cheap (mostly from rooftop-PV during the day and from wind during the night) and discharged in late afternoon to offset the demand when the electricity is most expensive. Note that the plots in the bottom two rows show a combined load profile of all aggregators in the system, which explains why storage is seemingly charged and discharged simultaneously. Observe how high amounts of storage (rightmost columns in Fig.s 3.9 and 3.10) flatten the demand profile. During the day, the flexible demand is supplied by rooftop-PV, which *reduces* the operational demand, while during the night, with sufficient wind generation, batteries are charged, which *increases* the operational demand. This has a significant beneficial effect on loadability and voltage stability, as discussed in the next section.

3.5.3 Loadability and voltage stability results

Dispatch results from the market simulations are used to perform a load flow analysis, which is then used in the assessment of loadability and voltage stability. In the analysis, only scenarios with 4 h of storage were considered. The prosumer scenarios are thus called, according to the respective penetration rates, zero (ZP), low (LP), medium (MP), and high (HP). Note that the market model only considers a simplified DC power flow with the maximum angle limit set to 30°. This can sometimes result in a non-convergent AC power flow in scenarios with a high RES penetration. The number of non-convergent hours is, respectively, 175, 37, 12, and 0, in scenarios ZP, LP, MP, and HP. An increased penetration of prosumers thus improves voltage stability, as explained in more detail later.

In loadability assessment, N-1 security is considered, so a contingency screening is performed first. We screened all credible N-1 contingencies to identify the most severe ones based on the maximum power transfer level [80]. Twenty most critical contingencies were selected for each hour of the simulated year.

Loadability calculation

To calculate system loadability (LDB), power flow is solved twice using the market dispatch results; first for the base case and then for each of the preselected critical contingency. When the load flow does not converge for a particular contingency, the last convergent load flow solution without a contingency is considered the loadability margin. We considered two different load increase patterns, where load and generation are increased uniformly, in proportion to the base case: (i) **NEM**: only load and generation in the NEM are increased; (ii)

Table 3.2 Loadability results

	LDB Cases	Scenarios				
		BAU	ZP	LP	MP	HP
Avg. LDB margin (GW)	NEM	7.8	2.5	4.3	5.9	7.1
	SA/VIC	2.2	0.8	1.1	1.5	1.7

SA/VIC: only load in VIC and generation in SA are increased. The results are summarised in Table 3.2. Comparing the BAU scenario and the renewable scenario with conventional demand (ZP), it can be seen that with the increased RES penetration, the average loadability margin over the simulated year in the demand increase scenario NEM is decreased from 7.8 GW to 2.5 GW. Similarly, the average loadability margin in the demand increase scenario SA/VIC is reduced from 2.2 GW to 0.8 GW. With a high RES penetration, conventional synchronous generation is replaced by inverter-based generation with inferior reactive power support capability[5], which results in a reduced reactive power margin in the system and hence lower stability margin. With an increased penetration of prosumers, the system loadability improves. Observe that the average system loadability margin in both load increase scenarios, NEM and SA/VIC, is increased from 2.5 GW and 0.8 GW for the renewable scenario with no prosumers (ZP) to 7.1 GW and 1.7 GW for high penetration of prosumers (HP), respectively, which indicates a considerable improvement in the system loadability margin. This is explained by a demand reduction when prosumer demand is supplied by rooftop-PV. In the night hours, however, even with high prosumer penetration, the loadibility can be reduced when prosumers charge their batteries, as observed in Fig.s 3.9 and 3.10. The situation is further illustrated in Fig. 3.11 that compares the loadability margin for the load increase scenario NEM and the results of the modal analysis, discussed next.

Modal analysis

Using the market dispatch results, modal analysis of the reduced V-Q sub-matrix of the power flow Jacobian is performed to assess voltage stability. The smallest real part of the V-Q sub-matrix' eigenvalues is used as a relative measure of the proximity to voltage instability. Furthermore, the associated eigenvectors provide information on the critical voltage modes and the weak points in the grid, that is, the areas that are most prone to voltage instability. The results are summarised in Table 3.3. With the increased RES penetration, the average of

[5]For synchronous generation, a 0.8 power factor is assumed. For RES, we used the reactive power capability curve for the generic GE Type IV wind farm model [81], in which the reactive power generation is significantly constrained close to the nominal active power generation.

Table 3.3 Modal analysis results

	Scenarios				
	BAU	ZP	LP	MP	HP
Avg. of minimum Real(eig) (Neper/s)	49.5	42.3	44.8	45.6	48.4
Nodes with highest participation factor in critical voltage modes	506 306 308	506 505 410	506 505 410	505 506 410	505 410 408
Unstable hours	0	175	37	12	0

the minimum of the real part of all eigenvalues, henceforth called the minimum eigenvalue, is reduced from 49.5 Np/s for the BAU scenario to 42.3 Np/s for the ZP scenario. With an increased prosumer penetration, the average of the minimum eigenvalue over the simulated year increases from 42.3 Np/s (ZP) to 48.8 Np/s (HP). Observe in Fig. 3.11 that the results of the modal analysis confirm the results loadability analysis. The general trend remains the same; higher RES penetration with conventional demand reduces the minimum real value of an eigenvalue, which implies a lower voltage stability margin.

Another observation that can be made from the modal analysis concerns the location of the weak points in the system, that is, the buses with the highest participation factor in the critical voltage modes. These clearly change with the increased RES penetration. In the BAU Scenario, the weakest points are typically buses with large loads (e.g. 306 and 308, representing Melbourne). With the increased RES penetration and no prosumers (ZP), however, the weakest part of the system become buses located close to RESs (e.g. 505 and 410, representing, respectively a large wind farm in SA and a large solar PV farm in QLD).

Further, we observed that the voltage stability margin in the system improves significantly when there are more synchronous generators in the grid, due to their superior reactive power support capability compared to RES. The participation factor analysis of the renewable scenarios revealed that SA and QLD are the most voltage constrained regions where the penetration of WFs and utility PVs is higher compared to other regions in the NEM, which can be, to a large extent, mitigated with a sufficiently large penetration of prosumers. This clearly illustrates that RESs and prosumers change power system stability in ways that have not been experienced before, which requires a further in-depth analysis.

3.6 Summary

The emergence of demand side technologies, in particular rooftop-PV, battery storage and energy management systems, is changing the way electricity consumers source and consume

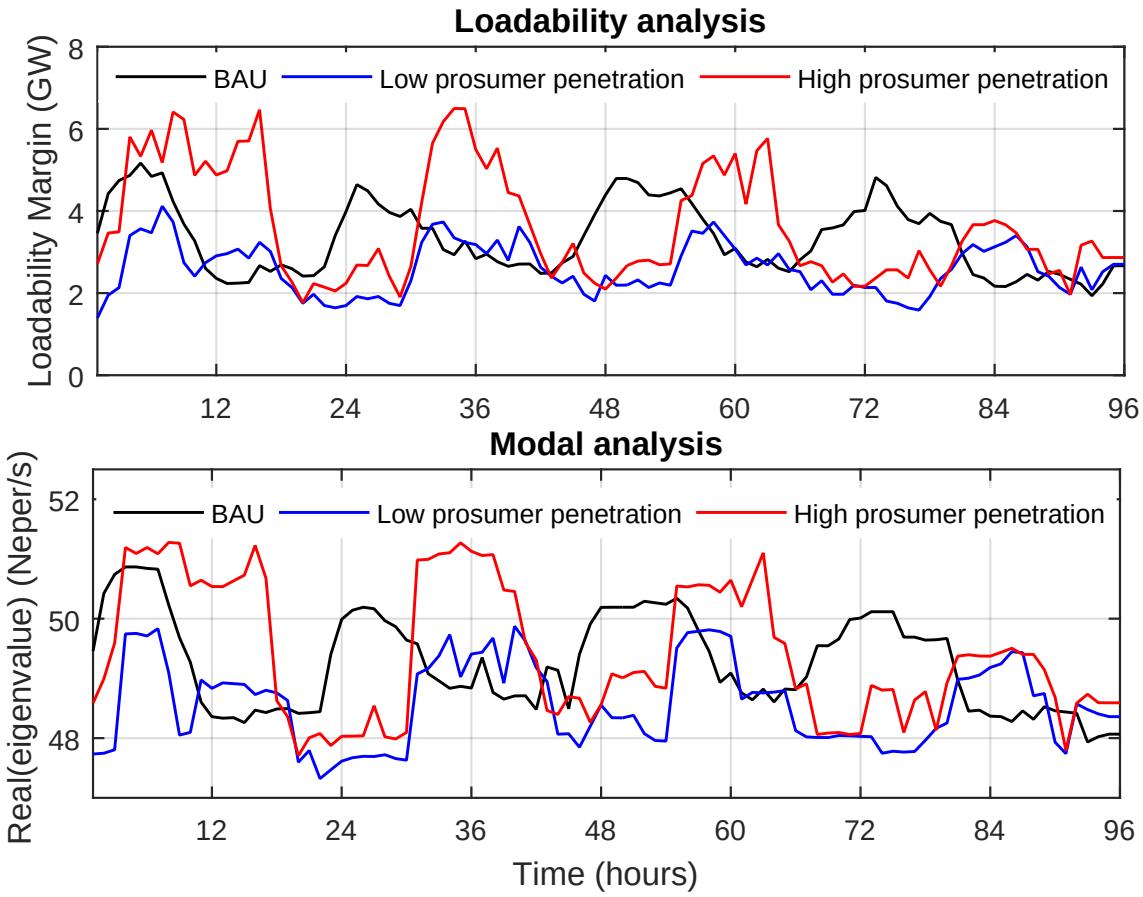

Fig. 3.11 Comparison of the loadability and modal analysis results for a typical summer week with high demand (12-15 January) for the load increase scenario NEM for the BAU, and low and high prosumer penetration.

electric power, which requires new demand models for the long-term analysis of future grids. In this chapter, a network model is incorporated into a generic demand model proposed in Chapter 2, capturing the aggregate effect of a large number of prosumers on the load profile. The model uses a bi-level optimisation framework, in which the upper level employs a unit commitment problem to minimise generation cost, and the lower-level problem maximises collective prosumers' self-consumption. To that effect, the model implicitly assumes an efficient mechanism for demand response aggregation, for example peer-to-peer energy trading or any other form of transactive energy. However, energy exchange between different aggregators is not advisable in the absence of transmission pricing and in the presence of protection devices that considers reverse power flow as sign of fault.

The impact of prosumers on the performance, loadability and voltage stability of the Australian NEM with a high RES penetration show that an increased prosumer penetration flattens the demand profile, which increases loadability and voltage stability, except in

situations with a low underlying demand and an excess of RES generation, where the aggregate demand might increase due to battery charging. The analysis also revealed that with a high RES penetration, the weakest points in the network move from large load centres to areas with high RES penetration. Also, loadability and voltage stability are highly dependent on the amount of synchronous generation due to their superior reactive power capability compared to RES, which requires further analysis. On other hand, prosumers do improve the stability in the wake of high RES scenario, which highlights the potential of prosumers as flexibility providers for RES integration in future grids.

Chapter 4

Evaluation of Concentrated Solar-Thermal for Power System Flexibility

While Chapter 3 explains the potential of prosumers in providing flexibility to enable higher RES penetration, this chapter explores the role of CST for providing flexibility in FGs by limiting the ramping stress of conventional generators. In particular, this chapter proposes a joint dispatch of CST and utility-scale PV through a REA to restrict the rate of change of power export to the slope of residual demand[1]. This single factor is used to force the RES aggregation to operate in a manner that does not impose additional ramping stresses on other generators in the system. In addition, thermal reserves are maintained for CST to overcome solar variation, while PV variability is secured through CST spinning reserves. In other words, this aggregation tries to shape CST power dispatch so that when it is combined with power from PV it does not create any additional net ramp stress on other generators in the system.

To model participation of RES in the electricity market, a bi-level optimisation framework is developed. As discussed earlier in the context of prosumer aggregation, bi-level optimisation is a particular class of optimisation where one problem is nested within the other. Interaction of REA with the electricity market can be considered in this context. On the upper-level (leader problem), dispatch decisions are made by the ISO to minimise overall electricity cost using standard dispatch procedure, while on the lower level (follower problem), the REA tries to maximise profit in response to the ISO's decision.

[1] In this study, due to low penetration level of WG and rooftop-PV are modelled as negative demand. So residual demand is the load profile formed after taken into account effects of WG and rooftop-PV.

The proposed model is then demonstrated on the NEM using listed weather and load data from the AEMO [72]. In more detail, first a base case is analysed where a combination of coal, gas, WG, PV and hydro power plants are considered to meet the NEM demand requirement in 2020. Second, the effect of grid integration of utility PV without CST on the NEM is studied. Third, we explore the role of CST in providing flexibility to the network in the presence of utility-scale PV using the proposed REA. Although the analysis here is limited to PV, WG can also be used in the same context.

4.1 Background and Literature Regarding CST Modelling

Flexibility in FGs is the key to RES integration. Many RES, such as WG and PV, are constrained by the availability of their primary energy source. Thus, they lack the flexibility to follow demand. Nonetheless, existing FG studies shows that achieving a 100 % renewable scenario is possible with the flexibility provided by backup generation and storage [33, 34]. Chapter 3 established that the mentioned flexibility can be provided by demand side (i.e prosumers); this chapter aims to explores the potential of providing flexibility from the generation side. In particular, this chapter proposes aggregation of dispatchable RES (such as CST) with non-dispatchable RES to mitigate the additional ramp stress on CGs.

In contrast to WG and PV, CST is a RES with an integrated thermal energy storage (TES) system that provides flexibility in its operation, which overcomes the intermittent nature of its primary energy source. In regions with excellent solar resources, e.g. Australia, California and Chile, it may provide the cornerstone of future electric energy supply systems [33, 82]. The use of CST in future grids is not only advantageous from the power balancing point of view, but it can also provide the spinning reserves and inertia required for power system security.

Power systems with higher penetration level of PV have already observed a characteristic "duck" or "Nessie" curve effect [83], in which ramping stress on conventional generators has increased tremendously. Thus, finding a suitable economical solution to these problems is becoming increasingly urgent. Among feasible solutions, DR and utility storage are the most promising candidates to achieve required flexibility [40, 84, 85]. However, these solutions are not without their own challenges. DR programmes require users to change their consumption behaviour, which may cause discomfort for users, whereas utility storage chemical storage is still not economically feasible. Although pumped hydro can provide an economical utility storage solution, it is limited by the geographical features of the region.

Despite the prevalence of works modelling CST, its operational role in electricity markets has not been widely discussed [86]. In particular, most studies treat CST as a non-strategic

Table 4.1 Installed TES Capacity deployed in some CSTs.

Name or Location	Country	Storage (hours)
Gemasolar	Spain	15
Crescent Dunes	USA	10
Termosol	Spain	9
Archimede	Italy	8
Aste	Spain	8
Andasol, Extresol, Manchasol, Valle, Alvarado, Sesmero	Spain	7.5
Solana	USA	6

unit [33, 87] in which CST dispatch is moved to peak evening hours. Other studies try to optimise the operation of CST against pricing signals from a electricity market, assuming CST itself has no effect on market clearing prices [86, 88–90]. These studies seek to maximise the profit of CST by controlling the dispatch level, using an electricity price forecast. In [86], the costs of CST for different operating modes along with a backup boiler are considered to maximise profit. In contrast, [88] incorporates electricity buy-back from the grid to utilise thermal storage to maximise the revenue. A robust stochastic optimisation approach is used to build offer curves in [90]. Although these studies provide a solid foundation for integrating CST into electricity markets, they all treat CST as a price-taker, which is acceptable for lower penetration levels. However in a future with higher penetrations levels, CST should be treated as a price anticipator, to reflect its capability to impact the market clearing price. Thus, a modelling framework is proposed in this chapter to capture the impact of CST on the electricity market.

TES and backup boilers enable CST to shift its output and provide operational flexibility. Moreover, this flexibility can be shared with other intermittent RES. Many reports suggest that high RES penetration is possible with large-scale storage [34, 91]. A novel approach is used in [85] where WG hedges unfavourable wind realisations using third party storage. Also, in [8] joint optimisation of WG and pumped storage is proposed to alleviate the risk of paneltaties when bidding in the day ahead market. Along parallel lines, the TES of CST can be used to circumvent other undesirable RES dispatch scenarios.

Given the potential uses of CST above, numerous recent studies concluded that TES potentially increases the value of CST [86, 88, 89]. TES enables CST to have a larger solar field (SF) and shift its energy to peak hours. In [89] a comparison of the size of the power block (PB), TES and SF is discussed and concluded that 6-hour storage will provide maximum profit. In [34], 15-hour storage is used to analyse a 100 % RES scenario and Zero Carbon Australia proposed storage of 17 hours [33]. Table 4.1 reflects installed TES capacity of some currently operating CSTs [33].

Electricity markets have also started to recognise that traditional reserves will not be able to provide enough flexibility in response to RES fluctuations [92, 93]. For instance, California ISO has identified a need for an additional ramp up and down reserves as wind penetration increases [94]. In another related study, an enhanced reliability evaluation is presented in [95]. This study put emphasis on the development of a *flexiramp* market by introducing flexible ramping constraints in the optimisation model of California ISO. In the same direction, [94] provides an initial evaluation of a flexiramp market design against stochastic optimisation ideal. Thus, the role of CST in providing grid flexibility in future markets is very interesting and worthwhile to study. To the best of our knowledge, CST for providing flexibility is yet to be studied.

4.2 Conceptual Framework

The general conceptual framework adopted for this chapter is described in this section. Given that increasing RES penetration will likely require different market structures, we have adopted a generic modelling framework, previously used in major national FG studies in Ireland [39], the US [96] and continental Europe [38]. The model is based on a unit commitment problem aiming to minimise system cost, and is intended specifically for modelling the role of REA in FG scenario studies. However, the model does not presume any particular market structure. As such, it is not suitable for modelling REA's participation in existing electricity markets, but rather its aim is to capture the behaviour of REAs in future electricity markets, provided an appropriate market structure is adopted. Nevertheless, our objective is to derive insight into the benefit of storage, that will be helpful in forming the basis of future high penetration RES markets. With the emergence of flexibility markets, electricity networks can support high penetration levels of RES. As noted earlier, such markets for flexibility are already being proposed to limit ramp rates introduced by RES [94, 95].

The REA accounts for of all the technical requirements and operational limitation of RES. On one side, it handles ramp rate limitation and power contribution requirements imposed by the ISO, while trying to maximise the profit for participant RES. The RES are assumed to have bilateral agreements to maintain reserves and providing flexibility to one another. Furthermore, this aggregation is constrained such that power export to the electricity grid does not increase net ramping stress on other available generators. This strategy aims to avoid additional ramp effects appearing in the power system due to the intermittent nature of the RES. In the absence of flexible RES, the REA will resort to spilling excessive amount of power from inflexible RES, an arrangement that is likely to be inefficient. In this work, thermal storage of CST is utilised to provide operational flexibility. However,

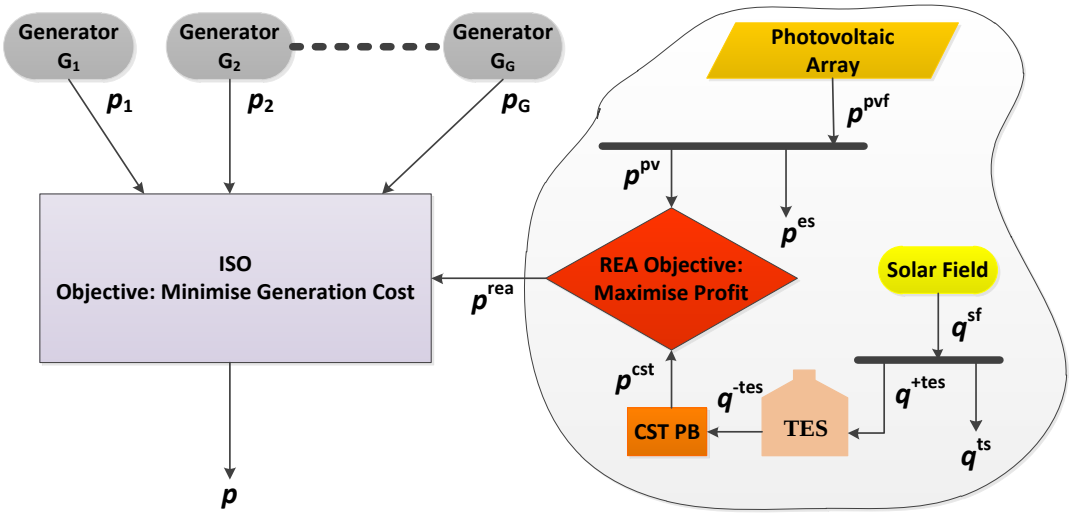

Fig. 4.1 Conceptual framework of this work. ISO minimises electricity generation cost and REA maximises profit.

this modification requires modelling the problem as a bi-level optimisation problem. The model used in this paper is illustrated in Fig. 4.1.

Bi-level optimisation problems are usually known as Stackelberg games [97]. The objective of the leader, ISO, is to minimise the cost of energy, subject to the power balancing and operational requirements of generators. At the lower level, REA (follower) maximises its profit, subject to RES constraints and market regulations. RES usually have zero SRMC hence they will always be prioritised for dispatch. However, their limited energy resources makes dispatch decisions a challenging task.

4.3 Mathematical Model of REA

The mathematical model adopted is a two-level optimisation problem cast in the framework of MPEC. As in standard UC problems, generators and the REA submit bids to the ISO, which computes a clearing price and returns dispatch instructions. Conventional generators' bids are a piece-wise linear supply functions, subject to operational constraints; without an REA, this is a standard UC problem [98]. However, the REA's bidding is complicated by its dispatch energy limts each day, so to maximise its profit, the REA has to supply energy strategically. Accordingly, the REA's optimal bid calculation problem is nested within the ISO's UC problem. We approach difficulty by reformulating the two-level problem as a single-level MILP. Specifically, the REA's operational constraints are included as KKT

conditions in the ISO's UC problem along with additional slack variables [97], with the resulting problem solved efficiently by standard MILP solvers.

4.3.1 Leader objective function

The ISO's objective is to schedule the generator fleet such that the overall cost is reduced keeping an account of various generation cost:

$$\underset{\Omega}{\text{minimise}} \quad \sum_{t\in\mathcal{T}} \left\{ \sum_{g\in\mathcal{G}} \left(c_g^{\text{fix}} s_{g,t} + c_g^{\text{su}} u_{g,t} + c_g^{\text{sd}} d_{g,t} + c_g^{\text{var}} p_{g,t} \right) + \lambda^{\text{rea}} p_t^{\text{rea}} \right\}, \tag{4.1}$$

$$\{p_{g,t}, p_t^{\text{rea}}\} \in \mathbb{R}^+,$$
$$\{s_{g,t}, u_{g,t}, d_{g,t}\} \in \{0,1\}.$$

where $\Omega = \{s_{g,t}, u_{g,t}, d_{g,t}, p_{g,t}, p_t^{\text{rea}}\}$ are the decision variables of the problem, and c_g^{fix}, c_g^{su}, c_g^{sd}, c_g^{var} and λ^{rea} are fixed, startup, shutdown and variable cost of generator g and REA bid, respectively.

4.3.2 Leader constraints

The decision taken by the leader must be within the feasible region defined by constraints (4.2) to (4.9)[2]:

$$\sum_{g\in\mathcal{G}} p_{g,h} + p_t^{\text{rea}} = p_t, \tag{4.2}$$

$$\sum_{g\in\mathcal{G}^{\text{syn}}} \overline{p}_g s_{g,t} - p_{g,t} \geq p_t^{\text{r}}, \tag{4.3}$$

$$\underline{p}_g s_{g,t} \leq p_{g,t} \leq \overline{p}_g s_{g,t}, \tag{4.4}$$

$$u_{g,t} - d_{g,t} = s_{g,t} - s_{g,t-1}, \tag{4.5}$$

$$u_{g,t} + \sum_{\tilde{t}=0}^{\tau_g^{\text{u}}-1} d_{g,t+\tilde{t}} \leq 1, \tag{4.6}$$

$$d_{g,t} + \sum_{\tilde{t}=0}^{\tau_g^{\text{d}}-1} u_{g,t+\tilde{t}} \leq 1, \tag{4.7}$$

[2] All the constraints must be satisfied in all time slots t, however, for sake of notational brevity, this is not explicitly mentioned.

$$-r_g^- \leq p_{g,t} - p_{g,t-1} \leq r_g^+. \tag{4.8}$$

$$\underset{p^{\text{cst}},p^{\text{pv}}}{\arg\min}\{\sum_{t\in\mathcal{T}} \lambda_t^* p_t^{\text{rea}} \text{ s.t. equation } (4.11)-(4.24)\}, \tag{4.9}$$

In the above set of expressions, p_t, p_t^{rea} and p_t^{r} represent nett load demand, power dispatch from REA and the spinning reserve requirements for time slot t. Whereas, r_g^+, r_g^- ,τ_g^{u} and τ_g^{d} represent corresponding ramp-up, ramp-down rates MUT and MDT of generator g. Constraints (4.2) forces the power required by the load to be fulfilled. Constraint (4.3) ensures spinning reserves[3] for system stability are provided. Constraint (4.4) bounds the dispatch level of a generating unit between its respective minimum and maximum stable limits. These restrictions on thermal units are linked to their fuel burning process limitations. Constraint (4.5) links the status of a generator unit to up and down binary decision variables. Constraints (4.6) and (4.7) ensure MUT (τ^u) and MDT (τ^d) associated with power generation units are observed. Constraint (4.8) restricts intertemporal power change of a generator to within its corresponding maximum ramp-down and ramp-up rates. Constraint (4.9) takes into account REA optimisation as explained in Section 4.3.3.

4.3.3 Follower objective function

On the lower level, the REA (follower) maximises its profit by maximising its output to the grid. Because of the higher penetration levels of CST and PV, the REA will act as a price anticipator. Also it will try to export more power during high price hours to maximise profit and can potentially lower the market clearing price. The REA cost function is given by:

$$\underset{\Omega}{\text{maximise}} \quad \sum_{t\in\mathcal{T}} \lambda_t^* p_t^{\text{rea}}, \tag{4.10}$$

where $\Omega = \{p_t^{\text{rea}}, p_t^{\text{cst}}, p_t^{\text{pv}}, q_t^{\text{tes+}}, p_t^{\text{es}}, q_t^{\text{ts}}, s_t^{\text{cst}}, u_t^{\text{cst}}, d_t^{\text{cst}}\}$ are the decision variables and λ_t^* is market clearing price set by the most expensive dispatched unit. Furthermore,

$$\{p_t^{\text{rea}}, p_t^{\text{cst}}, p_t^{\text{pv}}, q_t^{\text{tes+}}, p_t^{\text{es}}, q_t^{\text{ts}}, q_t^{\text{tes+}}, q_t^{\text{tes-}}, e_t^{\text{tes}}\} \in \mathbb{R}^+,$$
$$s_t^{\text{cst}}, u_t^{\text{cst}}, d_t^{\text{cst}} \in [0,1].$$

[3]Usually 10 % reserves are maintained to overcome small unseen load deviations.

4.3.4 Follower constraints

The REA have to fulfil following constraints:

$$l^{-}\Delta p_t^{'} \leq \Delta p_t^{\text{rea}} \leq l^{+}\Delta p_t^{'}, \tag{4.11}$$

$$p_t^{\text{rea}} = p_t^{\text{cst}} + p_t^{\text{pv}}, \tag{4.12}$$

$$p_t^{\text{pvf}} = p_t^{\text{pv}} + p_t^{\text{es}}, \tag{4.13}$$

$$\eta^{\text{sf}} q_t^{\text{sf}} = q_t^{\text{tes+}} + q_t^{\text{ts}}, \tag{4.14}$$

$$p_t^{\text{cst}} = \eta^{\text{cst}} q_t^{\text{tes-}}, \tag{4.15}$$

$$\alpha p_t^{\text{pv}} \leq s_t^{\text{cst}} \overline{p}_t^{\text{cst}} - p_t^{\text{cst}}, \tag{4.16}$$

$$p_t^{\text{cst}} \leq \eta^{\text{tes}} e_{t-1}^{\text{tes}} \tag{4.17}$$

$$s_t^{\text{cst}} \underline{p}_t^{\text{cst}} \leq p_t^{\text{cst}} \leq s_t^{\text{cst}} \overline{p}_t^{\text{cst}}, \tag{4.18}$$

$$u_t^{\text{cst}} - d_t^{\text{cst}} = \Delta s_t^{\text{cst}}, \tag{4.19}$$

$$-r^{-} \leq \Delta p_t^{\text{cst}} \leq r^{+}, \tag{4.20}$$

$$u_t^{\text{cst}} - \sum_{\tilde{t}=0}^{\tau^{\text{u}}-1} d_{t+\tilde{t}}^{\text{cst}} \leq 1, \tag{4.21}$$

$$d_t^{\text{cst}} - \sum_{\tilde{t}=0}^{\tau^{\text{d}}-1} u_{t+\tilde{t}}^{\text{cst}} \leq 1, \tag{4.22}$$

$$e_t^{\text{tes}} = \eta^{\text{tes}} e_{t-1}^{\text{tes}} + q_t^{\text{tes+}} - q_t^{\text{tes-}}, \tag{4.23}$$

$$\underline{e}^{\text{tes}} \leq e_t^{\text{tes}} \leq \overline{e}^{\text{tes}}, \tag{4.24}$$

where: l^{-} and l^{+} are binary inputs to indicate the intertemporal decrease or increase in power demand; $\Delta p_t{}'$ represents a change in net residual power demand between two hours; p_t^{pvf} represents total electrical power output of PV field for a particular hour h; q_t^{sf} represents thermal power output of SF; η^{sf} represents SF sunlight capturing efficiency; η^{cst} represents CST power conversion efficiency, α represents percentage spinning reserves to be maintained by CST for PV, and; η^{tes} represents TES thermal contents holding efficiency. The Follower constraints are explained below.

REA dispatch rule

To limit the ramp stress imposed by RES, constraint (4.11) is introduced. This constraint forces changes in the dispatch level of REA to follow the residual demand profile; that is, they must be less than the rate of change of residual demand. This ensures that ramp stress on other generators is not increased by the RES participation in the system. However, it will be challenging for the REA to abide by this dispatch condition. To remain within operational limits, the REA might have to spill some energy. This principle controls the variation in the REA dispatch and makes them align with the changes in demand. That means the REA can increase its dispatch level if and only if demand is increasing and vice versa. If demand remains constant, the REA have to maintain constant dispatch level. In doing this, the power profile of the REA is shaped to fit within demand profile thus reducing system wide ramps.

REA energy balancing equations

Constraints (4.12) to (4.15) ensure that both thermal and electrical energy balanced out. Constraint (4.12) ensures that electrical power dispatched is the sum of the power from CST and PV. Constraint (4.13) balances power from PV field by declaring it as the sum of electric power spilled and dispatched from PV. Constraint (4.14) ensures that energy from the SF is the sum of thermal energy spilled and transferred to TES. Constraint (4.15) make sure that the CST converts thermal power by utilising energy from TES.

Reserve constraints

Constraints (4.16) and (4.17) force the REA to maintain enough spinning and thermal reserves to overcome the stochastic nature of the primary energy sources of these generators. In this set-up, PV is able to dispatch its power while backed by the spinning reserves provided by CST. This provides enough flexibility to ensure the REA bid is met despite solar variation on the PV field. The second reserve constraint allows CST power dispatch to be independent of SF output of current hour. These reserves provide time to overcome solar insolation variation.

CST power block constraints

CST is subject to the same operational constraints as any other thermal generation unit, including minimum and maximum stable power dispatch levels, ramp rates, and τ^u and τ^d restrictions, as defined by constraints (4.18) to (4.22).

TES constraints

Constraint (4.23) accounts for the storage loss in TES, while constraint (4.24) ensure that the energy stored in TES should not exceed operational capacity.

The model above is not directly computationally realisable due to the nested optimisation constraint of the REA. However, nested optimisation can be replaced by KKT conditions and complementary slackness variables. The KKT are necessary and sufficient conditions for optimality provided that lower level problem is convex. In our problem this is the case, we can recast the model above as a large MILP [64].

4.4 Case Study

In this section, the simulation set-up and discussion of results are presented. Assumptions and different parameters used in the simulation are described next, followed by a discussion of results from different scenarios.

4.4.1 Simulation set-up

The simulations use the NEM 14-generator model as a starting point and incorporate a market model, primarily developed for small signal stability studies [69]. Generation data from this model are modified to meet demand for 2020. Hydro, black coal, brown coal, OCGT and CCGT are considered as CGs. Further, it is assumed that the generators bid at their respective variable O&M cost and predicted regional fuel prices for 2020, as derived from [70] and [71]. SRMC of RES is assumed to be always less than CG, therefore it will always be prioritised for demand. Hourly demand and RES generation traces are taken from the AEMO published National Transmission Network Developed Plan (NTNDP) 2013. The resulting market model is a MILP that can be solved using an off-the-shelf solver. The system model is developed in MATLAB and then CPLEX is used to solve the optimisation problem.

For the BAU scenario, a generation mix of 5.32 % hydro, 67.18 % coal, 13.17 % gas, and 5.56 % wind is adopted. In addition to this, 3850 MW of rooftop-PV is also considered in all scenarios. Further, minimum stable limits of 50 % and 40 % are imposed on coal generators and CCGT, respectively. Ramp rates of coal-fired generators are set between 50 % to 60 % of rating capacity per hour, while CCGT have much higher ramping rates ranging between 70 % to 80 %. The Minimum stable limit and ramp rate per hour for CST are taken as 40 % and 60 %, respectively.

Simulation is completed for one year (2020), using a rolling horizon approach to find dispatch decisions. Hourly resolution data from different sources is used for a two-day

Table 4.2 Generation mix for cases I to V.

	Hydro (GW)	Coal (GW)	Gas (GW)	Wind (GW)	PV (GW)	REA	
						Utility-PV (GW)	CST (GW h)
Case I	2.34	29.50	5.78	2.44	3.85	-	-
Case II	2.34	29.50	5.78	2.44	13.85	-	-
Case III	2.34	29.50	5.78	2.44	3.85	10	-
Case IV	2.34	29.50	5.78	2.44	3.85	-	10
Case V	2.34	29.50	5.78	2.44	3.85	4	6

planning horizon with perfect foresight. Any variation in the solar isolation is covered by the thermal and spinning reserves maintained by CST.

4.4.2 Cases

First, in **Case I** (BAU scenario), the load demand is met only by CG, WG and rooftop-PV. For **Case II**, 10 GW of PV offers its energy without ramp concerns into the electricity market. This scenario adds significant operational uncertainty into the system, as no additional reserves for the operation of PV are considered.

In Cases III, IV and V, the proposed the REA framework comprising combinations of PV and CST is used to investigate the effect on system power balancing. In all of the Cases III-V, 10 GW of RES is introduced. The REA framework first considers 10 GW of PV for maximising revenue, named as **Case III**. This scenario does not reflect the purpose of this paper. However, it provides a useful insight towards the operation of the REA. This demonstrates that even without flexibility, the REA is able to export some energy at the expense of additional uncertainty included in the system. Also, in this the REA spills a lot of energy due to the lack of flexibility.

Next for **Case IV**, the role of the REA is explored with 10 GW of CST with 6 h of thermal storage. This scenario analyses the role of the REA in presence of only flexible RESs.

Finally in **Case V**, the complete set-up is analysed by introducing both 4 GW of PV and 6 GW of CST, aggregated by a REA. This case adequately reflects the dynamics of proposed model by scheduling PV in the envelope of energy dispatched by CST. This scenario also utilises spinning reserves from CST to mitigate any variability introduced by PV. It is worth mentioning that the level of PV should be less than the CST to provide adequate reserves. A brief summary of different cases is described in Table 4.2.

Table 4.3 Comparison of Results from different cases.

Case	I	II	III	IV	V
Energy from CG (%)	91.37	79.08	90.26	81.46	81.44
Energy from RES (%)	8.63	20.92	8.63	8.63	8.63
Energy from REA (%)	NA	NA	1.11	9.91	9.94
Elect. energy spilled (%)	NA	0	89.40	NA	2.31
Therm. energy spilled(%)	NA	NA	NA	0	0
Maximum power dispatched by CG (GW)	33.41	33.41	33.41	27.82	28.57
Max. ramping stress induced on CG ($GW\,h^{-1}$)	6.26	8.87	6.26	5.66	5.86
net ramp rate variation of CG w.r.t BAU (%)	0	61.99	−9.48	−50.69	−35.25

4.4.3 Discussion

The following benchmarks are selected to summarise the results from different cases:

- the energy contribution of CG, RES and REA;
- the electrical and thermal energy spilled in order to abide by the system constraints;
- the maximum power dispatched by the CG;
- the maximum ramp stress the CGs undergo;
- the net ramping stress born by CGs.

Table 4.3 lists values of these benchmarks for five cases. In this, the energy contribution of RES represents the aggregated energy from WG, rooftop-PV and any other RES not included under REA (i.e. not including CST).

In the Case I (BAU scenario), all the demand of 2020 is met by the generation mix described in Section 4.4.1. Fig. 4.2 shows a typical generation mix for summer (left) and winter (right) seasons. Most of the load is met with hydro and coal-based generators. The contribution of gas turbines is relatively small and mostly during peak demand hours or during intervals with high ramp requirements. Given the generation mix energy contribution from WG and rooftop-PV is 8.6 % except for Case II. In this case the RES contribution reached a maximum of 20.9 % with 12.3 % energy contribution from 10 GW additional utility PV fields.

If a penetration of PV is introduced directly into electricity network, it will not only compromise the stability of the system but also exert more ramp stress on existing thermal plants. This effect is more prominent during the winter when demand peaks are shifted to morning and evening hours rather than mid-day, as shown in Fig. 4.3. When 10 GW PV is

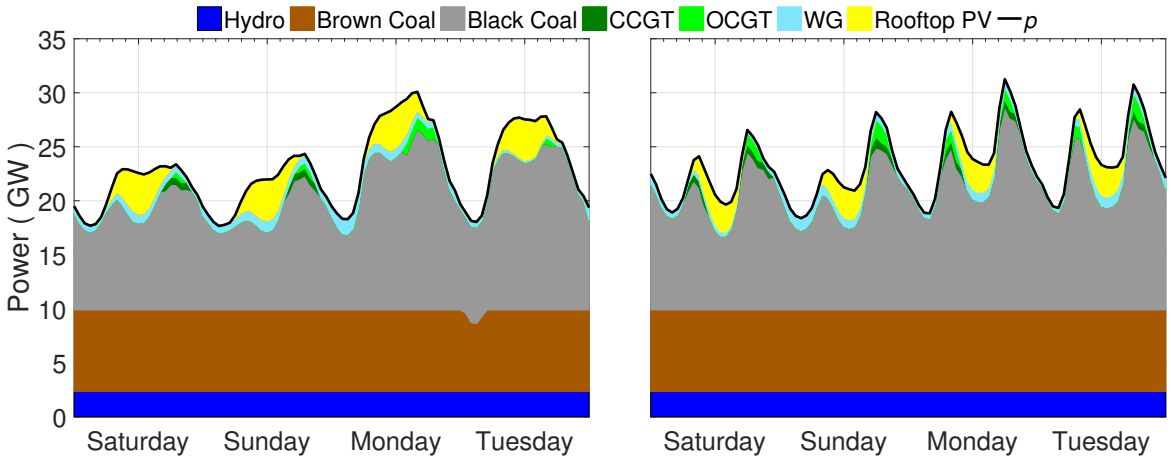

Fig. 4.2 Generation mix for Case I (BAU scenario) for typical summer (left) and winter (right) load. Vertical lines mark noon for each day.

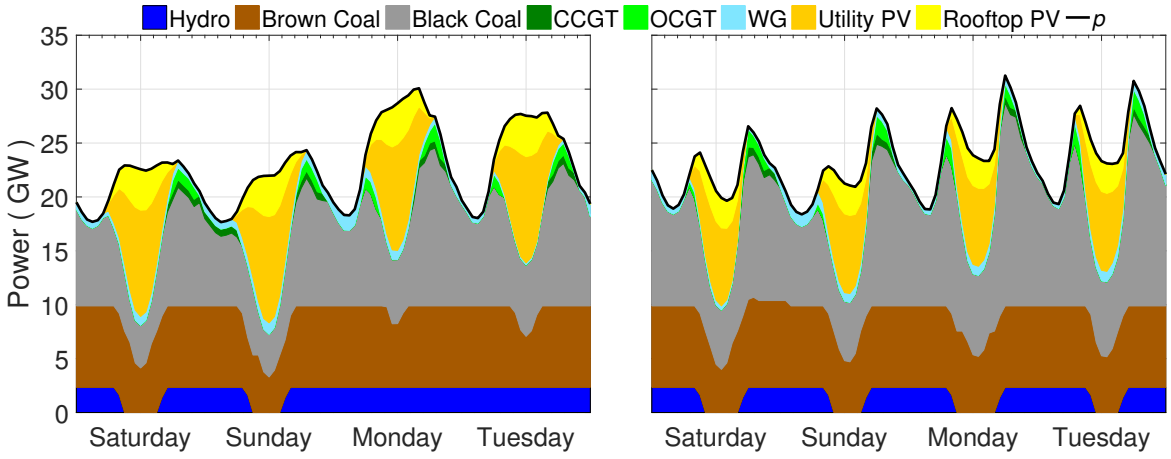

Fig. 4.3 Generation mix in the presence of 10 GW of Utility PV (Case II) for summer (left) and winter (right). Vertical lines mark noon for each day.

introduced (Case II), it increases the ramp rates of CG by 61.99 % over the BAU. These ramp rates can have highly detrimental effects on the system's reliability and security. In contrast to PV, TES provides operational flexibility and enables CST to generate more revenue without imposing large ramp rates on the system.

Next we take into account the REA. The REA handles the flexible operation of all RES attached to it. The backbone of the REA is a dispatch rule that does not allow its associated RES to undertake actions that increase the ramp stress on the system. Hence for Case III when 10 GW of PV is integrated through the REA without any other flexible RES, ramp stress on CG decreases by 9.5 %. However to fulfil the dispatch rule requirements it ends up spilling 89.4 % energy from the field, as illustrated in Fig. 4.4. These spill levels indicate

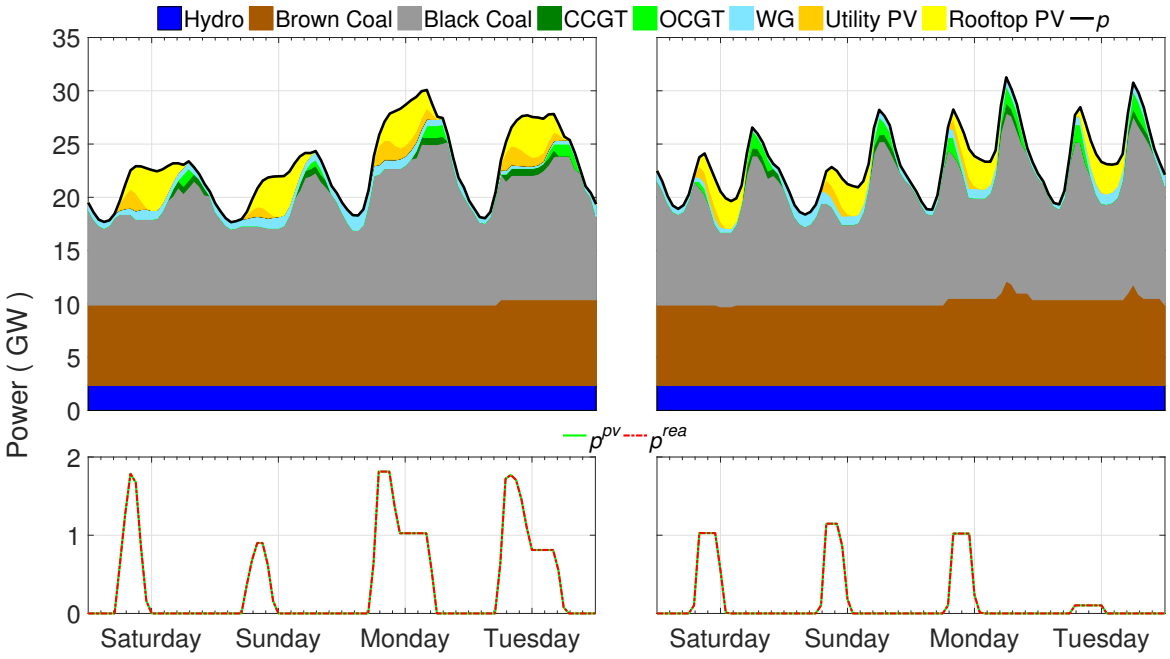

Fig. 4.4 Dispatch decisions if 10 GW of Utility PV (Case III) is subjected to the REA for summer (left) and winter (right) demand profile. Vertical lines mark noon for each day.

that PV is an inflexible RES. Also, no backup reserves are maintained for PV, thereby adding operational uncertainties to the system. This is not an efficient solution, and is only analysed to show the operation of the REA without flexible dispatch.

In contrast, in Case IV when 10 GW of CST is introduced in the system, ramp stress on CG is reduced by 50.7 %. Additionally, no energy is spilled, and TES enables CST to shift most of the REA energy towards peak load hours, as indicated in Fig. 4.5.

Fig. 4.6 presents dispatch for Case V, when 4 GW of PV aggregated with 6 GW of CST to form the REA. In this situation, the REA maximises the profit for both PV and CST by utilising the flexibility available from CST. CST provides spinning reserves to overcome PV variabilities. It would be fair to provide some incentive for those reserves using bilateral agreements, as the real value of PV comes from the flexibility provided by CST, which significantly reduces spill levels and hence generate more revenues. An interesting observation is that the energy contribution from the REA in Case V is greater than Case IV. This is due to the thermal efficiency of the TES; to shift more energy, the losses in the TES increase, causing slightly less energy contribution in total.

Results show that the complementary arrangement between flexible and inflexible RES can yield benefits for all the market participants. The REA approach acts as stepping stone towards the establishment of market structures supporting high penetrations of RES. Specifically in this study we only consider demand profile to define REA dispatch rule.

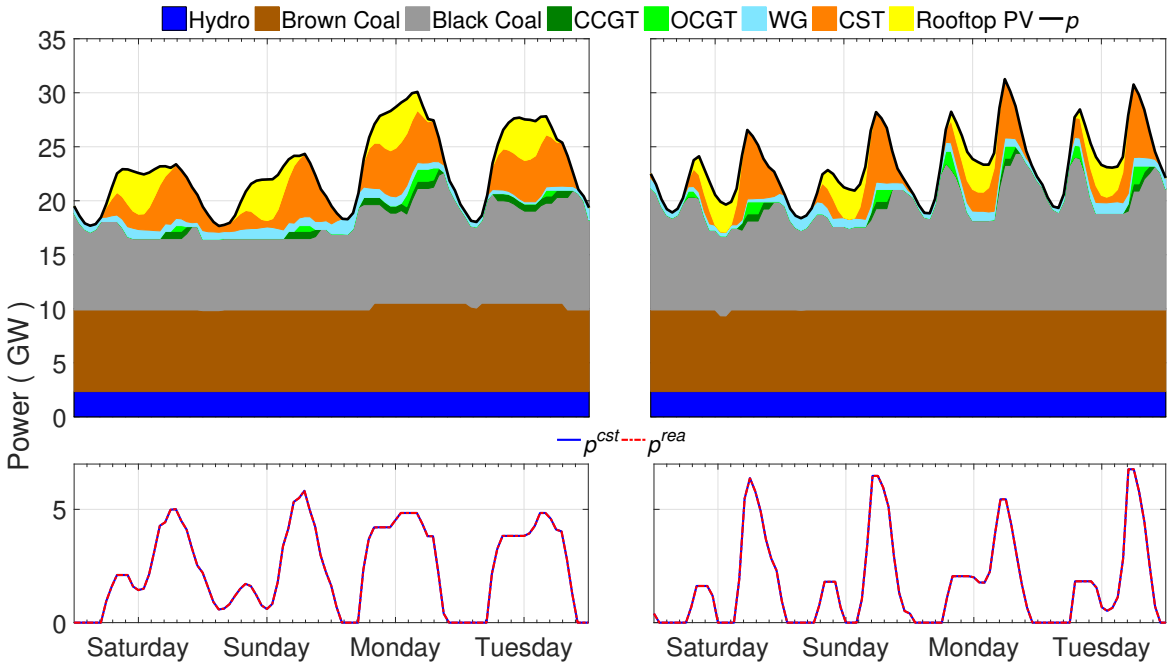

Fig. 4.5 Result when 10 GW of CST is subjected to the REA (Case IV) for typical summer (left) and winter (right) load profile. Vertical lines mark noon for each day.

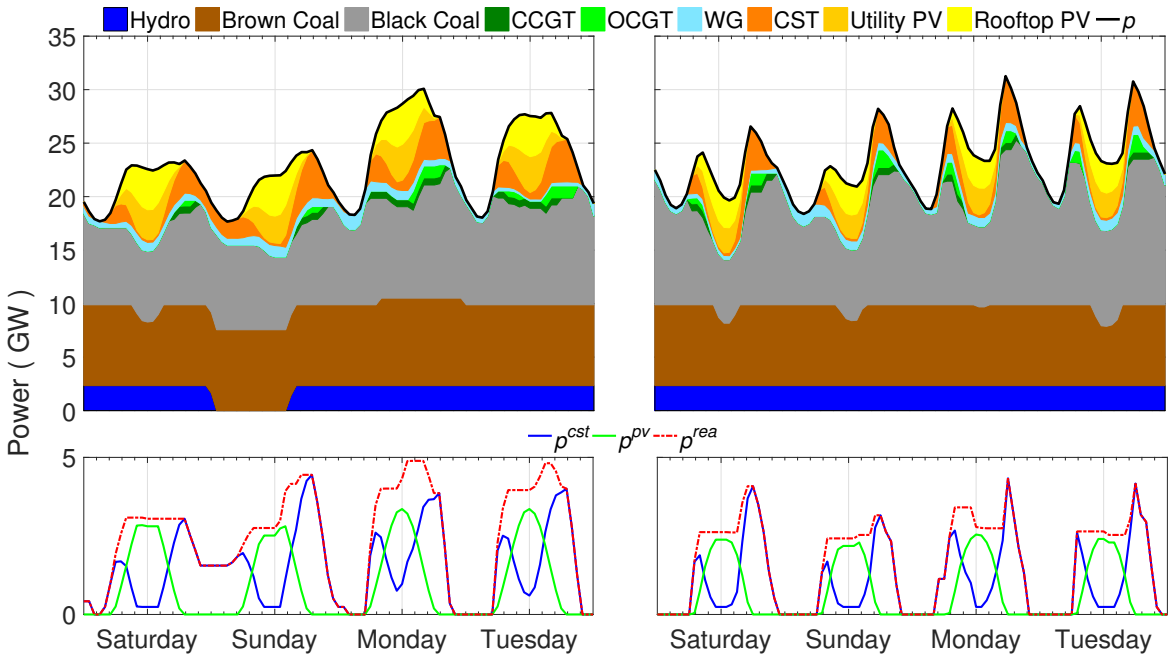

Fig. 4.6 Dispatch decisions for typical summer (left) and winter (right) load when 4 GW of PV and 6 GW of CST formed the REA (Case V). Vertical lines mark noon for each day.

However, REA dispatch rule could also include ramping limitations from other market participants for a much more refined outcome. The case studies here demonstrate the

flexibility provided by CST to PV, however, WG also can be examined in the same context. Furthermore, if the spinning reserve constraint required for PV is removed from the REA, and electrical spill levels are set to zero, then this system can also be used to optimise dispatch of CST to mitigate the effect of rooftop-PV.

4.5 Summary

A new institutional arrangement is explored to exploit generation flexibility in FGs, to ensure RES integration does not exceed system ramping constraints. Specifically, RES are not allowed to offer their energy directly into the wholesale electricity market. Rather an aggregation is structured from the combination of inflexible and flexible RES to offer power in the electricity market, while confining their effect on aggregate ramping rates to be at most equal to the rate of change in residual load.

This model is used to explore methods to mitigate the intermittent nature of RES by utilising other, complimentary RES. The challenge is to contribute power without imposing additional ramp stress on conventional generators. For this purpose, a REA dispatch rule is designed to fulfil this condition.

Case study show that this arrangement can provide benefits to all market participants, not just the RES. For PV, it will enable it to export more energy to the grid while CST can make profit by strategically shifting its output to peak hours all without increasing ramping stresses on conventional generators.

Chapter 5

Computationally Efficient Market Simulation Tool for Future Grid Scenario Analysis

This chapter integrates the advancements described in previous chapters with computationally efficient techniques to derive a generic market model that is capable of evaluating a wide range of future grid evolution pathways. The focus of this MST is to provide system planners and policy makers with an instrument to access and evaluate the integration of emerging technologies and their impact on long term decision making as detailed in Section 1.3. The existing literature on FG scenario analysis concentrates on simple balancing and the use of copper plate models (with a notable exception of the pan-European studies [31, 38] that use a DC load flow model). This ignores network related issues, which limits these models' applicability for stability assessment [33, 35, 39–41]. These studies have failed to include emerging technologies within the optimisation framework [31, 33, 35, 38–41, 44]. The FG research program funded by CSIRO was the first to propose a comprehensive modelling framework for future grids that also include stability [42]. The platform has been used, with additional improvements, to study fast stability scanning [43], modelling of prosumers for market simulation (Chapter 2), utility storage (Chapter 2), impact of prosumers on voltage stability (Chapter 3), power system flexibility using CST (Chapter 4) and system frequency performance (Chapter 6).

Specifically, in order to capture the inter-seasonal variations in the renewable generation, computationally intensive time series analysis needs to be used. A major computation bottleneck of the framework is the market simulation. Computation overhead is major challenge in realisation of such MST as acknowledged by [31]. Inclusion of new elements in the dispatch engine results in an increase of the size and the complexity of the underlying

optimisation problem. The major contributor to this computation expense are: (i) an network representation, which alters the dispatch of generator and limits aggregation of different components; (ii) prosumers, which introduce a bi-level structure and subsequent inlcusion of KKT and slackness variables; (iii) storage, which links intertemporal dispatch decisions; (iv) combinatorial structure in the generation commitment; and (v) high variability of RES, resulting in an increased cycling of conventional generators.

Within this context, the contribution of this chapter is a unified generic MST based on a UC problem suitable for FG scenario analysis, including stability assessment. The tool incorporates the following key features:

- a market structure-agnostic modelling framework,
- integration of various types and penetrations of RES and emerging demand-side technologies,
- a generic demand model considering the impact of prosumers,
- an explicit network representation, including HVDC lines, using a DC power flow model,
- an explicit representation of the number of online synchronous generators,
- an explicit representation of system inertia and reactive power support capability of synchronous generators,
- computational efficiency with sufficient accuracy.

The model builds on the research contributions presented in other chapters, combining utility storage model from Chapter 2; prosumers and network constraints from Chapter 3; minimum set of constraints from Chapter 4 to capture operation of CST; and minimum inertia constraint that will be elaborated in Chapter 6 in a single coherent formulation. Also, for simulation simplicity in Chapters 2, Chapters 3 and Chapters 4, identical units at each generation station are combined and their aggregated status is tracked by one single variable as previously used in [44]. This approach reduces the computation time at the expense of information regarding online units, which is quite important for stability studies as explained in Section 5.1.1.

5.1 Market Simulation Tool

This section begins by enumerating the functional requirement of the MST, which is followed by a discussion about the techniques used to improve computational performance. To

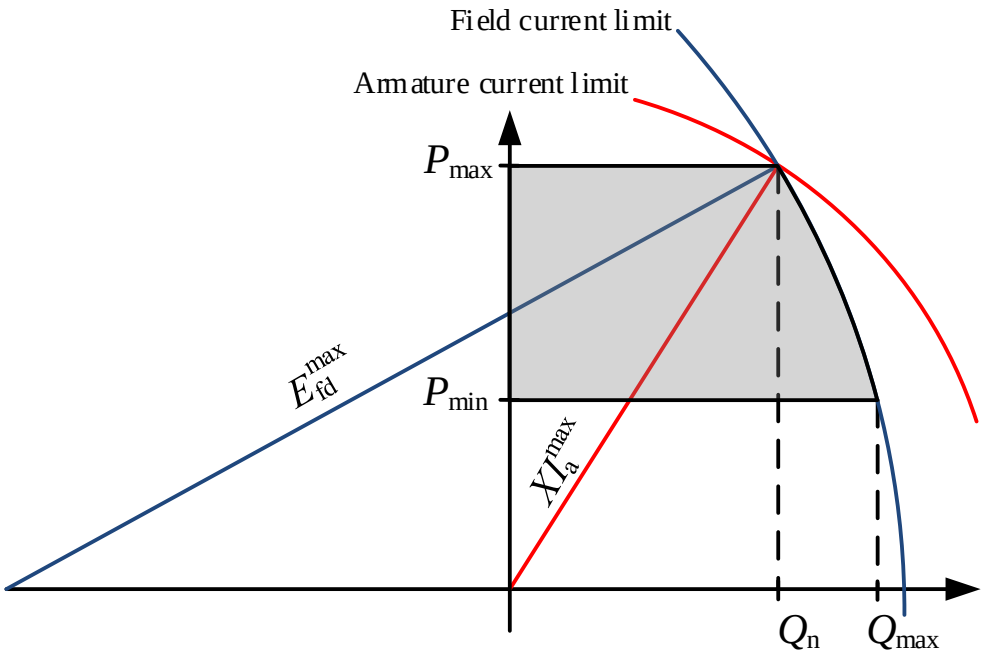

Fig. 5.1 Illustrative operating chart a synchronous generator in an over-excited mode (shaded region).

overcome the computation burden and to retain the information regarding number of online generators, unit clustering, rolling horizon, and constraint clipping techniques are used. Finally the resulting modified UC model is presented considering network, utility storage, prosumers, CST and minimum system inertia requirement.

5.1.1 Functional requirements

The focus of our work is stability assessment of future grid scenarios. Thus, the MST must produce dispatch decisions that accurately capture the kinetic energy stored in rotating masses (inertia), active power reserves and reactive power support capability of synchronous generators, which all depend upon the number of online units and the respective dispatch levels.

For the sake of illustration, consider a generation plant consisting of three identical (synchronous) thermal units, with the following characteristics: (i) constant terminal voltage of 1 pu; (ii) minimum technical limit $P_{\text{min}} = 0.4\,\text{pu}$; (iii) power factor of 0.8; (iv) maximum excitation limit $E_{\text{fd}}^{\text{max}} = 1.5\,\text{pu}$; and (v) normalized inertia constant $H = 5\,\text{s}$. We further assume that in the over-excited region, the excitation limit is the binding constraint, as shown in Fig. 5.1. Observe that the maximum reactive power capability depends on the active power generated, and varies between Q_{n} at $P_{\text{max}} = 1\,\text{pu}$ and Q_{max} at P_{min}. We consider three

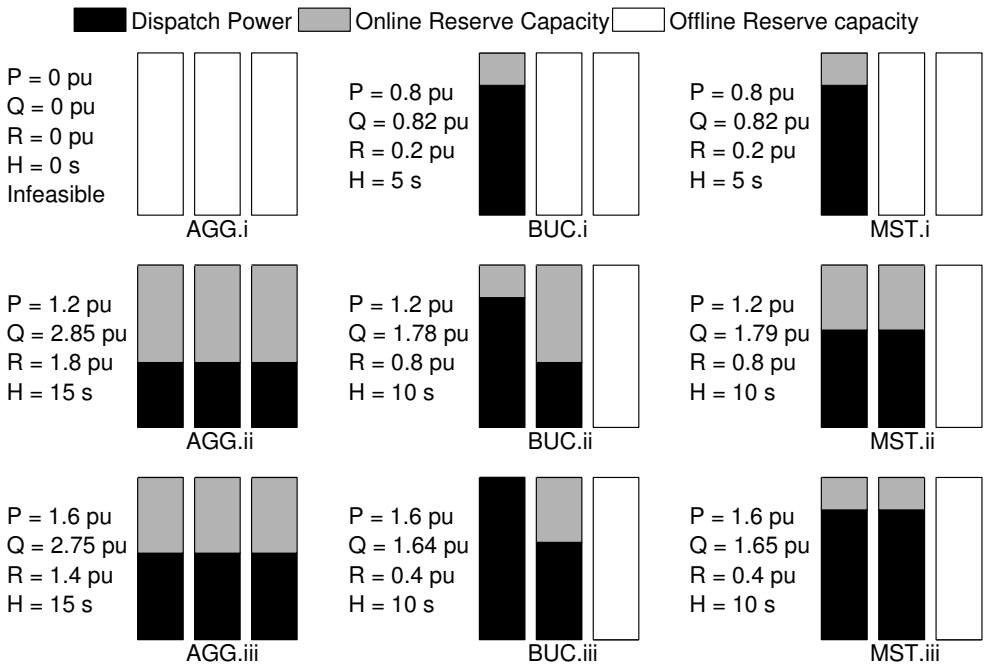

Fig. 5.2 Illustrative operating cases, (i) $P = 0.8\,\text{pu}$, (ii) $P = 1.2\,\text{pu}$, (iii) $P = 1.6\,\text{pu}$, showing active power dispatch level P, reactive power support capability Q, online active power reserves R and generator inertia H. The columns correspond to three different UC formulations: aggregated (AGG), binary (BUC) and the proposed MST formulation.

cases defined by the total active power generation of the plant: (i) 0.8 pu, (ii) 1.2 pu, and (iii) 1.6 pu. The three scenarios correspond to the rows in Fig. 5.2, which shows the active power dispatch level P, reactive power support capability Q, online active power reserves R, and generator inertia H. The three columns show feasible solutions for three different UC formulations: all three units are aggregated into one equivalent unit (AGG), standard binary UC (BUC) when each unit is modeled individually, and the proposed market simulation tool (MST). A detailed comparison of the three formulations is given in Section V.

Although the results are self-explanatory, a few things are worth emphasising. In case (i), aggregating the units into one equivalent unit results in the unit being shut down due to the minimum technical limit. The individual unit representation (BUC), on the other hand, does allow the dispatch of one or two units, but with significantly different operational characteristics. In cases (ii) and (iii), the total inertia in the AGG formulation is much higher, which has important implications for frequency stability. A similar observation can be made for the reactive power support capability, which affects voltage stability. Also, dispatching power from all three units results in a significantly higher active power reserve. And last, a higher reactive power generation due to a lower P reduces the internal machine angle, which improves transient stability.

In conclusion, a faithful representation of the number of online synchronous machines is of vital importance for stability assessment. An individual unit representation, however, is computationally expensive, so the computation burden should be reduced, as discussed in the following section. Next, an explicit network representation is required. An AC load flow formulation, however, is nonlinear (and non-convex), which results in an intractable mixed-integer nonlinear problem. Therefore, we use a DC load flow representation with a sufficiently small voltage angle difference on transmission lines. Our experience shows that an angle difference of 30° results in a manageable small number of infeasible operating conditions that can be dealt with separately.

5.1.2 Computational speedup

The MST is based on the UC formulation using constant fixed, startup, shutdown and production costs. To improve its computational efficiency, the dimensionality of the optimisation problem is reduced employing: (i) unit clustering [9] to reduce the number of variables needed to represent a multi-unit generation plant; (ii) a rolling horizon approach [10, 1, 39] to reduce the time dimension; and (iii) constraint clipping to remove most non-binding constraints.

Unit clustering

Linearised UC models are computationally efficient for horizons of up to a few days, which makes them extremely useful for operational studies. For planning studies, however, where horizon lengths can be up to a year, or more, these models are still computationally too expensive. Our work builds on the clustering approach proposed in [9], where identical units at each generation plant are aggregated by replacing binary variables with fewer integer variables. The clustering approach is adopted and the status of online units, startup/shutdown decisions and dispatched power are tracked by three integer variables and one continuous variable *per plant* per period, as opposed to three binary and one continuous variable *per unit* per period. Further clustering proposed in [9] is not possible in our formulation because of the explicit network representation required in the MST.

Rolling horizon

Solving the UC as one block, especially for long horizons, is computationally too expensive. This can be overcome by breaking the problem into several smaller intervals called sub-horizons [10, 1, 39]. To ensure accuracy and consistency of the solution, a proper overlap between sub-horizons is maintained and the terminating state of the previous sub-horizon

is used as the initial condition of the next sub-horizon. The minimum sub-horizon length depends on the time constants associated with the decision variables. While these might be in the order of hours for thermal power plants, they can be significantly longer for energy storage. Large-scale hydro dams, for example, require horizon lengths of several weeks, or even months. In our research, however, the sub-horizon length is up to a few days to cater for thermal energy storage of CST plants and battery storage. The optimisation of hydro dams is not explicitly considered, as it requires horizons spanning over several months. However it can be taken into account heuristically, if needed.

Constraint clipping

The size of the problem can be reduced by removing non-binding constraints, which doesn't affect the feasible region. For instance, an MUDT constraint on a unit with an MUDT less than the time interval is redundant[1]. Similarly, a ramp constraint for flexible units is redundant if the time step is sufficiently long. With a higher RES penetration, in particular, where backup generation is provided by fast-ramping gas turbines, this technique can significantly reduce the size of the optimisation problem, and hence improves the computational performance due to a larger number of units with higher ramp rates and smaller MUDTs. It should be noted that optimisation pre-solvers might not able to automatically remove these constraints.

5.1.3 MST UC Formulation

The MST model builds on a three-variable UC formulation and modifies it according with the above mentioned computationally efficient techniques. In addition to that, it also incorporates utility storage, prosumers, DC power flow, CST and minimum inertia constraints. It is worth mentioning that a careful revaluation of these constraints is required to combine them in a unified framework. For example, unit clustering enables accurate tracking of online generators without any additional computation overhead, however, it requires a modification of the decision variables from binary to integer, which also requires a modification of inter-temporal coupling variables in the the rolling horizon formulation. Although the MST incorporates the emerging technologies that are introduced in this dissertation, it can incorporate also other emerging technologies such as electric vehicles.

[1] This is especially the case when the time resolution is coarse. In our studies, the time step is one hour. In operational studies, where the resolution can be as short as five minutes, constraint clipping is less useful.

Objective function

The objective of the MST is to minimise total generation cost for all sub-horizons h:

$$\underset{\Omega}{\text{minimise}} \sum_{t\in\mathcal{T}}\sum_{g\in\mathcal{G}}\Big(c_g^{\text{fix}}s_{g,t}+c_g^{\text{su}}u_{g,t}+c_g^{\text{sd}}d_{g,t}+c_g^{\text{var}}p_{g,t}\Big), \tag{5.1}$$

where $\Omega=\{s_{g,t},u_{g,t},d_{g,t},p_{g,t},p_{s,t},p_{l,t}\}$ are the decision variables of the problem, and c_g^{fix}, c_g^{su}, c_g^{sd}, and c_g^{var} are fixed, startup, shutdown and variable cost, respectively. As typically done in planning studies [9], [27], the costs are assumed constant to reduce the computation complexity. The framework, however, also admits a piece-wise linear approximation proposed in [4].

System constraints

System constraints[2] include power balance constraints, power reserve and minimum synchronous inertia requirements.

Power balance: Power generated at node n must be equal to the node power demand plus the net power flow on transmission lines connected to the node:

$$\sum_{g\in\mathcal{G}_n}p_{g,t}=\sum_{c\in\mathcal{C}_n}p_{c,t}+\sum_{p\in\mathcal{P}_n}p_{p,t}^{\text{g}+}-\sum_{p\in\mathcal{P}_n}p_{p,t}^{\text{g}-}+\sum_{s\in\mathcal{S}_n}p_{s,t}+\sum_{l\in\mathcal{L}_n}(p_{l,t}+\Delta p_{l,t}), \tag{5.2}$$

where $\mathcal{G}_n,\mathcal{C}_n,\mathcal{P}_n,\mathcal{S}_n,\mathcal{L}_n$ represent respectively the set of generators, consumers, prosumers[3], utility storage plants and lines connected to node n.

Power reserves: To cater for uncertainties, active power reserves provided by synchronous generation $g\in\mathcal{G}^{\text{syn}}$ are maintained in each region r:

$$\sum_{g\in\{(\mathcal{G}^{\text{syn}}-\mathcal{G}^{\text{cst}})\cap\mathcal{G}_r\}}(\overline{p}_g s_{g,t}-p_{g,t})+\sum_{g\in\{\mathcal{G}^{\text{cst}}\cap\mathcal{G}_r\}}\min(\overline{p}_g s_{g,t}-p_{g,t},e_{g,t}-p_{g,t})\geq\sum_{n\in\mathcal{N}_r}p_{n,t}^{\text{r}}. \tag{5.3}$$

For synchronous generators other than concentrated solar thermal, reserves are defined as the difference between the online capacity and the current operating point. For CST, reserves can either be limited by their online capacity or energy level of their thermal energy system. Variable $s_{g,t}$ in (5.3) represents the total number of online units at each generation plant, and $\mathcal{G}_r$ and $\mathcal{N}_r$ represent the sets of generators and nodes in region r, respectively.

[2] All the constraints must be satisfied in all time slots t, however, for sake of notational brevity, this is not explicitly mentioned.

[3] Price-responsive users equipped with small-scale PV-battery systems.

Minimum synchronous inertia requirement: To ensure frequency stability, a minimum level of inertia provided by synchronous generation must be maintained at all times. The need of explicit minimum synchronous inertia constraint is justified and derived in Chapter 6, here is it mentioned for the sake of completeness:

$$\sum_{g\in\{\mathcal{G}^{\text{syn}}\cap\mathcal{G}_r\}} s_{g,t}H_gS_g \geq \sum_{n\in\mathcal{N}_r} I_{n,t}, \tag{5.4}$$

where $I_{n,t}$ is the minimum synchronous inertia requirement of node n.

Network constraints

Network constraints include DC power flow constraints and thermal line limits for AC lines, and active power limits for HVDC lines.

Line power constraints: A DC load flow model is used for computation simplicity for AC transmission lines[4]:

$$p_{l,t}^{x,y} = B_l(\delta_{x,t} - \delta_{y,t}), \quad l \in \mathcal{L}^{\text{AC}}, \tag{5.5}$$

where the variables $\delta_{x,t}$ and $\delta_{y,t}$ represent voltage angles at nodes $x \in \mathcal{N}$ and $y \in \mathcal{N}$, respectively.

Thermal line limits: Power flows on all transmission lines are limited by the respective thermal limits of line l:

$$\mid p_{l,t} \mid \leq \overline{p}_l, \tag{5.6}$$

where $\overline{p}_l$ represents the thermal limit of line l.

Generation constraints

Generation constraints include physical limits of individual generation units. For the binary unit commitment (BUC), we adopted a UC formulation requiring three binary variables per time slot (on/off status, startup, shutdown) to model an individual unit. In the MST, identical units of a plant are clustered into one individual unit [9]. This requires three *integer* variables (on/of status, startup, and shutdown) *per generation plant* per time slot as opposed to three *binary* variables *per generation unit* per time slot in the BUC, as discussed in Section 5.1.2.

Generation limits: Dispatch levels of a synchronous generator g are limited by the respective stable operating limits:

$$s_{g,t}\underline{p}_g \leq p_{g,t} \leq s_{g,t}\overline{p}_g, \quad g \in \mathcal{G}^{\text{syn}}. \tag{5.7}$$

[4] A sufficiently small ($\sim 30°$) voltage angle difference over a transmission line is used to reduce the number of nonconvergent AC power flow cases.

The power of RES[5] generation is limited by the availability of the corresponding renewable resource (wind or sun):

$$s_{g,t}\underline{p}_g \leq p_{g,t} \leq s_{g,t}\overline{p}^{\text{res}}, \quad g \in \{\mathcal{G}^{\text{res}} \cap \mathcal{G}^{\text{cst}}\}. \tag{5.8}$$

Unit on/off constraints: A unit can only be turned on if and only if it is in off state and vice versa:

$$u_{g,t} - d_{g,t} = s_{g,t} - s_{g,t-1}, \quad t \neq 1,\ g \in \mathcal{G}^{\text{syn}}. \tag{5.9}$$

In a rolling horizon approach, consistency between adjacent time slots is ensured by:

$$u_{g,t} - d_{g,t} = s_{g,t} - \hat{s}_g, \quad t = 1,\ g \in \mathcal{G}^{\text{syn}}, \tag{5.10}$$

where $\hat{s}_g$ is the initial number of online units of generator g. Equations (5.9) and (5.10) also implicitly determine the upper bound of $u_{g,t}$ and $d_{g,t}$ in terms of changes in $s_{g,t}$.

Number of online units: Unlike the BUC, the MST requires an explicit upper bound on status variables:

$$s_{g,t} \leq \overline{U}_g, \tag{5.11}$$

where $\overline{U}_g$ is total number of identical units of generator g.

Ramp-up and ramp-down limits: Ramp rates of synchronous generation should be kept within the respective ramp-up (5.12), (5.13) and ramp-down limits (5.14), (5.15):

$$p_{g,t} - p_{g,t-1} \leq s_{g,t} r_g^+, \qquad t \neq 1, g \in \{\mathcal{G}^{\text{syn}} | r_g^+ < \overline{p}_g\}, \tag{5.12}$$

$$p_{g,t} - \hat{p}_g \leq s_{g,t} r_g^+, \qquad t = 1, g \in \{\mathcal{G}^{\text{syn}} | r_g^+ < \overline{p}_g\}, \tag{5.13}$$

$$\hat{p}_g - p_{g,t} \leq s_{g,t-1} r_g^-, \qquad t \neq 1, g \in \{\mathcal{G}^{\text{syn}} | r_g^- < \overline{p}_g\}, \tag{5.14}$$

$$\hat{p}_g - p_{g,t} \leq \hat{s}_g r_g^-, \qquad t = 1, g \in \{\mathcal{G}^{\text{syn}} | r_g^- < \overline{p}_g\}. \tag{5.15}$$

In the MST, a ramp limit of a power plant is defined as a product of the ramp limit of an individual unit and the number of online units in a power plant $s_{g,t}$. If $s_{g,t}$ is binary, these ramp constraints are mathematically identical to ramp constraints of the BUC. If a ramp rate multiplied by the length of the time resolution Δt is less than the rated power, the rate limit has no effect on the dispatch, so the corresponding constraint can be eliminated. Constraints explicitly defined for $t = 1$ are used to join two adjacent sub-horizons in the rolling-horizon approach.

[5]For the sake of brevity, by RES we mean "unconventional" renewables like wind and solar, but excluding conventional RES, like hydro, and dispatchable unconventional renewables, like concentrated solar thermal.

Minimum up and down times: Steam generators must remain on for a period of time τ_g^{u} once turned on (minimum up time):

$$s_{g,t} \geq \sum_{\tilde{t}=\tau_g^{\mathrm{u}}-1}^{0} u_{g,t-\tilde{t}}, \qquad t \geq \tau_g^{\mathrm{u}},\ g \in \{\mathcal{G}^{\mathrm{syn}} | \tau_g^{\mathrm{u}} > \Delta t\}, \tag{5.16}$$

$$s_{g,t} \geq \sum_{\tilde{t}=t-1}^{0} u_{g,t-\tilde{t}} + \hat{u}_{g,t}, \qquad t < \tau_g^{\mathrm{u}},\ g \in \{\mathcal{G}^{\mathrm{syn}} | \tau_g^{\mathrm{u}} > \Delta t\}. \tag{5.17}$$

Similarly, they must not be turned on for a period of time τ_g^{d} once turned off (minimum down time):

$$s_{g,t} \leq \overline{U}_g - \sum_{\tilde{t}=\tau_g^{\mathrm{d}}-1}^{0} d_{g,t-\tilde{t}}, \qquad t \geq \tau_g^{\mathrm{d}},\ g \in \{\mathcal{G}^{\mathrm{syn}} | \tau_g^{\mathrm{d}} > \Delta t\}, \tag{5.18}$$

$$s_{g,t} \leq \overline{U}_g - \sum_{\tilde{t}=t-1}^{0} d_{g,t-\tilde{t}} - \hat{d}_{g,t}, \qquad t < \tau_g^{\mathrm{d}},\ g \in \{\mathcal{G}^{\mathrm{syn}} | \tau_g^{\mathrm{d}} > \Delta t\}. \tag{5.19}$$

Similar to the rate limits, if the minimum up and down times are smaller than the time resolution Δt, the corresponding constraints can be eliminated. Due to integer nature of discrete variables in the MST, the definition of the MUDT constraints in the RH approach requires the number of online units for the last $\tau^{\mathrm{u/d}}$ time interval to establish the relationship between the adjacent sub-horizons. If the $\tau_g^{\mathrm{u/d}}$ is smaller than time resolution Δt, then these constraints can be eliminated.

CST constraints

CST constraints include thermal energy storage energy balance and storage limits.

TES state of charge determines the thermal energy storage energy balance subject to the accumulated energy in the previous time slot, thermal losses, thermal power provided by the solar farm and electrical power dispatched from the CST plant:

$$e_{g,t} = \eta_g e_{g,t-1} + p_{g,t} - p_{g,t}, \qquad t \neq 1,\ g \in \mathcal{G}^{\mathrm{cst}}, \tag{5.20}$$

$$e_{g,t} = \eta_g \hat{e}_g + p_{g,t} - p_{g,t}, \qquad t = 1,\ g \in \mathcal{G}^{\mathrm{cst}}, \tag{5.21}$$

where, $p_{g,t}$ is the thermal power collected by the solar field of generator $g \in \mathcal{G}^{\mathrm{cst}}$.

TES limits: Energy stored is limited by the capacity of a storage tank:

$$\underline{e}_g \leq e_{g,t} \leq \overline{e}_g, \quad g \in \mathcal{G}^{\mathrm{cst}}. \tag{5.22}$$

Utility storage constraints

Utility-scale storage constraints include energy balance, storage capacity limits and power flow constraints. The formulation is generic and can capture a wide range of storage technologies.

Utility storage SOC limits determine the energy balance of storage plant s:

$$e_{s,t} = \eta_s e_{s,t-1} + p_{s,t}, \qquad t \neq 1, \tag{5.23}$$

$$e_{s,t} = \eta_s \hat{e}_s + p_{s,t}, \qquad t = 1. \tag{5.24}$$

Utility storage capacity limits: Energy stored is limited by the capacity of storage plant s:

$$\underline{e}_s \leq e_{s,t} \leq \overline{e}_s. \tag{5.25}$$

Charge/discharge rates limit the charge and discharge powers of storage plant s:

$$\overline{p}_s^- \leq p_{s,t} \leq \overline{p}_s^+, \tag{5.26}$$

where $\overline{p}_s^-$ and $\overline{p}_s^+$ represent the maximum power discharge and charge rates of a storage plant, respectively.

Prosumer sub-problem

The prosumer sub-problem captures the aggregated effect of prosumers. It is modeled using a bi-level framework in which the upper-level unit commitment problem described above minimises the total generation cost, and the lower-level problem maximises prosumers' self-consumption. The coupling is through the prosumers' demand, not through the electricity price, which renders the proposed model market structure agnostic. As such, it implicitly assumes a mechanism for demand response aggregation. The Karush-Kuhn-Tucker optimality conditions of the lower-level problem are added as the constraints to the upper-level problem, which reduces the problem to a single mixed integer linear program.

The model makes the following assumptions: (i) the loads are modeled as price anticipators; (ii) the demand model representing an aggregator consists of a large population of prosumers connected to an unconstrained distribution network who collectively maximise self-consumption; (iii) aggregators do not alter the underlying power consumption of the prosumers; and (iv) prosumers have smart meters equipped with home energy management systems for scheduling of the PV-battery systems, and, a communication infrastructure is

assumed that allows a two-way communication between the grid, the aggregator and the prosumers. More details can be found in Chapter 2 and Chapter 3.

Prosumer objective function: Prosumers aim to minimise electricity expenditure:

$$\underset{p_p^{g+/-}, p_p^b}{\text{minimise}} \sum_{t \in \mathcal{T}} p_{p,t}^{\mathrm{g}+} - \lambda\, p_{p,t}^{\mathrm{g}-}, \tag{5.27}$$

where λ is the applicable feed-in price ratio. In our research, we assumed $\lambda = 0$, which corresponds to maximization of self-consumption.

The prosumer sub-problem is subject to the following constraints:

Prosumer power balance: Electrical consumption of prosumer p, consisting of grid feed-in power, $p_{p,t}^{\mathrm{g}-}$, underlying consumption, $p_{p,t}$, and battery charging power, $p_{p,t}^{\mathrm{b}}$, is equal to the power taken from the grid, $p_{p,t}^{\mathrm{g}+}$, plus the power generated by the PV system, $p_{p,t}^{\mathrm{pv}}$:

$$p_{p,t}^{\mathrm{g}+} + p_{p,t}^{\mathrm{pv}} = p_{p,t}^{\mathrm{g}-} + p_{p,t} + p_{p,t}^{\mathrm{b}}. \tag{5.28}$$

Battery SOC limits: Battery state of charge is the sum of the power inflow and the state of charge in the previous period:

$$e_{p,t}^{\mathrm{b}} = \eta_p^{\mathrm{b}} e_{p,t}^{\mathrm{b}} + p_{p,t}^{\mathrm{b}}, \qquad t \neq 1, \tag{5.29}$$

$$e_{p,t}^{\mathrm{b}} = \eta_p^{\mathrm{b}} \hat{e}_p^{\mathrm{b}} + p_{p,t}^{\mathrm{b}}, \qquad t = 1, \tag{5.30}$$

where $\hat{e}_p^{\mathrm{b}}$ represents the initial state of charge and is used to establish the connection between adjacent sub-horizons.

Battery charge/discharge limits: Battery power should not exceed the charge/discharge limits:

$$\overline{p}_p^{\mathrm{b}-} \leq p_{p,t}^{\mathrm{b}} \leq \overline{p}_p^{\mathrm{b}+}, \tag{5.31}$$

where $\overline{p}_b^-$ and $\overline{p}_b^+$ represent the maximum power discharge and charge rates of the prosumer's battery, respectively.

Battery storage capacity limits: Energy stored in a battery of prosumer p should always be less than its capacity:

$$\underline{e}_p^{\mathrm{b}} \leq e_{p,t}^{\mathrm{b}} \leq \overline{e}_p^{\mathrm{b}}. \tag{5.32}$$

5.2 Simulation Setup

The case studies provided in this section compare the computational efficiency of the MST with alternative formulations. For detailed studies on the impact of different technologies on future grids, an interested reader can refer to Chapters 2, 3, 4 and 6.

5.2.1 Test system

We use a modified 14-generator IEEE test system that was initially proposed in [69] as a test bed for small-signal analysis. The system is loosely based on the Australian NEM, the interconnection on the Australian eastern seaboard. The network is stringy, with large transmission distances and loads concentrated in a few load centres. Generation, demand and the transmission network were modified to meet future load requirements. The modified model consists of 79 buses grouped into four regions, 101 units installed at 14 generation plants and 810 transmission lines.

5.2.2 Test cases

To expose the limitations of the different UC formulations, we have selected a typical week with sufficiently varying operating conditions. Four diverse test cases with different RES penetrations are considered. First, RES0 considers only conventional generation, including hydro, black coal, brown coal, combined cycle gas and open cycle gas. The generation mix consists of 2.31 GW hydro, 39.35 GW of coal and 5.16 GW of gas, with the peak load of 36.5 GW. To cater for demand and generation variations, 10 % reserves are maintained at all times. The generators are assumed to bid at their respective short run marginal costs, based on regional fuel prices [70].

Cases RES30, RES50, RES75 consider, respectively, 30 %, 50 % and 75 % annual energy RES penetration, supplied by wind, PV and CST. Normalized power traces for PV, CST and wind farms (WFs) for the 16-zones of the NEM are taken from the AEMO's planning document [99]. The locations of RESs are loosely based on the AEMO's 100% RES study [37].

5.2.3 Modelling assumptions

Power traces of all PV modules and wind turbines at one plant are aggregated and represented by a single generator. This is a reasonable assumption given that PV and WF don't provide active power reserves, and are not limited by ramp rates, MUDT, and startup and shutdown costs, which renders the information on the number of online units unnecessary.

Also worth mentioning is that RES can be modelled as negative demand, which can lead to an infeasible solution. Modelling RES (wind and solar PV) as negative demand is namely identical to preventing RES from spilling energy. Given the high RES penetration in future grids, we model RES explicitly as individual generators. Unlike solar PV and wind, CST requires a different modelling approach. Given that CST is synchronous generation it also contributes to spinning reserves and system inertia. Therefore, the number of online units in a CST plant needs to be modelled explicitly.

An optimality gap of 1% was used for all test cases. Simulation were run on Dell OPTIPLEX 9020 desktop computer with Intel(R) Core(TM) i7-4770 CPU with 3.40 GHz clock speed and 16 GB RAM.

5.3 Results and Discussion

To showcase the computational efficiency of the MST, we first benchmark its performance for different horizon lengths against the BUC formulation employing three binary variables *per unit per time slot* and the AGG formulation where identical units at each plant are aggregated into a single unit, which requires three binary variables *per plant per time slot*. We pay particular attention to the techniques used for computational speedup, namely unit clustering, rolling horizon, and constraint clipping. Last, we compare the results of the MST with BUC and AGG formulations for voltage and frequency stability studies.

5.3.1 Binary unit commitment (BUC)

We first run the BUC for horizon lengths varying from one to seven days, Fig. 5.3 (top). As expected, with the increase in the horizon length, the solution time increases exponentially. For a seven-day horizon, the solution time is as high as 25 000 s (7 h). Observe how the computation burden is highly dependent on the RES penetration. The variability of the RES results in an increased cycling of the conventional thermal fleet, which increases the number of on/off decisions and, consequently the computation burden. In addition to that, a higher RES penetration involves an increased operation of CST. This poses an additional computation burden due to the decision variables associated with thermal energy storage that span several time slots. In summary, the computation burden of the BUC renders it inappropriate for scenario analysis involving extended horizons.

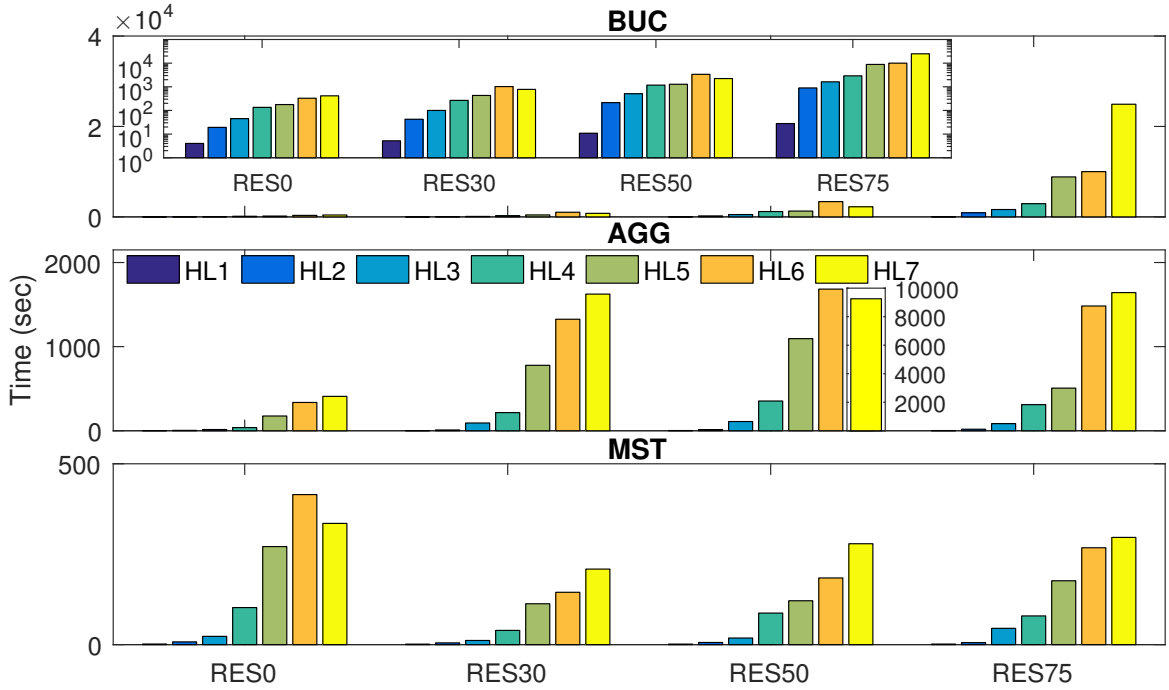

Fig. 5.3 Computation time requirements of BUC, AGG and MST for horizon lengths of one (HL1) to seven days (HL7) and different RES penetration levels. In the insets, a logarithmic scale is used for BUC, and a linear scale for AGG case RES50-HL7.

5.3.2 Aggregated formulation (AGG)

Aggregating identical units at a power plant into a single unit results in a smaller number of binary variables, which should in principle reduce the computation complexity. Fig. 5.3 confirms that this is mostly true, however, for RES50-HL7 the computation time is higher than in the BUC formulation. The reason for that is that, in this particular case, the BUC formulation has a tighter relaxation than the AGG formulation and, consequently, a smaller root node gap. Compared to the MST formulation, with a similar number of variables than the AGG formulation, the MST has considerably shorter computation time due to a smaller root node gap.

In terms of accuracy, the AGG formulation works well for balancing studies as demonstrated in Chapter 2 and Chapter 4. On the other hand, the number of online synchronous generators in the dispatch differs significantly from the BUC, which negatively affects the accuracy of voltage and frequency stability analysis, as shown later. Due to a large number of online units in a particular scenario, a direct comparison of dispatch levels and reserves from each generator is difficult. Therefore, we compare the total number of online synchronous generators, which serves as a proxy to the available system inertia. Fig. 5.4 shows the number of online generators of four different RES penetration levels for a horizon length of seven

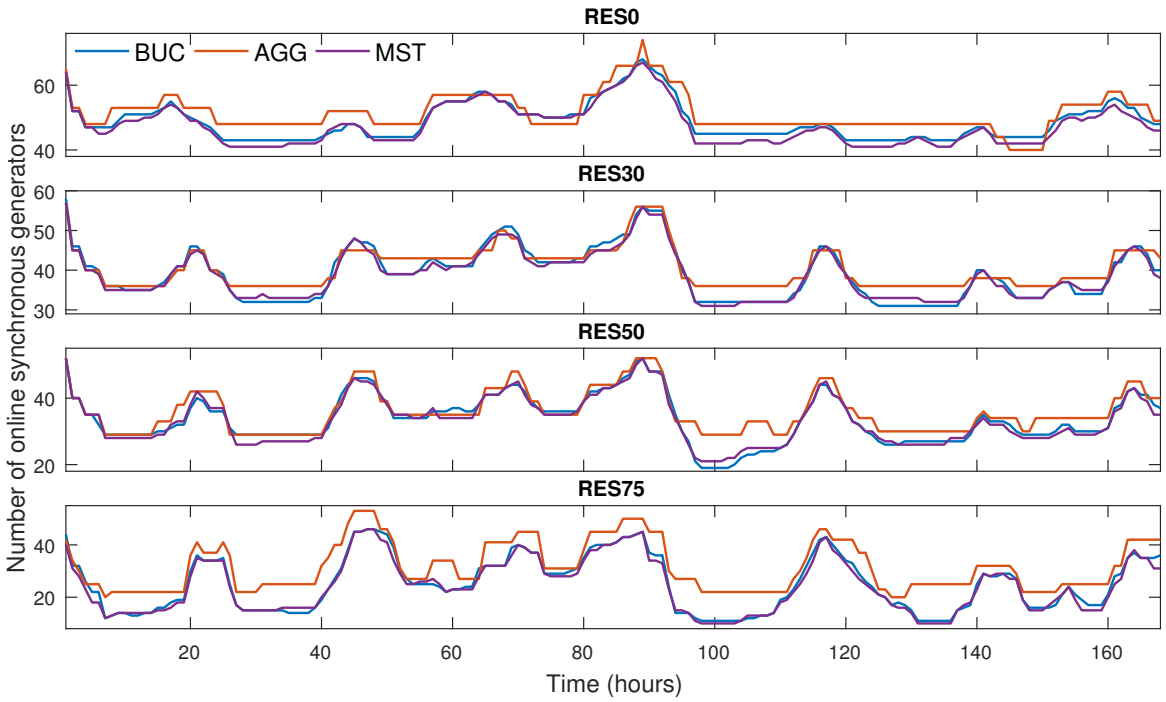

Fig. 5.4 Total number of online synchronous generators for BUC, AGG and MST for different RES penetration levels and a horizon length of seven days.

days. For most of the hours there is a significant difference between the number of online units obtained from the BUC and the AGG formulation.

In conclusion, despite its computational advantages, the AGG formulation is not appropriate for stability studies due to large variations in the number of online synchronous units in the dispatch results. In addition to that, the computation time is comparable to the BUC in some cases.

5.3.3 Computational speedup assessment

We now evaluate the effectiveness of the techniques for the computational speedup.

Unit clustering

In unit clustering, binary variables associated with the generation unit constraints are replaced with a smaller number of integer variables, which allows aggregating several identical units into one equivalent unit, but with the number of online units retained. This results in a significant reduction in the number of variables and, consequently, in the computational speedup. Compared to the BUC, the number of variables in the MST with this technique alone reduces from 24 649 to 5990 for RES75 with a horizon length of seven days. Therefore,

Table 5.1 Computation time comparison (MB = monolithic block, RH = rolling horizon, 7 = 7 days, 2+1 = 2 days with one day overlap).

	RES0 (minutes)	RES30 (minutes)	RES50 (minutes)	RES75 (minutes)
BUC MB 7	6.92	12.95	37.11	415.25
AGG MB 7	6.81	27.08	154.27	27.37
MST MB 7	2.12	3.34	4.73	5.32
BUC RH 2+1	2.38	4.03	24.18	74.70
AGG RH 2+1	0.15	0.20	0.27	0.25
MST RH 2+1	0.35	0.71	0.60	0.76

the solution time for RES75-HL7 reduces from 25 000 s in the BUC to 450 s in MST with unit clustering alone.

Rolling horizon approach

A rolling horizon approach splits the UC problem into shorter horizons. Given the exponential relationship between the computation burden and the horizon length, as discussed in Section 5.3.1, solving the problem in a number of smaller chunks instead of in one block results in a significant computational speedup. The accuracy and the consistency of the solution are maintained by having an appropriate overlap between the adjacent horizons. However, the overlap depends on the time constants of the problem. Long term storage, for example, might require longer solution horizons. The solution times for different RES penetrations are shown in Table 5.1. Observe that in the RES75 case, the effect of rolling horizon is much more pronounced, which confirms the validity of the approach for studies with high RES penetration.

Constraint clipping

Eliminating non binding constraints can speedup the computation even further. Table 5.2 shows the number of constraints for different scenarios with and without constraint clipping. Observe that the number of redundant constraints is higher in scenarios with a higher RES penetration. The reason is that a higher RES penetration requires more flexible gas generation with ramp rates shorter than the time resolution (one hour in our case). Note that the benefit of constraint clipping with a shorter time resolution will be smaller.

Table 5.2 The impact of constraint clipping (CC) on the total number of constraints for all cases with a horizon length of seven days.

Case	Number of Constraints		
	without CC	with CC	% reduction
RES0	64555	61332	4.99
RES30	62520	56617	9.44
RES50	62500	56777	9.15
RES75	62740	57017	9.12

5.3.4 MST computation time and accuracy

The MST outperforms the BUC and AGG in terms of the computation time by several orders of magnitude, as shown in Fig. 5.3 (bottom). The difference is more pronounced at higher RES penetration levels. For RES75, the MST is more than 500 times faster than the BUC. In terms of the accuracy, the MST results are almost indistinguishable from the BUC results, as evident from Fig. 5.4 that shows the number of online synchronous units for different RES penetration levels. Minor differences in the results stem from the nature of the optimisation problem. Due to its mixed-integer structure, the problem is non-convex and has therefore several local optima. Given that the BUC and the MST are mathematically not equivalent, the respective solutions might not be exactly the same. The results are nevertheless very close, which confirms the validity of the approach for the purpose of scenario analysis. The loadability and inertia results presented later further support this conclusion.

5.3.5 Stability assessment

To showcase the applicability of the MST for stability assessment, we analyse system inertia and loadability that serve as a proxy to frequency and voltage stability, respectively. More detailed stability studies are covered in Chapter 3 (voltage stability) and Chapter 6 (frequency stability).

System inertia

Fig. 5.5 (bottom) shows the system inertia for the BUC, AGG and the proposed MST, respectively, for RES0. Given that the inertia is the dominant factor in the frequency response of a system after a major disturbance, the minuscule difference between the BUC and the MST observed in Fig. 5.5 validates the suitability of the MST for frequency stability assessment. The inertia captured by the AGG, on the other hand, is either over or under estimated and so does not provide a reliable basis for frequency stability assessment.

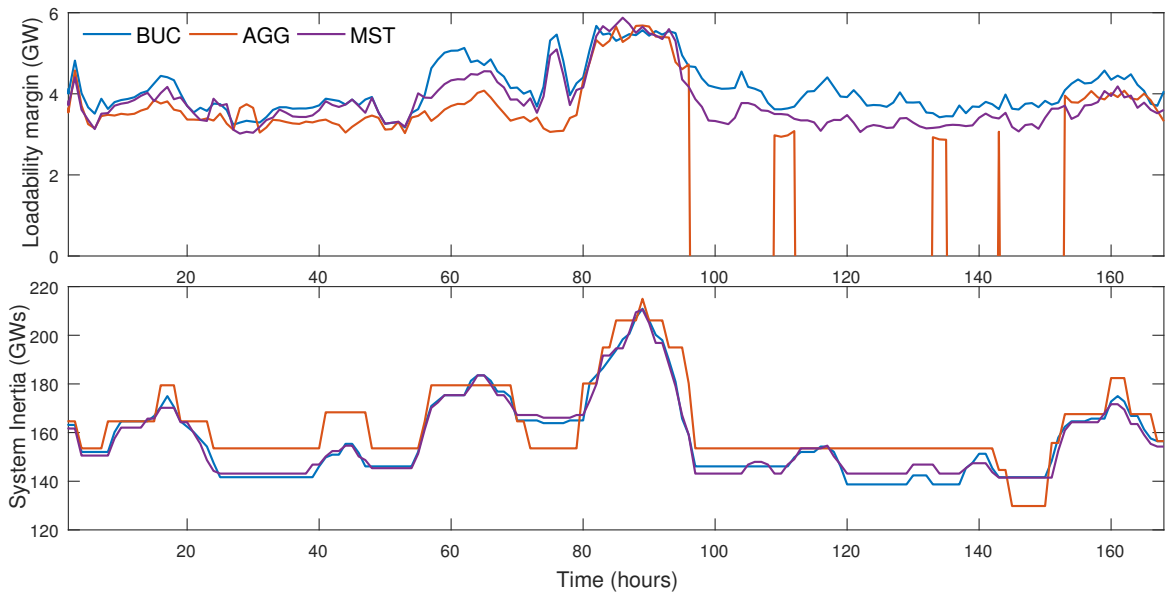

Fig. 5.5 Loadability margins (top) and system inertia (bottom) computed based on dispatch results of different techniques i.e BUC, AGG and proposed MST for RES0.

Loadability analysis

The dispatch results from the MST are used to calculate power flows, which are then used in loadability analysis[6]. Fig. 5.5 (top) shows loadability margins for the RES0 scenario for different UC formulations. Observe that the BUC and the MST produce very similar results. The AGG formulation, on the other hand, gives significantly different results. From hours 95 to 150, in particular, the AGG results show that the system is unstable most of the time, which is in direct contradiction to the accurate BUC formulation. Compared to the inertia analysis, the differences between the formulations are much more pronounced. Unlike voltage, frequency is a system variable, which means that it is uniform across the system. In addition to that, inertia only depends on the number of online units but not on their dispatch levels. Voltage stability, on the other hand, is highly sensitive both to the number of online units and their dispatch levels, which affects the available reactive power support capability, as illustrated in Fig. 5.2. Close to the voltage stability limit, the system becomes highly nonlinear, so even small variations in dispatch results can significantly change the power flows and, consequently, voltage stability of the system. One can argue that in comparison to BUC the MST result in the more conservative loadability margin, although this is not always the case (around hour 85, the MST is less conservative).

[6]The loadability analysis is performed by uniformly increasing the load in the system until the load flow fails to converge. The loadability margin is calculated as the difference between the base system load and the load in the last convergent load flow iteration.

5.4 Summary

This chapter built on the work presented in previous chapters and integrate them in the form of a computationally efficient electricity market simulation tool based on a UC problem suitable for FG scenario analysis. The proposed UC formulation includes an explicit network representation and accounts for the uptake of emerging demand-side technologies in a unified generic framework while allowing for a subsequent stability assessment. We showed that unit aggregation, used in conventional planning-type UC formulations to achieve computational speedup, fails to properly capture the system inertia and reactive power support capability, which is crucial for stability assessment. To address this shortcoming, a UC formulation is proposed, which models the number of online generation units explicitly and is amenable to a computationally expensive time-series analysis required in FG scenario analysis. To achieve a further speedup, we use a rolling horizon approach and constraint clipping.

The effectiveness of the computational speedup techniques depends on the problem structure and the technologies involved so the results cannot be readily generalized. The computational speedup varies between 20 to more than 500 times, for a zero and 75% RES penetration, respectively, which can be explained by a more frequent cycling of the conventional thermal units in the high-RES case. The simulation results show that the computational speedup doesn't jeopardize accuracy. Both the number of online units, which serves as a proxy for the system inertia, and the loadability results, are in close agreement with more detailed UC formulations. This confirms the validity of the approach for long term future grid studies, where one is more interested in finding weak points in the system rather than in a detailed analysis of an individual operating condition. The MST presented here is used in Chapter 6 for detailed frequency stability assessment of the NEM.

Chapter 6

Future Grid Frequency Performance Assessment

An increasing penetration of relatively economical RES (such as PV and WG) will challenge future grid security due to their non-synchronous nature. Substituting synchronous generators with non-synchronous RES will result in reduced system inertia, which has adverse effects on system frequency performance. Frequency stability is defined as the ability of a power system to maintain steady frequency after a severe contingency, resulting in a considerable imbalance between generation and demand [100]. Increasing penetration of non-synchronous RES results in an increase in system dynamics' complexity, which makes it difficult to specify the worst case scenario for frequency assessment. In the wake of the uncertainty associated with these non-synchronous RES, even defining the worst case scenario is becoming a challenging task. Consequently, the traditional way of defining the worst case scenario to assess power system stability is no longer valid. This inherently makes it difficult to identify all vital conditions based on the widely accepted criterion for defining critical contingencies and critical points of operation. Thus, frequency performance of systems with high penetration of non-synchronous RES is profoundly affected due to the reduction in total inertia and governor response. Therefore, the system frequency control is adversely affected, which has an adverse effect on the frequency behaviour characterised by the rate of change of frequency (RoCoF) and frequency nadir [101–104].

The increasing complexity regarding frequency control due to the integration of RES should be dealt in a systematic way. There is a notable need for a frequency assessment framework that has the capability to evaluate the frequency performance for a large number of scenarios.

Remark on attribution: The work presented in this chapter resulted from a collaboration with another PhD student, Ahmad Shabir Ahmadyar. The author' contribution was in

developing the optimisation framework, including the identification of critical contingencies, the introduction of minimum inertia requirements. The literature review, load flow analysis and frequency assessment were carried out by Shabir.

6.1 Existing Literature for Frequency Performance

Restricting frequency within bounds is one of the critical factors for power system stability, but is one that is becoming increasingly challenging with higher penetration on non-synchronous RES [101–107]. WECC (an interconnection of the US west coast) stability assessment showed that 50 % non-synchronous instantaneous penetration (NSIP) degenerates frequency response when benchmarked against the existing practice [102]. Along similar lines, Ireland's transmission operator EirGrid has placed a 50 % NSIP limit to ensure that frequency deviations stay within bounds [105]. The above mentioned studies provide a good insight regarding the impacts of non-synchronous RES on system frequency, however they cannot be readily generalised. Other studies have shown that frequency performance is a serious emerging problem, particularly for small and stringy networks, for example, Ireland grid [103] and Australian NEM. Australian Energy Market Operator has recently listed frequency control as an immediate issue [107], owing to the long and weakly connected transmission system. Presently, eight frequency control and ancillary services markets are conjointly functioning alongside NEM spot market [108]. The primary role of these frequency control and ancillary services markets is to provide frequency support with 6 s, 1 min and 5 min speed responses. In the presence of frequency control and ancillary services and similar models, primary frequency control is not an immediate issue for future grid security. It is rather the rate of change of frequency (RoCoF) that is challenging for future grid frequency performance, resulting from lower inertia. This is also identified as one of the key reasons for the SA blackout [28]. Following the isolation of SA from the rest of the NEM on 28 September 2016, SA faced a low system inertia event resulting in a very steep RoCoF, which lead to a frequency drop below 47 Hz, triggering under frequency load shedding.

Steeper RoCoF does not give sufficient time for the activation and deployment of primary frequency response resulting in a tripping of RoCoF protection of generators. Consequently, the RoCoF becomes steeper and other synchronous generators also trip like falling dominos. Mechanical stress and maximum torque of machines also increase as RoCoF increases. It is also possible that if RoCoF is more than -1 Hz, the rotor of an under excited machine is unable to track the rapid decrease in the grid speed, thus losing the opposing force, which results in the machine's speedup and a pole slip [109]. It is also found in the literature that a

fast frequency event has a negative impact on combustion turbines because of the combustion lean-blowout [110].

Therefore, a frequency curtailment within limit is becoming increasingly challenging for power systems with higher non-synchronous RES penetration. To limit these impacts, the existing studies have proposed limiting the penetration of non-synchronous instantaneous penetration by requiring a certain portion of the power to come from synchronous generation, thus explicitly ensuring a specific level of system inertia [62, 111]. Along similar lines, studies [104, 112] proposed to include an explicit inertia constraint in market dispatch. It is vital to define inertia constraints precisely and identifying its limits. A comparison of different ways of defining inertia constraint and their impact on frequency are detailed in [113]. This work analyses the existing approaches for maintaining minimum inertia such as, meeting a minimum percentage of demand from synchronous generators and keeping a minimum amount of online synchronous generation. However, these approaches are not accurate as they ignore the inertia constant of synchronous generators and try to maintain the inertia by maintaining the dispatch levels. Furthermore, [113] provides a formulation of the inertia constraint based on the inertia constant of synchronous generators and the total system inertia requirement.

From the above discussion, one can conclude that with a high RES penetration, future grid frequency performance is becoming increasingly difficult to maintain. The existing literature deals with this issue in an ad hoc manner, instead of using more principled approaches, for example, limiting NSIP to ensure frequency limits. Existing literature lacks a systematic way of dealing with this subject and it is important to know the safe level of NSIP for a wide range of scenarios before drawing any general conclusions. With such an objective, this chapter proposes a time series analysis based frequency performance assessment framework. Using MST proposed in Chapter 5, extensive simulations are performed to assess the impact of RES on dispatch, and then a comprehensive scenario based sensitivity analysis is performed for selected nine RES penetration levels, which enabled an accurate assessment of the NEM frequency performance for all credible contingencies (CC). After the identification of the maximum NSIP from frequency performance of the NEM, a further step is made to restrict dispatch based on the dynamic constraint to keep in check the RoCoF and improve frequency performance.

6.2 Frequency Performance Assessment Framework

The frequency performance framework proposed in this chapter is based on [42, 43]. Algorithm 1 elaborates the salient features of the framework. It is capable of identifying and

Algorithm 1 Future grid Frequency Performance Assessment Framework

Inputs: Network data, generation data, ancillary service requirements (e.g. spinning reserve), wind, solar and demand traces for each scenario $s \in \mathcal{S}$ in the studied year.

```
for s ← 1, |S| do
    for t ← 1, |T| do
        Market simulation (generation dispatch);
        Identify credible contingencies;
        Load-flow analysis;
    end for
    for c ← 1, |C| do
        for t ← 1, |T| do
            Frequency performance assessment by;
            Considering all the credible contingencies;
        end for
    end for
end for
```

Outputs: Frequency performance indices (i.e. minimum RoCoF and frequency nadir) for each time slot $t \in \mathcal{T}$, for each sensitivity case $c \in \mathcal{C}$, and for each scenario $s \in \mathcal{S}$.

capturing the frequency response and other relevant aspects of the power system following a credible contingency, for a vast range of scenarios using a time series analysis.

6.2.1 Inputs and scenarios

Previous frequency performance assessments relied heavily upon deterministic studies considering only specific operating points [102]. Whereas, the framework presented here identifies principal challenges for future grid frequency performance utilising a large number of scenarios. For such a large number of scenarios, a simplified network model is more efficient and provides a balance between computation time and accuracy [104]. It is also valid to use a simplified grid model based on the fact that, under steady state, inertia and in turn frequency is a system variable and only depend upon online synchronous generators but not on generators' dispatch levels. Hence, a frequency variation across the network is negligible. The network under consideration, the Australian NEM, is more than 5000 km long , connecting five states (QLD, NSW, VIC, SA, and TAS) that are weakly interconnected. A simplified model of the NEM used for this study is presented in Fig. 6.1, represented each state as one bus in the network model. We consider year 2040 for simulation and thus existing interconnects are reinforced in the light of the AEMO 100 % renewable study [82]. Along similar lines of the BAU scenario described in Section 4.4.1, the current generation mix is considered as a base case with around 10 % of non-synchronous annual penetration (NSAP). However, generation is slightly modified to meet the demand requirement in 2040. Then progressively,

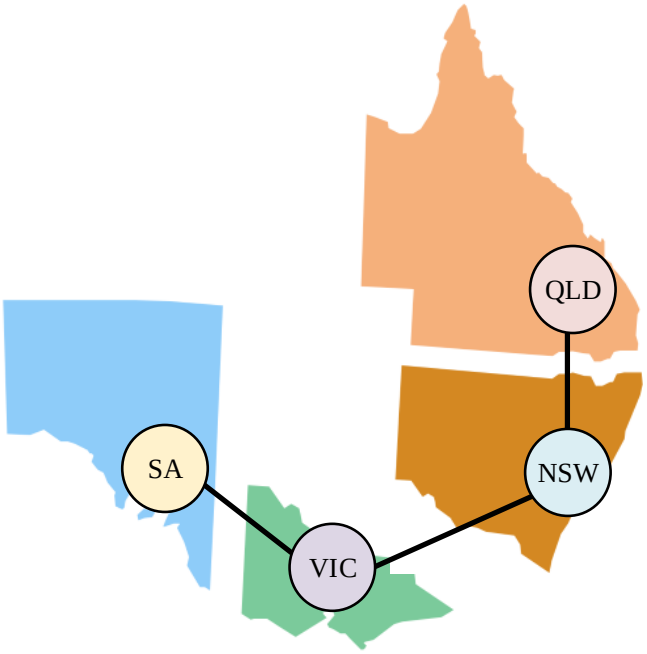

Fig. 6.1 Simplified NEM representation.

coal fired generators are retired and replaced by RES (WG, PV and CST) to increase NSAP to 90 %, following Australian 100 % renewable studies roadmap [33, 45, 82]. To limit the computation burden of the expensive time series analysis, nine distinct scenarios ($|\mathcal{S}| = 9$) are selected in a way that the non-synchronous annual penetration is incremented with a step size of 10 %. Each scenario is then analysed for one year ($|\mathcal{T}| = 8784$)[1] to capture the wide range possible variations on the generation side, inter seasonal and intra day demand and RES generation variations.

6.2.2 Market simulation

Line 1-6, Algorithm 1 captures market dynamics, which has a great influence on the power system operation, including frequency control [114]. The frequency stability dynamics is quite complex and influenced by many factors as follows [62]:

$$\frac{df}{dt} = \frac{f_0}{2I_s(t)} p_t^{cc} - \frac{f_0}{2I_s D_{load}} f, \tag{6.1}$$

where df/dt represents the RoCoF, f_0 is the system nominal frequency, p^{cc} is the size of credible contingency, D_{load} is the frequency damping of the system load, I_s is the system inertia and f represents the system frequency. The system inertia can be represented as

[1] Year 2040 is a leap year.

follows:

$$I_s(t) = \sum_{g \in \mathcal{G}^{syn}} s_{g,t} H_g S_g, \tag{6.2}$$

where, $g \in \mathcal{G}^{syn}$ represents the set of synchronous generators, H_g and S_g and $s_{g,t}$ represents the inertia constant, MVA rating and number of online units for generator g, respectively. As evident from the above equation, the time dependant system inertia will change based on the market commitment decision. Thus, to capture the relationship between the commitment decision and system inertia, market dispatch is executed using the MST proposed in Chapter 5. Market simulations modelling assumptions are the same as explained in Section 5.2.3. As, RES are bidding with zero SRMC, they can push synchronous generators out of the merit list, thereby resulting in smaller credible contingency events (such as loss of the largest generator or transmission line). Therefore, the dispatch level of a credible contingency is identified during the market simulations as follows[2]:

$$p_t^{cc} = \text{maximum}(p_{g,t}) \quad g \in \mathcal{G}^{syn}. \tag{6.3}$$

After running the market simulations, load flow analysis is performed, which provides the starting point for dynamic simulations.

6.2.3 Sensitivity cases and frequency performance assessment

A comprehensive stability assessment (line 7-13, Algorithm 1) is then carried out by taking into account the sensitivity of most vital components presented by equation (6.1) namely: (i) load model; (ii) size and (iii) location of contingency. Fig. 6.2 represents the scenarios and all the associated sensitivity cases. A constant impedance, current and power (ZIP) model is used as static load model, and denoted (Ls) [115], where as 60 % ZIP and 40 % induction machines are considered for dynamic load model (Ld) [116]. For a fixed contingency (Cf), the size of the largest in-feed generator currently operating in the NEM i.e. 666 MW [69], whereas for variable contingency (Cv), values obtained from equation (6.3) are used. All the above cases are considered in all four areas (i.e. QLD, NSW, VIC and SA). This gives us a total of nine scenarios ($|\mathcal{S}| = 9$) and and $2 \times 2 \times 4 = 16$ sensitivity cases; while yearly simulation are performed for 144 cases ($|\mathcal{C}| = 144$,$|\mathcal{T}| = 8784$), resulting in 1 264 896 simulation instances. As shown in Fig. 6.2, the following convention is used to distinguish between different cases: $NSxx - Ls/d, Cv/f, Location - Meter$; $\boldsymbol{Nsxx}$ is the NSAP varying from 10 % to 90 % with

[2]Due to the enormous computation burden only the biggest in-feed unit is examined as credible contingency and its operating point is considered. However, one can examine all nodes in the network to determine the node with the highest in-feed power for a more comprehensive analysis at the cost of a increased computation time.

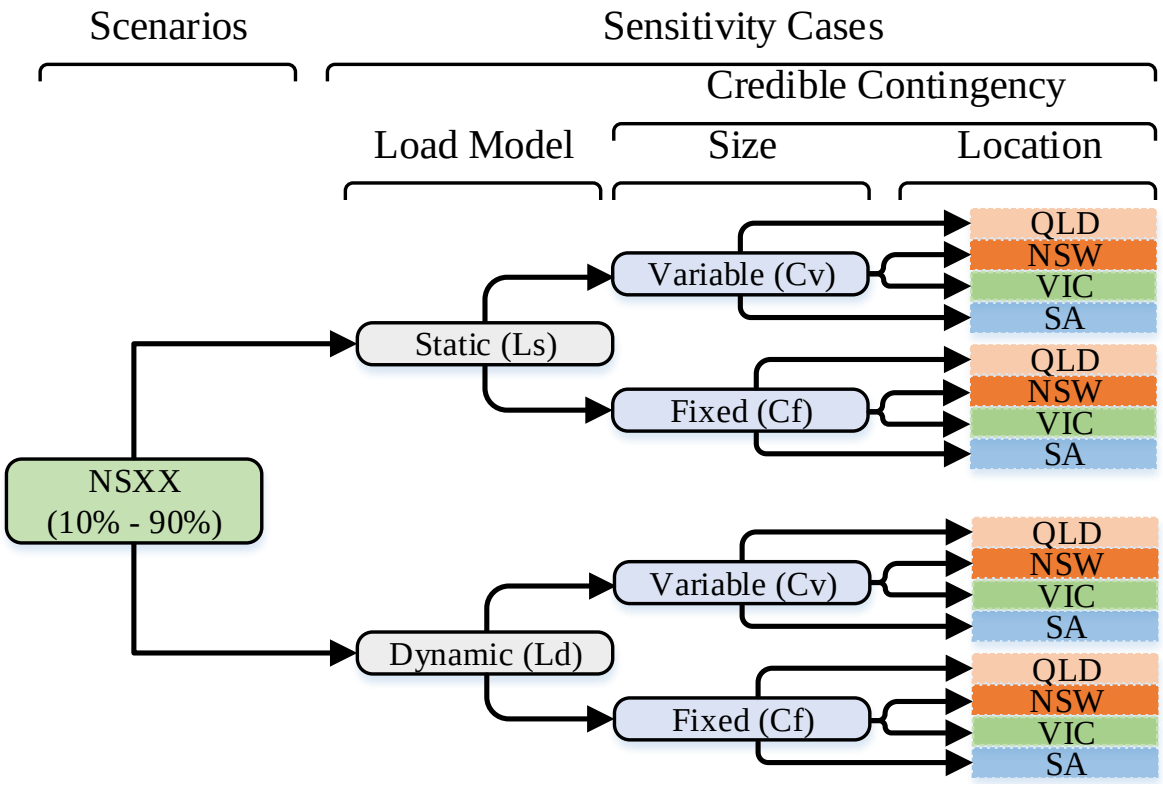

Fig. 6.2 Summary of scenarios and sensitivity cases, NSXX is the NSAP and varies from 10 % to 90 % with increment of 10

incremental step of 10 ; ***Ls/d*** distinguishes static (***Ls***) and dynamic ***Ld*** load models; ***Cv/f*** represents fixed ***Cf*** and variable ***Cv*** contingency size; **Location** is the location of credible contingency; and **Meter** is the bus where measurement is taken. An example is given as follows:

- $NS60 - LsCvVIC - QLD$: represents the case for 60 %; static load model is used; contingency is obtained from equation (6.3); credible contingency location is VIC; and measurement is done at QLD bus.

Furthermore, for frequency performance analysis, all synchronous generators are modelled with their governors, power system stabilisers and excitation systems [69, 113]. Also utility PV plants are modelled as full converter interfaced generators, and all WFs are moddeled as Type IV wind turbines.

6.2.4 Output

The proposed framework provides an information regarding the RoCoF and the frequency nadir for each simulated hour. These outputs are then used as indicators to estimate the range

of NSIP the Australian future grid can handle from a frequency performance point of view. The NSIP for every hour is calculated as follows:

$$\text{NSIP} = \frac{p_t^{\text{NS-RES}}}{p_t^{\text{NS-RES}} + p_t^{\text{syn}}}, \tag{6.4}$$

where p_t^{syn} and $p_t^{\text{NS-RES}}$ represents power dispatched from synchronous generators and non-synchronous RES, respectively.

6.3 Results and Discussion

Market dispatch and frequency performance results are discussed in this section.

6.3.1 Market dispatch

As explained previously, the current generation mix in the NEM, with about 10 % non-synchronous RES, is considered as the base case and annual market dispatch is calculated with different RES penetration. From theses simulations nine distinct cases are selected that provide non-synchronous RES penetration from 10 % to 90 % with an incremental step of 10. Note that non-synchronous RES penetration is aposteriori information and can not be calculated apriori, as the RES dispatch is limited by numerous factors, e.g. renewable resource availability in that particular year, network capacity, market limitations, reserve requirements etc. It was found out that in the presence of 10 % reserve constraint (5.3) non-synchronous RES penetration cannot be increase beyond 83 %; therefore for *NS*90 this constraint is removed from the market dispatch.

The impact of a high non-synchronous RES penetration on the primary frequency reserves and system inertia was evaluated as both serve as a proxy for the frequency nadir and the RoCoF [62]. With a higher non-synchronous RES penetration the system power reserve requirement gains importance and becomes a binding constraint more often as compared to cases with a lower non-synchronous RES penetration, as shown in Fig. 6.3. For cases *NS*40 to *NS*80 a negligible change in the lower limit of system inertia resulting from the reserve requirement becomes a binding constraint, which requires the system synchronous inertia to be maintained at specific level. However, in *NS*90 when dispatch is not restricted by (5.3), there is a sharp decrease in the minimum and the mean value of inertia as compared to *NS*80, as shown in Fig. 6.3. It is also interesting to note that with an increasing non-synchronous RES penetration not only the mean value of inertia decreases but its variance increases too. For example, the *NS*10 inertia histogram shape is close to a normal distribution with a maximum,

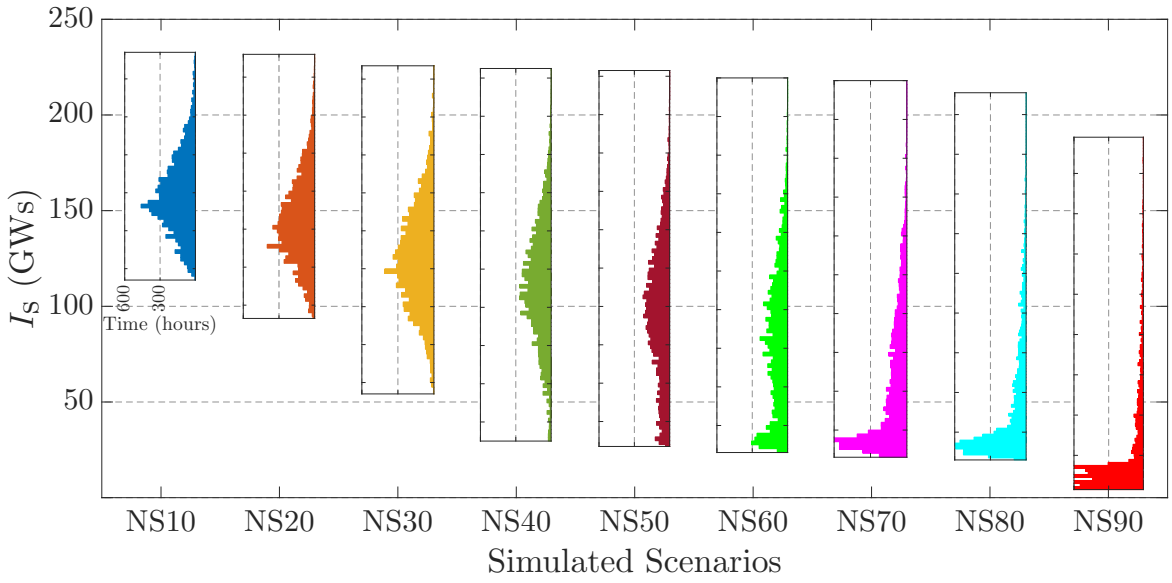

Fig. 6.3 Synchronous inertia histogram for all scenarios; histograms are drawn on same scale to maintain consistency.

mean and minimum value of 234 GW s, 159 GW s and 114 GW s, respectively. However, for the *NS*90 histogram, most of the hours (mean value 18 GW s) are concentrated toward the lower end (4 GW s) and long thin trailing tail extending to higher values (178 GW s). System primary reserves shown in Fig. 6.4 also verify the above discussion. Note that the system primary reserves trend for case NS90 is vastly different from the rest of the cases as seen in Fig. 6.4. In the presence of a 10 % reserve constraint, the non-synchronous RES penetration cannot be increased beyond 83 %. Hence, for the NS90 case only, the reserve constraint was eliminated resulting in much lower inertia and primary reserves as compared to the remaining cases. The NS90 case is interesting from the point that it shows the importance of the reserve constraint on the system inertia and primary reserves. The reductions in system primary reserves and inertia have significant deteriorating effects on frequency performance, as discussed in Section 6.3.2.

Fig. 6.5 shows the size of credible contingency for cases *NS*10 to *NS*90 obtained from (6.3). The average size of credible contingency decreases with the progressive increase of the non-synchronous RES penetration. In *NS*10, the size of credible contingency drops below 666 MW for around 10 % of the time, which increases to almost 95 % for *NS*80. For *NS*90, 95 % of the time there is no synchronous generator online, hence in this scenario credible contingency is set at minimum value, i.e. 333 MW. Note that for the case of fixed contingency, 666 MW is considered as credible contingency. Although the minimum value of credible contingency comes out to be 333 MW, as shown in Fig. 6.4, the minimum size of synchronous generator is much lower than this value; the minimum synchronous generator

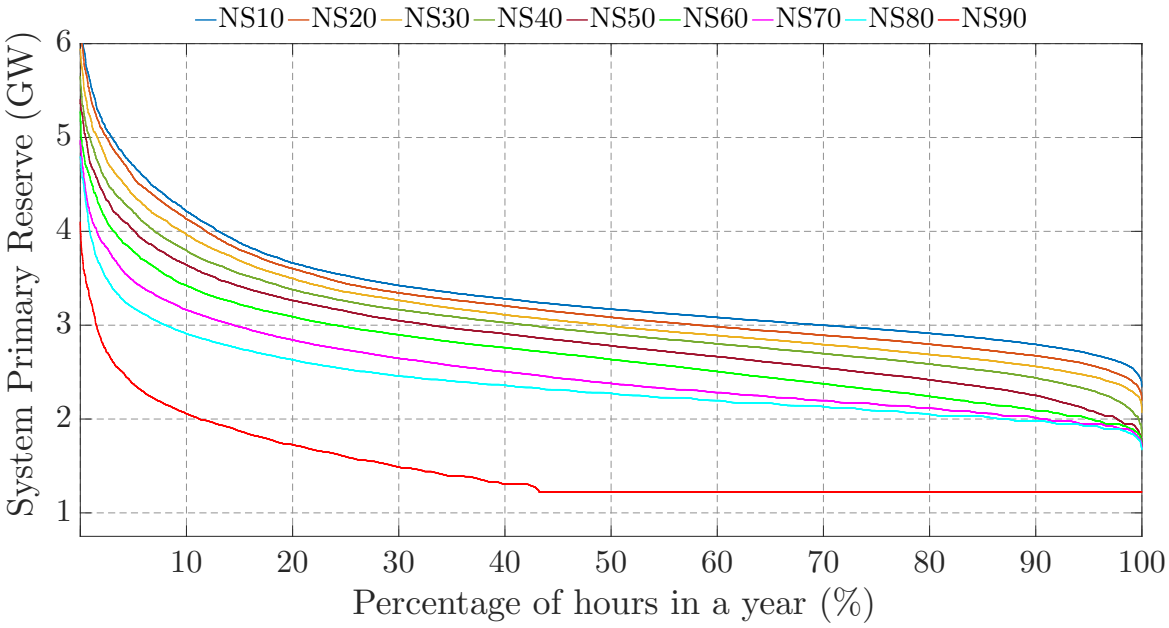

Fig. 6.4 System primary reserves for all scenarios.

assumed is OCGT with a maximum active power rating of 166 MW however, these are peaking plant and never set the value of credible contingency. In summary, power system frequency performance with a high non-synchronous RES penetration deteriorates with the decrease in system primary reserves and inertia, however it also improves due to the size reduction of the credible contingency. Therefore, it is important to include all these factors when performing a comprehensive frequency performance assessment. These dispatch results are then used to calculate load flow, which provides the basis for frequency performance assessment.

6.3.2 Frequency performance

For all cases, the frequency behaviour of the system following a credible contingency is analysed for the first 50 s. This enabled the assessment of the impact of system inertia and primary reserves reduction on frequency performance by assessing the RoCoF and the frequency nadir. Minimum RoCoF for all scenarios of $NSxx - LsCvQLD - QLD$ is summarised in Fig. 6.6. With higher penetration levels of RES, the RoCoF and system inertia decreases and observe that, with NSAP 60 % and above, the minimum RoCoF start to violate critical RoCoF (i.e 0.5 $\mathrm{Hz\,s^{-1}}$). For $NS90$, lack of spinning reserves results in lower levels of system inertia. Also some regions may face lower inertia events despite the fact that system inertia is quite high as shown in Fig. 6.6; simulations show that in such events, the RoCoF for these regions is also quite high. Case $NS90 - LsCvQLD - QLD$ shows the importance

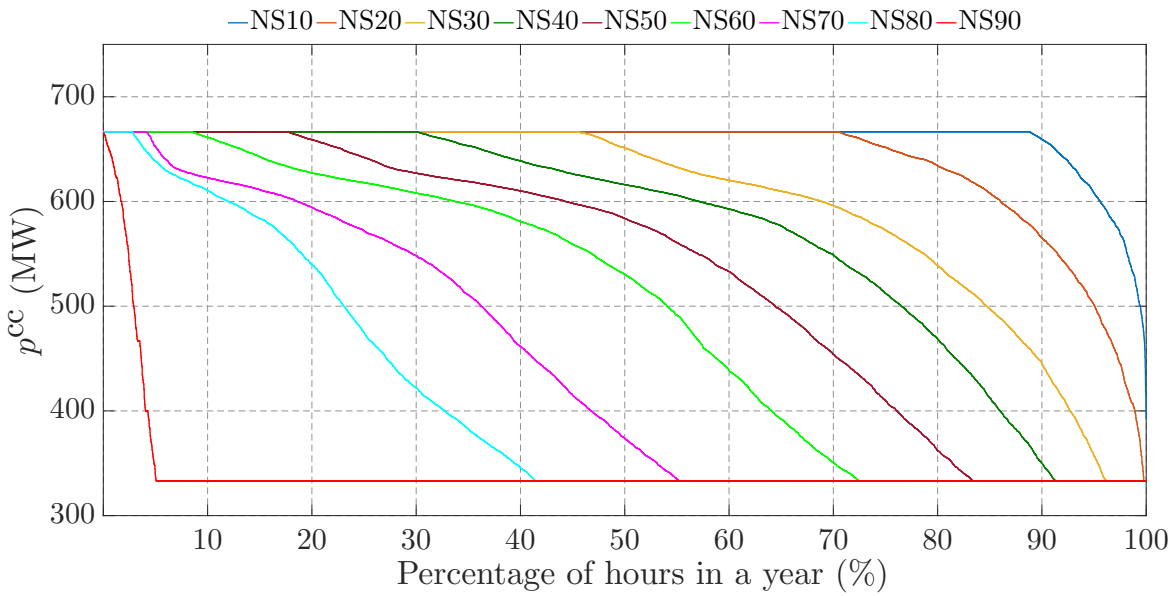

Fig. 6.5 Variable credible contingency (*Cv*) size obtained from equation (6.3).

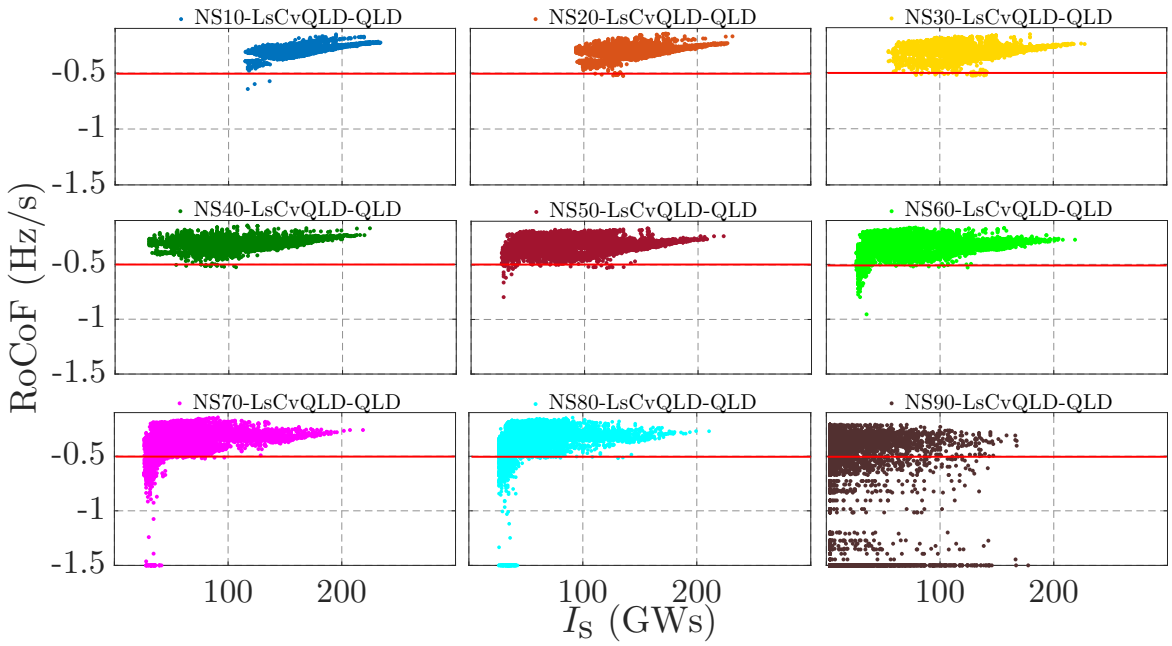

Fig. 6.6 Minimum RoCoF following the loss of credible contingency; red line shows critical RoCoF.

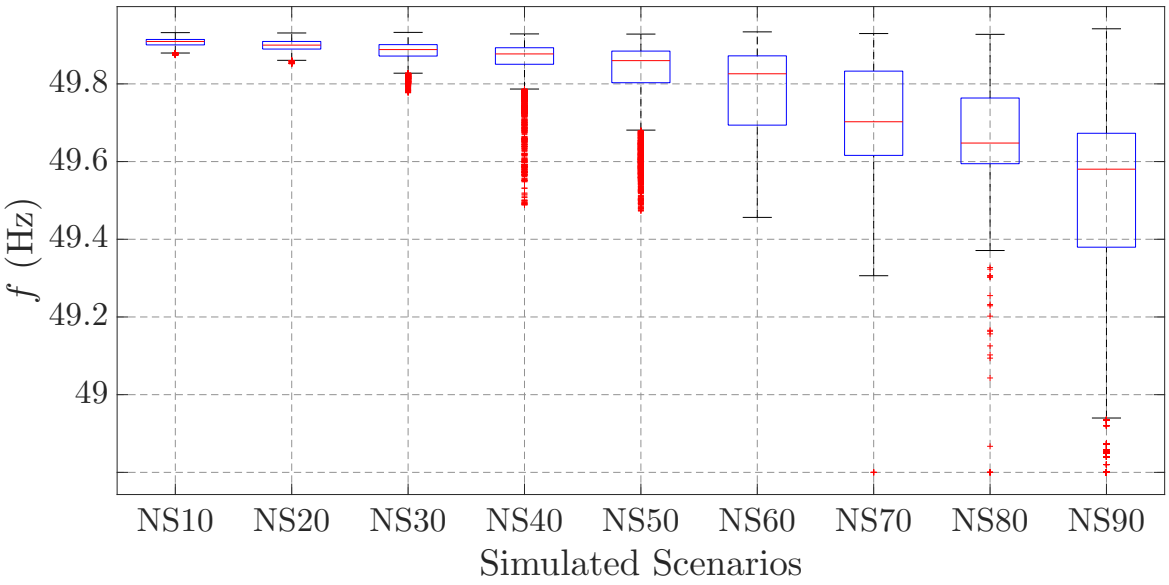

Fig. 6.7 Frequency nadir following loss of credible contingency for cases $NSxx-LsCvQLD-QLD$.

of the location of the inertia on system frequency. This point will be discussed later on in Section 6.4, presenting options for improving frequency performance. The frequency nadir also follows the same trend as the RoCoF; for NSAP 60 % and above, the number of hours that the frequency drops below 49.5 Hz[3] (minimum allowable frequency limit for power systems with the nominal frequency of 50 Hz) increases significantly. For $NS90$ even the mean value is close to 49.5 Hz, as shown in Fig. 6.7. It is interesting to see that the reduction in system inertia and primary reserves in Fig. 6.3 and Fig. 6.4 have an impact on the RoCoF and the frequency nadir of system shown in Fig. 6.6 and Fig. 6.7, respectively. Inertia is an important factor for frequency performance and serves as the proxy to the frequency behaviour of the system, however, it is not the only parameter and other parameters has to be considered before an accurate estimation of the NSIP limit can be defined. For illustration, in Fig. 6.6, scenario $NS60$, $NS70$ and $NS80$ shows that for the inertia levels between 30 GW s to 50 GW s, some cases violates minimum the RoCoF while others don't, suggesting that other factors also influence the outcome of frequency performance. These factors as mentioned in Section 6.2.3 along with their impacts are discussed as follows:

Impact of load model

The impact of load model on system frequency performance is significant and cannot be ignored. Fig. 6.8a shows the impact of static and dynamic load models for $NS80-$

[3]Nominal operating frequency of the NEM is 50 Hz.

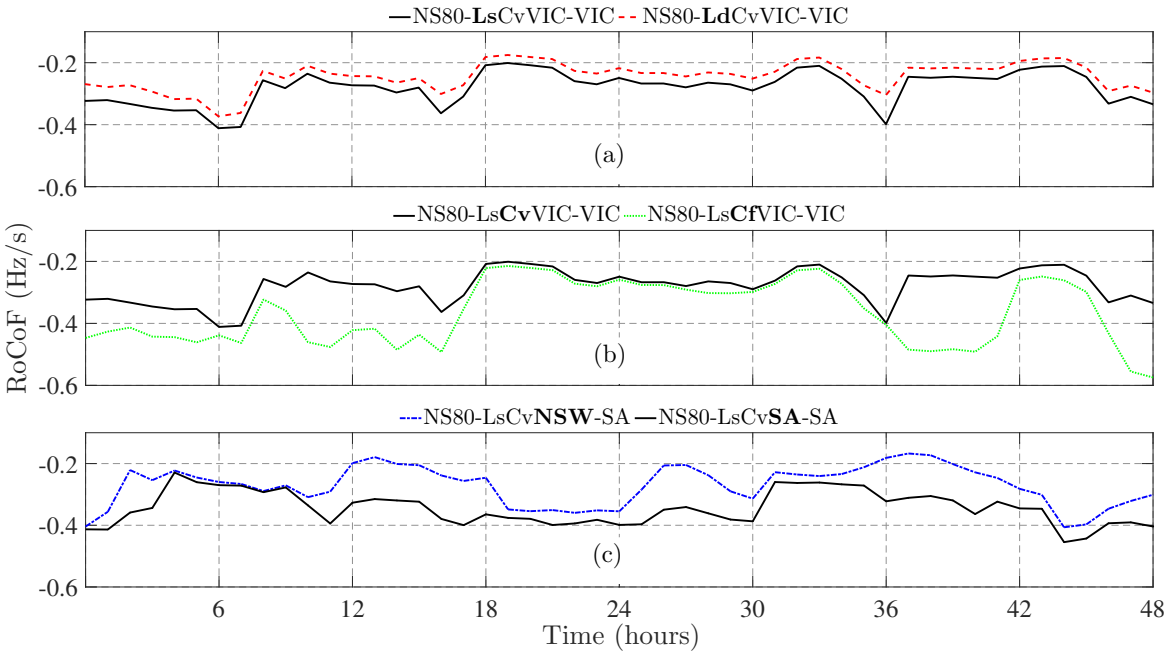

Fig. 6.8 RoCoF for two typical days considering sensitivity of: (a) load model, (b) credible contingency size and (c) credible contingency location.

$LxCvVIV-VIC$ on the RoCoF. System RoCoF drops more in case of a static load as compared to the dynamic load. This effect is more prominent during the interval of high NSIP and high demand resulting in lower system inertia and higher frequency damping of system load (D_{load}). Therefore, D_{load} in (6.1) becomes more dominant and the load dynamics becomes a significant factor. The deviation at hour 36 in Fig. 6.8a makes this point more prominent.

Impact of contingency size

Contingency size is an important factor for establishing power system frequency performance. Equation 6.1 shows a direct relationship between the size of credible contingency and the RoCoF. Furthermore, Fig. 6.5 shows a vast deviation between the variable (obtained from equation (6.3)) and the fixed contingency size. For $NS80$, only 5 % of the time the variable contingency (Cv) matches with the fixed contingency (Cf) size, whereas, for more than 55 % of the time is it almost half of the size a compared to the fixed contingency. Fig. 6.8b shows a comparison between the variable and the fixed contingency for two typical days, for the $NS80-LsCxVIV-VIC$ case. Note that the RoCoF is better in the case of a variable contingency size owing to the decrease in the credible contingency with the increase penetration of non-synchronous RES. This also highlights the need for a correct identification

of the credible contingency size and its importance on the frequency performance assessment of future grids.

Impact of contingency location

Contingency location is another important aspect to be considered in frequency performance assessment. Network strength plays an important role in this regard. Weakly connected end regions of the NEM (i.e. SA and QLD) are more vulnerable to an incident as compared to strongly connected NSW and VIC. Fig. 6.8c shows two cases for $NS80-LsCvXXX-SA$, first is when the contingency occurred in NSW and measurement is taken in SA bus and second, when contingency occurred in SA and measurement is also taken in SA bus. Observe that in the former case, the RoCoF is more severe. Hence, the location of contingency also play a vital role in assessment of the system frequency behaviour.

Impact of prosumers

As mentioned in Chapter 2, due to the increasing electricity cost and the decreasing PV-battery prices, the number of prosumers in the NEM is expected to rise, thus their impact on frequency performance cannot be ignored. For this purpose, 6.3 %, 8.6 %, 16 % and 22 % demand of NSW, VIC, QLD and SA is aggregated as prosumers. Furthermore, two sensitivity cases of 1.8 kW h and 3 kW h of battery storage per 1 kW of rooftop-PV are considered. In the presence of the prosumers system peak demand decreases and is shifted to the off peak hours as shown in Fig. 6.9a, that has important implications for system inertia and size of credible contingency. Prosumers utilise power from rooftop-PV, which pushes expensive synchronous generators out of the merit order, resulting in a decrease in system inertia as shown in Fig. 6.9b. However, with the increase in the number of prosumers, not only system inertia but also the size of credible contingency reduces, as shown in Fig. 6.9c. The overall effect of prosumers i.e. the reduction in inertia (deteriorating frequency behaviour) and the decrease in the size of the credible contingency (improving frequency behaviour) improves the system RoCoF as demonstrated in Fig. 6.9d. Also, frequency performance deteriorates negligibly for off peak intervals, where prosumers shift their energy requirements using battery storage. Moreover, it was observed that the cases with battery storage had the least amount of hours for which RoCoF limit is violated.

Outcome

System frequency depends on many time varying factors, making it difficult to define a safe level of NSIP that ensures stable operation. Therefore, it makes more sense to defining

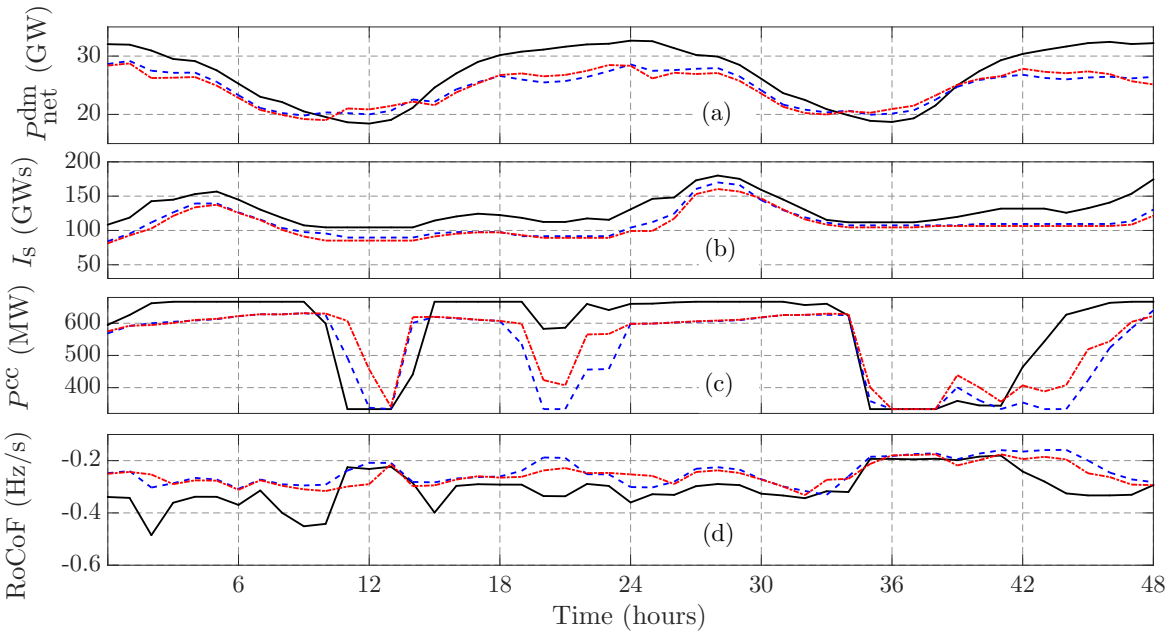

Fig. 6.9 Impact of prosumers with different battery storage on: (a) net system demand, (b) system inertia, (c) size of credible contingency and (d) RoCoF for two typical days for $NS80-LsCvVIC-VIC$.

a critical range of NSIP rather than a single number as shown in Fig. 6.10. The figure summarises the results of the most vulnerable cases, i.e. with the highest RoCoF violations found during the analysis of different sensitivity cases. The results indicated that the critical RoCoF $df_{\text{crt}}/dt = -0.5\,\text{Hz}\,\text{s}^{-1}$, the system critical NSIP range is around 60 % to 67 %, which can be increased up to 84 % if the critical RoCoF df_{crt}/dt is selected as $-1\,\text{Hz}\,\text{s}^{-1}$. However, these bounds can be improved as discussed next.

6.4 Improving Frequency Response

The frequency response of the system can be improved by restricting the dispatch, to meet the critical RoCoF limit. To acheive that, first, an global inertia constraint was introduced in the market model. However, the NEM is very long and weakly connected transmission network and the impact of the location of the inertia is important. Therefore, the global inertia constraint (designed to meet minimum level of inertia taking into account credible contingency and critical RoCoF) failed to control the RoCoF violation in certain regions of the network. To assure that critical the RoCoF is met for each region, a set of inertia restrictions is included in the market dispatch to ensure frequency performance for each

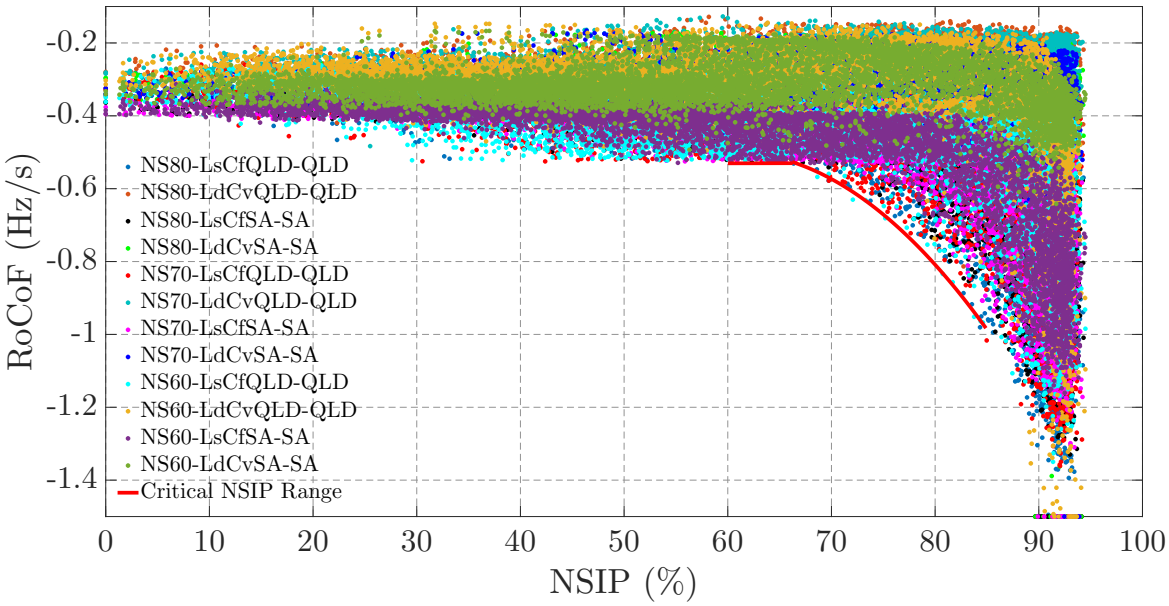

Fig. 6.10 Minimum RoCoF following a credible contingency based on NSIP .

region as follows:

$$I_{r,t} \geq \frac{f_0 p^{\text{cc}}_{r,t}}{2\,|df_{\text{crt}}/dt|}, \tag{6.5}$$

where I_r represents the minimum inertia requirement of region r established based on the critical RoCoF on df_{crt}/dt and the nominal system frequency f_0 and a credible contingency $p^{\text{cc}}_{r,t}$ calculated as follows:

$$p^{\text{cc}}_{r,t} = \text{maximum}(p_{g,t}) \quad g \in \{\mathcal{G}^{\text{syn}} \cap \mathcal{G}_r\}, \tag{6.6}$$

where $\mathcal{G}_r$ denotes the set of generators in region r. The inertia for each region is given by:

$$I_{\text{r,t}} = \sum_{\{g \in \mathcal{G}^{\text{syn}} \cap \mathcal{G}_r\}} s_{g,t} H_g S_g, \tag{6.7}$$

It is also worth mentioning that, (6.6) restricts the use of clustering implemented to improve the MST computation time. The inclusion of this constraint naively in to the MST framework would change the optimisation problem from linear to quadratic, due to the lack of power dispatch from each individual unit in the power plant. Hence for these cases, the unit clustering was dropped and the simulation took more time as compared to the previous cases. Simulations are then performed for critical RoCoF $df_{\text{crt}}/dt = -0.5\,\text{Hz}\,\text{s}^{-1}$ and results are summarised in Fig. 6.11. With an explicit inertia constraint, market decisions are made in such a way that the system inertia is improved for lower inertia cases and remained

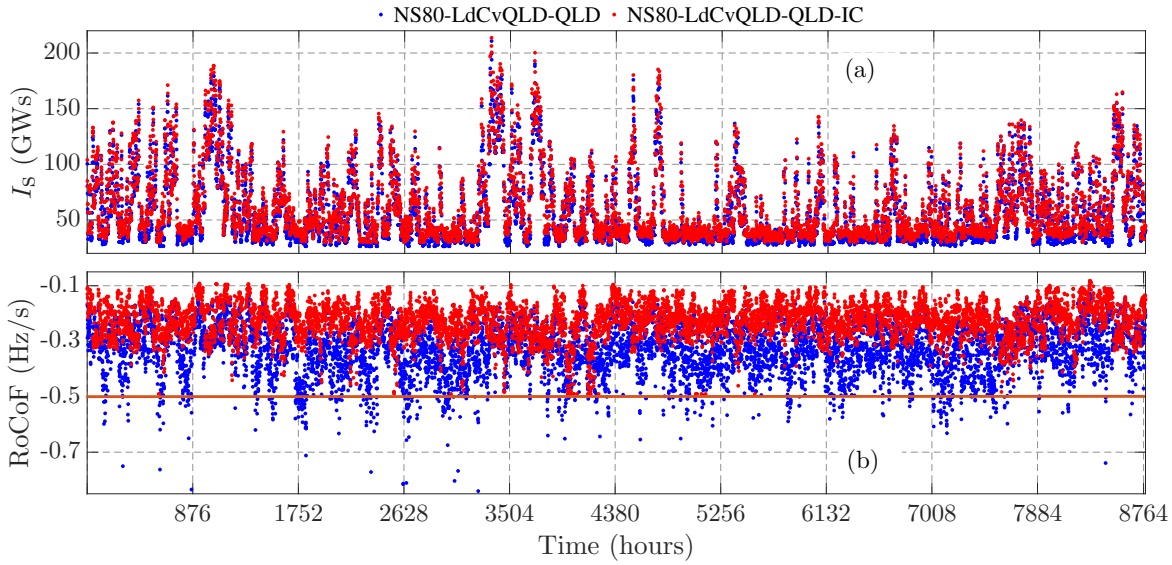

Fig. 6.11 Impact of dynamic inertia constraint on: (a) synchronous inertia of system and (b) RoCoF for QLD; brown line indicate the critical value of RoCoF.

almost unaltered for interval of high inertia events. Instances where previously for case $NS80-LdCvQLD-QLD$ the RoCoF violations are observed are rectified. In the case with inertia constraint $NS80-LdCvQLD-QLD-IC$ no violation of the critical RoCoF are observed. However the inclusion of these constraints to improve system frequency performance comes with the price of addition RES spillage, resulting in a 380 GW of additional spillage from WFs. Hence, for a higher non-synchronous RES penetration, there exists a trade off between frequency performance and RES energy spillage.

6.5 Summary

Utilising the MST presented in Chapter 5, a range of scenarios were analysed to understand the impact of non-synchronous RES on system frequency performance. An accurate estimation of the NSAP is difficult due to factors like weather and market conditions. Therefore, simulations are first performed for different RES penetration levels. Second, nine distinct scenarios were selected such that the increase in the NSAP changes from the present case (around 10 %) to 90 % with a step size of approximately 10. Furthermore, framework for future grid frequency performance assessment is also described in this chapter. This framework is used to perform a comprehensive assessment the frequency performance of the NEM and to identify a critical range of the NSIP that the NEM can accommodate. It also shows that factors such as load model, contingency location and size play a vital role in such studies and can vary from time to time. Therefore, to compensate for these changes and for higher

non-synchronous RES penetrations, a dynamic inertia constraint is proposed that restricts the dispatch to keep the frequency within permissible bounds at the cost of energy curtailment.

Chapter 7

Conclusion

The main contribution of the dissertation is a fast generic market simulation tool (MST) suitable for future grid (FG) scenario analysis that considers DC power flow, utility storage, prosumers, concentrated solar thermal (CST) and minimum inertia requirements. This tool is market structure agnostic, making it suitable for long-term studies, characterised by a high degree of uncertainty about future market structure. Unlike the existing literature on future grid scenario analysis, this dissertation explicitly considers network constraints that are important for stability studies and focuses on the incorporation of prosumers within the optimisation framework. The integration of high penetration of renewable energy resources is challenging from both balancing and stability points of view. The most significant advantage of the presented MST is its flexibility to incorporate a wide range of emerging technologies. Therefore, policy-makers and system planners use it to provide a better understanding of the critical impacts of emerging technologies on future grids.

Starting from the standard unit commitment (UC) model, numerous simplifications are proposed for computational speed-up, as detailed out in Section 1.2. In the future, prosumers will likely be one of the key players in electricity markets. Thus, a mathematically principled way of establishing prosumers' behaviour and capturing their interaction with the electricity market is proposed in Chapter 2. This provides a vital step towards our understanding of the effect of a collective prosumers' behaviour on system dispatch.

Simulations are then performed to demonstrate the efficacy of the model. Results show that the proposed model behaves as expected; in particular, price-anticipating prosumers are: first, consuming power from rooftop-photovoltaic (PV); second, storing excess energy from rooftop-PV to batteries; third, leverage flexibility from their batteries to charge them when electricity price is low and utilising this energy during peak hours.

However, the prosumers' model presented in Chapter 2 ignores network constraints. Simple copper plate models do provide sensible results for balancing studies, however they

proved insufficient for stability studies. Chapter 3 proposes the same prosumers model with an explicit network representation.Two case studies are investigated looking at different prosumers strategies. In the first, aggregated consumers can exchange energy with the grid. This resulted in significant additional ramp stress on generators. Also, in the absence of an explicit transmission pricing, allowing feeding power from prosumer aggregators can create perverse outcomes, such as power exchange (using transmission network) between aggregators located in different parts of the network. To avoid these complications in the second, case study, prosumer aggregators on different buses are not allowed to send power to the bulk grid. Simulations are then performed using a simplified 14-generator model of the NEM, to test the model efficacy and to study the impact of renewable energy sources (RES) and prosumers on voltage stability.

In contrast to Chapter 3 (exploring flexibility from prosumers), Chapter 4 explores flexibility options from a generations side. Concentrated solar thermal plant presents a good solution regarding flexibility. Chapter 4 explores this flexibility and proposes a new institutional arrangement to exploit generation flexibility in FGs. In particular, non-dispatchable RES are not allowed to bid directly into the market but through a renewable energy aggregator. In a case study, an aggregator comprising CST and PV utilises the flexibility provided by thermal energy storage of CST to maximise profits for both CST and PV while abiding the market and network constraints. Results show that such methods have the potential to mitigate some of the problems associated with intermittent nature of RES.

The above contributions to state of the art are combined in Chapter 5, which presents a comprehensive MST suitable for FG scenario analysis. The inclusion of utility storage, network, prosumers, minimum inertia requirement and CST, however, adds a significant burden to the computation complexity. To improve computational efficiency, techniques such as, unit clustering, constraint clipping and rolling horizon are proposed. The results indicate that these techniques significantly reduce the computation time without jeopardising the accuracy.

An increasing penetration of non-synchronous RES can reduce system inertia, which deteriorates power system frequency performance. Chapter 6 first, provides a comprehensive frequency stability assessment framework followed by comprehensive simulations to establish a critical limit of non-synchronous instantaneous penetration. Results suggest that this critical range depends on range of factors like load model, contingency location and contingency size. Finally, a dynamic inertia constraint is proposed to restrict the dispatch based on the maximum allowed rate of change of frequency (RoCoF). This also confirms the need for comprehensive studies to identify critical issues and thus highlighting the potential role, flexibility and usefulness of the presented MST.

The MST developed in this thesis provides a powerful tool for policy-makers and system planners to analyse a wide range of future scenarios with different emerging technologies. It does not need to specify the market structure, and this makes it useful for future grid studies. The integration of prosumers within the optimisation framework is one of the most crucial aspects of the presented work. This will be helpful in answering some of the critical questions about prosumers' behaviour and offers a platform for the integration of RES by harnessing the prosumers' flexibility. The dissertation focuses on future grid scenario studies. Also, the state of the art is improved in terms of establishing new models capable of modelling the impact of prosumers' strategy and reflecting this in the generation dispatch. It is also improved in terms of exploring new control strategies and arrangement to deal with intermittent nature of RES and proposing a flexible and fast market simulation tool that is suitable for future grid scenario analysis. Comprehensive frequency performance assessment presented in this dissertation is only one of the examples of the application of the proposed MST and we hope that it will be used in further studies to inform a better policy making to enable a better and prosperous future.

References

[1] F. Ramos, C. Cañizares, and K. Bhattacharya, "Effect of price responsive demand on the operation of microgrids," in *18th International Conference on the Power Systems Computation (PSCC 2014)*, Aug 2014.

[2] D. Bertsimas, E. Litvinov, X. A. Sun, J. Zhao, and T. Zheng, "Adaptive Robust Optimization for the Security Constrained Unit Commitment Problem," *IEEE Transactions on Power Systems*, vol. 28, pp. 52–63, Feb. 2013.

[3] J. M. Arroyo and A. J. Conejo, "Optimal response of a thermal unit to an electricity spot market," *IEEE Transactions on Power Systems*, vol. 15, no. 3, pp. 1098–1104, 2000.

[4] Carrio, x, M. n, and J. M. Arroyo, "A computationally efficient mixed-integer linear formulation for the thermal unit commitment problem," *Power Systems, IEEE Transactions on*, vol. 21, no. 3, pp. 1371–1378, 2006.

[5] R. Gollmer, M. P. Nowak, W. Römisch, and R. Schultz, "Unit commitment in power generation – a basic model and some extensions," *Annals of Operations Research*, vol. 96, no. 1, pp. 167–189, 2000.

[6] K. Hara, M. Kimura, and N. Honda, "A method for planning economic unit commitment and maintenance of thermal power systems," *IEEE Transactions on Power Apparatus and Systems*, vol. PAS-85, no. 5, pp. 427–436, 1966.

[7] N. Langrene, W. v. Ackooij, and F. Breant, "Dynamic constraints for aggregated units: Formulation and application," *IEEE Transactions on Power Systems*, vol. 26, no. 3, pp. 1349–1356, 2011.

[8] J. Garcia-Gonzalez, R. M. R. d. l. Muela, L. M. Santos, and A. M. Gonzalez, "Stochastic joint optimization of wind generation and pumped-storage units in an electricity market," *IEEE Transactions on Power Systems*, vol. 23, no. 2, pp. 460–468, 2008.

[9] B. S. Palmintier and M. D. Webster, "Heterogeneous unit clustering for efficient operational flexibility modeling," *IEEE Transactions on Power Systems*, vol. 29, no. 3, pp. 1089–1098, 2014.

[10] A. Tuohy, P. Meibom, E. Denny, and M. O'Malley, "Unit commitment for systems with significant wind penetration," *Power Systems, IEEE Transactions on*, vol. 24, no. 2, pp. 592–601, 2009.

[11] B. Palmintier and M. Webster, "Impact of unit commitment constraints on generation expansion planning with renewables," in *2011 IEEE Power and Energy Society General Meeting*.

[12] A. Shortt, J. Kiviluoma, and M. O. Malley, "Accommodating variability in generation planning," *IEEE Transactions on Power Systems*, vol. 28, no. 1, pp. 158–169, 2013.

[13] S. A. Kazarlis, A. Bakirtzis, and V. Petridis, "A genetic algorithm solution to the unit commitment problem," *IEEE transactions on power systems*, vol. 11, no. 1, pp. 83–92, 1996.

[14] N. P. Padhy, "Unit commitment-a bibliographical survey," *IEEE Transactions on Power Systems*, vol. 19, no. 2, pp. 1196–1205, 2004.

[15] F. N. Lee, "Short-term thermal unit commitment-a new method," *IEEE Transactions on Power Systems*, vol. 3, no. 2, pp. 421–428, 1988.

[16] T. Senjyu, K. Shimabukuro, K. Uezato, and T. Funabashi, "A fast technique for unit commitment problem by extended priority list," *IEEE Transactions on Power Systems*, vol. 18, no. 2, pp. 882–888, 2003.

[17] Z. Ouyang and S. M. Shahidehpour, "An intelligent dynamic programming for unit commitment application," *IEEE Transactions on Power Systems*, vol. 6, no. 3, pp. 1203–1209, 1991.

[18] T. S. Dillon, K. W. Edwin, H. D. Kochs, and R. J. Taud, "Integer programming approach to the problem of optimal unit commitment with probabilistic reserve determination," *IEEE Transactions on Power Apparatus and Systems*, vol. PAS-97, no. 6, pp. 2154–2166, 1978.

[19] F. Zhuang and F. D. Galiana, "Unit commitment by simulated annealing," *IEEE Transactions on Power Systems*, vol. 5, no. 1, pp. 311–318, 1990.

[20] A. Merlin and P. Sandrin, "A new method for unit commitment at electricite de france," *IEEE Transactions on Power Apparatus and Systems*, vol. PAS-102, no. 5, pp. 1218–1225, 1983.

[21] M. Tahanan, W. van Ackooij, A. Frangioni, and F. Lacalandra, "Large-scale Unit Commitment under uncertainty," *4OR - A Quarterly Journal of Operations Research*, vol. 13, pp. 115–171, Jan. 2015.

[22] N. Chowdhury and R. Billinton, "Unit commitment in interconnected generating systems using a probabilistic technique," *IEEE Transactions on Power Systems*, vol. 5, no. 4, pp. 1231–1238, 1990.

[23] G. B. Sheblé, T. T. Maifeld, K. Brittig, G. Fahd, and S. Fukurozaki-Coppinger, "Unit commitment by genetic algorithm with penalty methods and a comparison of lagrangian search and genetic algorithm—economic dispatch example," *International Journal of Electrical Power & Energy Systems*, vol. 18, no. 6, pp. 339–346, 1996.

[24] Y. Hong-Tzer, Y. Pai-Chuan, and H. Ching-Lien, "Evolutionary programming based economic dispatch for units with non-smooth fuel cost functions," *IEEE Transactions on Power Systems*, vol. 11, no. 1, pp. 112–118, 1996.

[25] N. S. Sisworahardjo and A. A. El-Keib, "Unit commitment using the ant colony search algorithm," in *Power Engineering 2002 Large Engineering Systems Conference on, LESCOPE 02*.

[26] L. L. Garver, "Power generation scheduling by integer programming-development of theory," *Transactions of the American Institute of Electrical Engineers. Part III: Power Apparatus and Systems*, vol. 81, no. 3, pp. 730–734, 1962.

[27] L. Zhang, T. Capuder, and P. Mancarella, "Unified unit commitment formulation and fast multi-service lp model for flexibility evaluation in sustainable power systems," *IEEE Transactions on Sustainable Energy*, vol. 7, no. 2, pp. 658–671, 2016.

[28] Australian Energy Market Operator (AEMO), "Black System South Australia 28 September 2016. Third Preliminary Report.," report, 2016.

[29] L. Fahey and R. M. Randall, *Learning From the Future*. Wiley, 1998.

[30] J. Foster, C. Froome, C. Greig, O. Hoegh-Guldberg, P. Meredith, L. Molyneaus, T. Saha, L. Wagner, and B. Ball, "Delivering a competitive Australian power system Part 2: The challenges, the scenarios," Tech. Rep. Oct, 2013.

[31] G. Sanchis, "e-Highway2050: Europe's future secure and sustainable electricity infrastructure. Project results.," tech. rep., 2015.

[32] B. Elliston, J. Riesz, and I. MacGill, "What cost for more renewables? The incremental cost of renewable generation – An Australian National Electricity Market case study," *Renewable Energy*, vol. 95, pp. 127 – 139, 2016.

[33] M. Wright and P. Hearps, "Zero Carbon Australia Stationary Energy Plan," report, The University of Melbourne Energy Research Institute, 2010.

[34] B. Elliston, I. MacGill, and M. Diesendorf, "Least Cost 100% Renewable Electricity Scenarios in the Australian National Electricity Market," *Energy Policy*, vol. 59, pp. 270–282, Aug. 2013.

[35] C. Budischak, and et al., "Cost-Minimized Combinations of Wind Power, Solar Power and Electrochemical Storage, Powering the Grid up to 99.9% of the Time," *Journal of Power Sources*, vol. 225, pp. 60–74, Mar. 2013.

[36] I. Mason, S. Page, and A. Williamson, "A 100% renewable electricity generation system for New Zealand utilising hydro, wind, geothermal and biomass resources," *Energy Policy*, vol. 38, no. 8, pp. 3973–3984, 2010.

[37] Australian Energy Market Operator (AEMO), "100 per cent renewable study - modelling outcomes," tech. rep., 2013.

[38] Greenpeace Germany, "PowE[R] 2030 A European Grid for 3/4 Renewable Energy by 2030," report, 2014.

[39] R. Doherty, "All-Island Grid Study Workstream 2A-High level assessment of suitable generation portfolios for the All-Island system in 2020," report, Department of communications, marine and natural resources and the department of enterprise, trade and investment, January 2008.

[40] P. Denholm and M. Hand, "Grid flexibility and storage required to achieve very high penetration of variable renewable electricity," *Energy Policy*, vol. 39, no. 3, pp. 1817–1830, 2011.

[41] E. K. Hart and M. Z. Jacobson, "A monte carlo approach to generator portfolio planning and carbon emissions assessments of systems with large penetrations of variable renewables," *Renewable Energy*, vol. 36, no. 8, pp. 2278–2286, 2011.

[42] H. Marzooghi, D. J. Hill, and G. Verbic, "Performance and Stability Assessment of Future Grid Scenarios for the Australian NEM," in *Power Engineering Conference (AUPEC), 2014 Australasian Universities*.

[43] R. Liu, G. Verbič, J. Ma, and D. J. Hill, "Fast stability scanning for future grid scenario analysis," *IEEE Transactions on Power Systems*, vol. 33, pp. 514–524, Jan 2018.

[44] H. Marzooghi, G. Verbič, and D. J. Hill, "Aggregated demand response modelling for future grid scenarios," *Sustainable Energy, Grids and Networks*, vol. 5, pp. 94–104, 2016.

[45] D. J. Riesz, D. B. Elliston, D. P. Vithayasrichareon, and A. P. I. MacGill, "100% Renewables in Australia," research summary, March 2016.

[46] AEMO, "Detailed Summary of 2015 Electricity Forecasts," report, 2015.

[47] S. Lewis, "Carnarvon High PV Penetration Case Study," report, 2012.

[48] R. Tonkoski, D. Turcotte, and T. H. El-Fouly, "Impact of high PV penetration on voltage profiles in residential neighborhoods," *Sustainable Energy, IEEE Transactions on*, vol. 3, no. 3, pp. 518–527, 2012.

[49] CSIRO, "Change and Choice, The Future Grid Forum's Analysis of Australia's Potential Electricity Pathways to 2050," report, 2013.

[50] EPRI, "The Integrated Grid Realizing the Full Value of Central and Distributed Energy Resources," report, 2014.

[51] T. Szatow, and D. Moyse, "What Happens When We Un-Plug? Exploring the Consumer and Market Implications of Viable, off-Grid Energy Supply, Research Phase 1: Identifying off-Grid Tipping Points," tech. rep., Energy for the People and ATA, 2014.

[52] Rocky Mountain Institute, Homer Energy and Cohnreznick Think Energy, "The Economics of Grid Defection, When and Where Distributed Solar Generation Plus Storage Competes with Traditional Utility Service," report, 2014.

[53] Australian Energy Market Operator (AEMO), "Emerging Technologies Information Paper, National Electricity Forecasting Report," tech. rep., 2015.

[54] J. Aghaei and M.-I. Alizadeh, "Demand response in smart electricity grids equipped with renewable energy sources: A review," *Renewable and Sustainable Energy Reviews*, vol. 18, no. 0, pp. 64 – 72, 2013.

[55] E. Veldman, M. Gibescu, H. J. Slootweg, and W. L. Kling, "Scenario-based modelling of future residential electricity demands and assessing their impact on distribution grids," *Energy Policy*, vol. 56, pp. 233–247, 2013.

[56] Heussen, Kai and Koch, Stephan and Ulbig, Andreas and Andersson, Göran, "Unified system-level modeling of intermittent renewable energy sources and energy storage for power system operation," *Systems Journal, IEEE*, vol. 6, no. 1, pp. 140–151, 2012.

[57] C.-L. Su and D. Kirschen, "Quantifying the effect of demand response on electricity markets," *Power Systems, IEEE Transactions on*, vol. 24, no. 3, pp. 1199–1207, 2009.

[58] N. Li, L. Chen, and S. H. Low, "Optimal demand response based on utility maximization in power networks," in *Power and Energy Society General Meeting, 2011 IEEE*, pp. 1–8, IEEE.

[59] M. Gonzalez Vaya and G. Andersson, "Optimal bidding strategy of a plug-in electric vehicle aggregator in day-ahead electricity markets under uncertainty," *Power Systems, IEEE Transactions on*, vol. 30, no. 5, pp. 2375–2385, 2015.

[60] B. Biegel, L. H. Hansen, P. Andersen, and J. Stoustrup, "Primary control by on/off demand-side devices," *Smart Grid, IEEE Transactions on*, vol. 4, no. 4, pp. 2061–2071, 2013.

[61] K. Bruninx, D. Patteeuw, E. Delarue, L. Helsen, and W. D'haeseleer, "Short-term demand response of flexible electric heating systems: the need for integrated simulations," in *European Energy Market (EEM), 2013 10th International Conference on the*, pp. 1–10, IEEE.

[62] P. Kundur, *Power System Stability and Control*. Power System Engineering, McGraw-Hill, Inc., 1994.

[63] T. Van Cutsem, and C. Vournas, *Voltage Stability of Electric Power Systems*. Kluwer international series in engineering and computer science, Springer, 1998.

[64] M. Zugno, J. M. Morales, P. Pinson, and H. Madsen, "A bilevel model for electricity retailers' participation in a demand response market environment," *Energy Economics*, no. 36, pp. 182–197, 2013.

[65] H. Marzooghi, D. J. Hill, and G. Verbič, "Aggregated Effect of Price-Taking Users Equipped with Emerging Demand-Side Technologies on Performance of Future Grids," in *2016 IEEE International Conference on Power System Technology (POWERCON)*, 2016.

[66] H. Tischer, and G. Verbič, "Towards a Smart Home Energy Management System-A Dynamic Programming Approach," in *Innovative Smart Grid Technologies Asia*, 2011.

[67] A. C. Chapman, G. Verbič, and D. J. Hill, "Algorithmic and strategic aspects to integrating demand-side aggregation and energy management methods," *IEEE Transactions on Smart Grid*, vol. 7, pp. 2748–2760, Nov 2016.

[68] H. Marzooghi, G. Verbic, and D. J. Hill, "Aggregated effect of demand response on performance of future grid scenarios," in *PowerTech, 2015 IEEE Eindhoven*, pp. 1–6, IEEE.

[69] M. Gibbard and D. Vowles, "Simplified 14-generator model of the SE Australian power system," report, The University of Adelaide, South Australia, 2010.

[70] A. Tasman, "Fuel resource, new entry and generation costs in the nem," *ACIL Tasman Melbourne*, 2009.

[71] A. Frontier Economics Pty. Ltd., "Input assumptions for modelling wholesale electricity costs," 2013.

[72] Australian Energy Market Operator (AEMO), "2012 NTNDP Assumptions and Inputs," tech. rep., 2012.

[73] Morgan Stanley, "Australia Utilities Asia Insight: Solar & Batteries," tech. rep., 2016.

[74] Energy Networks Australia and CSIRO, "Electricity Network Transformation Roadmap: Key Concepts Report," Tech. Rep. December, 2016.

[75] B. Kampman, M. Afman, and J. Blommerde, "The potential of energy citizens in the European Union," tech. rep., CE Delft, 2016.

[76] S. Mathieu, Q. Louveaux, D. Ernst, and B. Cornelusse, "A quantitative analysis of the effect of flexible loads on reserve markets," in *18th International Conference on the Power Systems Computation (PSCC 2014)*, Aug 2014.

[77] O. Mégel, J. L. Mathieu, and G. Andersson, "Scheduling distributed energy storage units to provide multiple services under forecast error," *International Journal of Electrical Power & Energy Systems*, vol. 72, pp. 48 – 57, 2015.

[78] AEMO, "Planning Methodology and Input Assumptions," report, 2014.

[79] AEMO, "Integrating renewable energy - wind integration studies report for nem," 2013.

[80] E. Vaahedi, C. Fuchs, W. Xu, Y. Mansour, H. Hamadanizadeh, and G. K. Morison, "Voltage stability contingency screening and ranking," *IEEE Transactions on Power Systems*, vol. 14, pp. 256–265, Feb 1999.

[81] K. Clark, N. W. Miller, and J. J. Sanchez-Gasca, "Modeling of GE Wind Turbine Generators for Grid Studies," tech. rep., 2013.

[82] Australian Energy Market Operator (AEMO), *100 Per Cent Renewables Study–Modelling Outcomes, 2013*.

[83] A. Olson, A. Mahone, E. Hart, J. Hargreaves, R. Jones, N. Schlag, G. Kwok, N. Ryan, R. Orans, and R. Frowd, "Halfway there: Can california achieve a 50pp. 41–52, 2015.

[84] P. Denholm and R. M. Margolis, "Evaluating the limits of solar photovoltaics (pv) in electric power systems utilizing energy storage and other enabling technologies," *Energy Policy*, vol. 35, no. 9, pp. 4424–4433, 2007.

[85] T. W. Haring, M. A. Bucher, A. Ratha, and G. Andersson, "On wind farm operation with third-party storage,"

[86] J. L. Gonzalez, I. Dimoulkas, and M. Amelin, "Operation planning of a csp plant in the spanish day-ahead electricity market," in *European Energy Market (EEM), 2014 11th International Conference on the*, pp. 1–5, IEEE.

[87] H. L. Zhang, J. Baeyens, J. Degrève, and G. Cacères, "Concentrated solar power plants: Review and design methodology," *Renewable and Sustainable Energy Reviews*, vol. 22, pp. 466–481, 2013.

[88] E. Lizarraga-Garcia, A. Ghobeity, M. Totten, and A. Mitsos, "Optimal operation of a solar-thermal power plant with energy storage and electricity buy-back from grid," *Energy*, vol. 51, pp. 61–70, 2013.

[89] R. Sioshansi and P. Denholm, "The value of concentrating solar power and thermal energy storage," *Sustainable Energy, IEEE Transactions on*, vol. 1, no. 3, pp. 173–183, 2010.

[90] R. Dominguez, L. Baringo, and A. J. Conejo, "Optimal offering strategy for a concentrating solar power plant," *Applied Energy*, vol. 98, 2012.

[91] C. Budischak, D. Sewell, H. Thomson, L. Mach, D. E. Veron, and W. Kempton, "Cost-minimized combinations of wind power, solar power and electrochemical storage, powering the grid up to 99.9% of the time," *Journal of Power Sources*, vol. 225, pp. 60–74, 2013.

[92] U. Helman and C. Loutan, "Operational Requirements and Generation Fleet Capability at 20% RPS," *Aug*, vol. 31, pp. 784–790, 2010.

[93] Y. Chen, P. R. Gribik, L. Zhang, R. Merring, J. Gardner, K. Sperry, and X. Ma, "Real time ramp model in midwest iso co-optimized energy and ancillary service market design," in *Power & Energy Society General Meeting, 2009. PES'09. IEEE*, pp. 1–8, IEEE.

[94] B. Wang and B. F. Hobbs, "Flexiramp market design for real-time operations: Can it approach the stochastic optimization ideal?," in *Power and Energy Society General Meeting (PES), 2013 IEEE*, pp. 1–5, IEEE.

[95] K. H. Abdul-Rahman, H. Alarian, M. Rothleder, P. Ristanovic, B. Vesovic, and B. Lu, "Enhanced system reliability using flexible ramp constraint in caiso market," in *Power and Energy Society General Meeting, 2012 IEEE*, pp. 1–6, IEEE.

[96] N. W. Miller, M. Shao, S. Pajic, and R. D. Aquila, "Western Wind and Solar Integration Study, Phases 1-3," tech. rep., 2014.

[97] M. Zugno, J. M. Morales González, P. Pinson, and H. Madsen, "Modeling demand response in electricity retail markets as a stackelberg game," in *12th IAEE European Energy Conference: Energy challenge and environmental sustainability*.

[98] E. Castillo, A. J. Conejo, P. Pedregal, R. Garcia, and N. Alguacil, *Building and solving mathematical programming models in engineering and science*, vol. 62. John Wiley & Sons, 2011.

[99] Australian Energy Market Operator (AEMO), "National Transmission Network Development Plan 2016," report, 2016.

[100] P. Kundur, J. Paserba, V. Ajjarapu, G. Andersson, A. Bose, C. Canizares, N. Hatziargyriou, D. Hill, A. Stankovic, C. Taylor, T. V. Cutsem, and V. Vittal, "Definition and classification of power system stability ieee/cigre joint task force on stability terms and definitions," *IEEE Transactions on Power Systems*, vol. 19, pp. 1387–1401, Aug 2004.

[101] N. W. Miller, M. Shao, and S. Venkataraman, "California ISO (CAISO) Frequency Response Study," Tech. Rep. Nov, 2011.

[102] N. W. Miller, M. Shao, S. Pajić, and R. D. Aquila, "Western Wind and Solar Integration Study Phase 3 Frequency Response and Transient Stability ," Tech. Rep. DRS8.3020, NREL, Dec 2014.

[103] EirGrid and System Operator for Northern Ireland (SONI), "All Island Tso Facilitation of Renewables Studies," tech. rep., 2010.

[104] R. Doherty, A. Mullane, G. Nolan, D. Burke, A. Bryson, and M. O'Malley, "An Assessment of the Impact of Wind Generation on System Frequency Control," *IEEE Transactions on Power Systems*, vol. 25, pp. 452–460, Feb 2010.

[105] The EirGrid Group, "The DS3 Programme - Delivering a secure, sustainable electricity system," tech. rep., EirGrid Group, 2015.

[106] ERCOT, "ERCOT CONCEPT PAPER: Future Ancillary Services in ERCOT," Tech. Rep. Version 1.0, ERCOT, Sep 2013.

[107] AEMO, "Future Power System Security Program," Tech. Rep. Aug, 2016.

[108] AEMO, "Guide to Ancillary Services in the National Electricity Market," Tech. Rep. Apr, AEMO, 2015.

[109] DNV KEMA Energy & Sustainability, "RoCoF An independent analysis on the ability of Generators to ride through Rate of Change of Frequency values up to 2Hz /s .," Tech. Rep. 4478894, London, 2013.

[110] NERC, "Industry Advisory -Turbine Combustor Lean Blowout," tech. rep., NERC, Jun 2008.

[111] J. O'Sullivan, A. Rogers, D. Flynn, S. Member, P. Smith, A. Mullane, and M. O'Malley, "Studying the Maximum Instantaneous Non-Synchronous Generation in an Island System - Frequency Stability Challenges in Ireland," *IEEE Transactions on Power Systems*, vol. 29, no. 6, pp. 2943–2951, 2014.

[112] H. Ahmadi and H. Ghasemi, "Maximum penetration level of wind generation considering power system security limits," *IET Generation, Transmission & Distribution*, vol. 6, pp. 1164–1170, Nov 2012.

[113] A. S. Ahmadyar, S. Riaz, G. Verbič, J. Riesz, and A. C. Chapman, "Assessment of Minimum Inertia Requirement for System Frequency Stability," in *2016 IEEE International Conference on Power Systems Technology (POWERCON)*, (Wollongong), 2016.

[114] F. L. Alvarado, J. Meng, C. L. DeMarco, and W. S. Mota, "Stability analysis of interconnected power systems coupled with market dynamics," *IEEE Transactions on Power Systems*, vol. 16, pp. 695–701, Nov 2001.

[115] IEEE Task Force on Load Representation for Dynamic Performance, "Load representation for dynamic performance analysis," *IEEE Transactions on Power Systems*, vol. 8, no. 2, pp. 472–482, 1993.

[116] L. Hiskens and J. V. Milanović, "Load modelling in studies of power system damping," *IEEE Transactions on Power Systems*, vol. 10, no. 4, pp. 1781–1788, 1995.

Appendix A

Transformation of bi-level optimisation to MILP

Bi-level optimisation problem presented in Section 2.4 is precise in narration, it cannot be solved directly due to nested optimisation. Given that the prosumer problem is convex, it can be translated in to a computationally retractable model by incorporating its KKT conditions along with slackness variables in the upper level optimisation to form a MILP. Prosumer nested optimisation problem along with the dual variables associated with relative constraints is represented in equation (A.1).

$$\underset{p^{\mathrm{g+}}_{p,t},\, p^{\mathrm{b}}_{p,t}}{\text{minimise}} \quad \sum_{t\in\mathcal{T}} p^{\mathrm{g+}}_{p,t}, \tag{A.1a}$$

$$p^{\mathrm{g+}}_{p,t} + p^{\mathrm{pv}}_{p,t} = p_{p,t} + p^{\mathrm{b}}_{p,t} \qquad (\lambda^{\mathrm{p}}_{p,t}), \tag{A.1b}$$

$$e^{\mathrm{b}}_{p,t} = \eta^{\mathrm{b}}_{p} e^{\mathrm{b}}_{p,t-1} + p^{\mathrm{b}}_{p,t} \qquad (\lambda^{\mathrm{e}}_{p,t}), \tag{A.1c}$$

$$p^{\mathrm{g+}}_{p,t} \geq 0 \qquad (\mu^{\mathrm{g+}}_{p,t}), \tag{A.1d}$$

$$\overline{p}^{\mathrm{b\text{-}}}_{p,t} \leq p^{\mathrm{b}}_{p,t} \qquad (\mu^{\underline{\mathrm{p}}}_{p,t}), \tag{A.1e}$$

$$p^{\mathrm{b}}_{p,t} \leq \overline{p}^{\mathrm{b+}}_{p,t} \qquad (\mu^{\overline{\mathrm{p}}}_{p,t}), \tag{A.1f}$$

$$\underline{e}^{\mathrm{b}}_{p,t} \leq e^{\mathrm{b}}_{p,t} \qquad (\mu^{\underline{\mathrm{e}}}_{p,t}), \tag{A.1g}$$

$$e^{\mathrm{b}}_{p,t} \leq \overline{e}^{\mathrm{b}}_{p,t} \qquad (\mu^{\overline{\mathrm{e}}}_{p,t}). \tag{A.1h}$$

$$\tag{A.1i}$$

The Lagrangian of follower (A.1) can be expressed as:

$$\begin{aligned}\mathcal{L}(p^{\mathrm{g+}}_{p,t}, p^{\mathrm{b}}_{p,t}, e^{\mathrm{b}}_{p,t}, \mu^{\mathrm{g+}}_{p,t}, \lambda^{\mathrm{p}}_{p,t}, \mu^{\underline{\mathrm{p}}}_{p,t}, \mu^{\overline{\mathrm{p}}}_{p,t}, \mu^{\underline{\mathrm{e}}}_{p,t}, \mu^{\overline{\mathrm{e}}}_{p,t}, \lambda^{\mathrm{e}}_{p,t}) = \\ &\sum_{t\in\mathcal{T}} p^{\mathrm{g+}}_{p,t} \\ &+ \lambda^{\mathrm{p}}_{p,t}(p^{\mathrm{g+}}_{p,t} + p^{\mathrm{pv}}_{p,t} - p_{p,t} - p^{\mathrm{b}}_{p,t}) \\ &+ \lambda^{\mathrm{e}}_{p,t}(e^{\mathrm{b}}_{p,t} - \eta^{\mathrm{b}}_{p} e^{\mathrm{b}}_{p,t-1} - p^{\mathrm{b}}_{p,t}) \\ &+ \mu^{\mathrm{g+}}_{p,t}(-p^{\mathrm{g+}}_{p,t}) \\ &+ \mu^{\underline{\mathrm{p}}}_{p,t}(\overline{p}^{\mathrm{b\text{-}}}_{p,t} - p^{\mathrm{b}}_{p,t}) \\ &+ \mu^{\overline{\mathrm{p}}}_{p,t}(p^{\mathrm{b}}_{p,t} - \overline{p}^{\mathrm{b+}}_{p,t}) \\ &+ \mu^{\underline{\mathrm{e}}}_{p,t}(\underline{e}^{\mathrm{b}}_{p,t} - e^{\mathrm{b}}_{p,t}) \\ &+ \mu^{\underline{\mathrm{e}}}_{p,t}(e^{\mathrm{b}}_{p,t} - \overline{e}^{\mathrm{b}}_{p,t}). \end{aligned} \tag{A.2}$$

The partial derivative of Lagrangian presented in equation (A.2) can be written as:

$$\frac{\partial \mathcal{L}(.)}{p^{\mathrm{g+}}_{p,t}} = 1 - \mu^{\mathrm{g+}}_{p,t} + \lambda^{\mathrm{p}}_{p,t}, \tag{A.3a}$$

$$\frac{\partial \mathcal{L}(.)}{p^{\mathrm{b}}_{p,t}} = -\lambda^{\mathrm{p}}_{p,t} - \lambda^{\mathrm{e}}_{p,t} - \mu^{\underline{\mathrm{p}}}_{p,t} + \mu^{\overline{\mathrm{p}}}_{p,t}, \tag{A.3b}$$

$$\frac{\partial \mathcal{L}(.)}{e^{\mathrm{b}}_{p,t}} = \lambda^{\mathrm{e}}_{p,t} - \eta^{\mathrm{b}}_{p}\lambda^{\mathrm{e}}_{p,t+1} - \mu^{\underline{\mathrm{e}}}_{p,t} + \mu^{\overline{\mathrm{e}}}_{p,t}. \tag{A.3c}$$

As optimisation problem (A.1) is convex minimisation problem with linear constraints, the KKT condition are necessary and sufficient conditions for optimality. Therefore the

problem is equivalent to set of conditions (A.4).

$$1-\mu^{\mathrm{g+}}_{p,t}+\lambda^{\mathrm{p}}_{p,t}=0, \tag{A.4a}$$
$$-\lambda^{\mathrm{p}}_{p,t}-\lambda^{\mathrm{e}}_{p,t}-\mu^{\underline{\mathrm{p}}}_{p,t}+\mu^{\overline{\mathrm{p}}}_{p,t}=0, \tag{A.4b}$$
$$\lambda^{\mathrm{e}}_{p,t}-\eta^{\mathrm{b}}_{p}\lambda^{\mathrm{e}}_{p,t+1}-\mu^{\underline{\mathrm{e}}}_{p,t}+\mu^{\overline{\mathrm{e}}}_{p,t}=0, \tag{A.4c}$$
$$0 \quad \leq \quad \mu^{\mathrm{g+}}_{p,t} \quad \perp \quad p^{\mathrm{g+}}_{p,t} \quad \geq \quad 0, \tag{A.4d}$$
$$\lambda^{\mathrm{p}}_{p,t} \quad \text{free} \quad p^{\mathrm{g+}}_{p,t}+p^{\mathrm{pv}}_{p,t}-p_{p,t}-p^{\mathrm{b}}_{p,t} \quad = \quad 0, \tag{A.4e}$$
$$\lambda^{\mathrm{e}}_{p,t} \quad \text{free} \quad e^{\mathrm{b}}_{p,t}-\eta^{\mathrm{b}}_{p}e^{\mathrm{b}}_{p,t-1}-p^{\mathrm{b}}_{p,t} \quad = \quad 0, \tag{A.4f}$$
$$0 \quad \leq \quad \mu^{\underline{\mathrm{p}}}_{p,t} \quad \perp \quad -\overline{p}^{\mathrm{b\text{-}}}_{p,t}+p^{\mathrm{b}}_{p,t} \quad \geq 0, \tag{A.4g}$$
$$0 \quad \leq \quad \mu^{\overline{\mathrm{p}}}_{p,t} \quad \perp \quad -p^{\mathrm{b}}_{p,t}+\overline{p}^{\mathrm{b+}}_{p,t} \quad \geq 0, \tag{A.4h}$$
$$0 \quad \leq \quad \mu^{\underline{\mathrm{e}}}_{p,t} \quad \perp \quad -\underline{e}^{\mathrm{b}}_{p,t}+e^{\mathrm{b}}_{p,t} \quad \geq 0, \tag{A.4i}$$
$$0 \quad \leq \quad \mu^{\overline{\mathrm{e}}}_{p,t} \quad \perp \quad -e^{\mathrm{b}}_{p,t}+\overline{e}^{\mathrm{b}}_{p,t} \quad \geq 0. \tag{A.4j}$$

In (A.4d)- (A.4j), orthogonality ($\perp$) conditions ensures that primal constraint is zero when its dual variable is non zero and vice versa. Although these constraint are still non-linear however they can converted into MILP by introducing a binary variable to maintain orthognality, for example equation (A.4d) is identical to equations (A.5):

$$0 \quad \leq \quad p^{\mathrm{g+}}_{p,t}, \tag{A.5a}$$
$$p^{\mathrm{g+}}_{p,t} \quad \leq \quad M^{\mathrm{g+}}b^{\mathrm{g+}}_{p,t}, \tag{A.5b}$$
$$0 \quad \leq \quad \mu^{\mathrm{g+}}_{p,t}, \tag{A.5c}$$
$$\mu^{\mathrm{g+}}_{p,t} \quad \leq \quad M^{\mathrm{g+}}(1-b^{\mathrm{g+}}_{p,t}), \tag{A.5d}$$

where addition of $b^{\mathrm{g+}}_{p,t} \in \{0,1\}$ is used to deal with the non-linearity of the equation (A.4d) and ensures that constraints (A.5a) and (A.5c) are always orthogonal. Also, $M^{\mathrm{g+}}$ is a large enough constant that ensure that the constraints (A.5b) and (A.5d) are never binding when corresponding variable has non-zero value. Thus, follower problem (A.4) is equivalent

to (A.6).

$$
\begin{aligned}
1-\mu^{\mathrm{g+}}_{p,t}+\lambda^{\mathrm{p}}_{p,t} &= 0, && \text{(A.6a)}\\
-\lambda^{\mathrm{p}}_{p,t}-\lambda^{\mathrm{e}}_{p,t}-\mu^{\underline{\mathrm{p}}}_{p,t}+\mu^{\overline{\mathrm{p}}}_{p,t} &= 0, && \text{(A.6b)}\\
\lambda^{\mathrm{e}}_{p,t}-\eta^{\mathrm{b}}_{p}\lambda^{\mathrm{e}}_{p,t+1}-\mu^{\underline{\mathrm{e}}}_{p,t}+\mu^{\overline{\mathrm{e}}}_{p,t} &= 0, && \text{(A.6c)}\\
p^{\mathrm{g+}}_{p,t}+p^{\mathrm{pv}}_{p,t}-p_{p,t}-p^{\mathrm{b}}_{p,t} &= 0, && \text{(A.6d)}\\
e^{\mathrm{b}}_{p,t}-\eta^{\mathrm{b}}_{p}e^{\mathrm{b}}_{p,t-1}-p^{\mathrm{b}}_{p,t} &= 0, && \text{(A.6e)}\\
p^{\mathrm{g+}}_{p,t} &\leq M^{\mathrm{g+}}b^{\mathrm{g+}}_{p,t}, && \text{(A.6f)}\\
\mu^{\mathrm{g+}}_{p,t} &\leq M^{\mathrm{g+}}(1-b^{\mathrm{g+}}_{p,t}), && \text{(A.6g)}\\
\overline{p}^{\mathrm{b\text{-}}}_{p,t} &\leq p^{\mathrm{b}}_{p,t}, && \text{(A.6h)}\\
p^{\mathrm{b}}_{p,t} &\leq M^{\underline{\mathrm{p}}}b^{\underline{\mathrm{p}}}_{p,t}, && \text{(A.6i)}\\
\mu^{\underline{\mathrm{p}}}_{p,t} &\leq M^{\underline{\mathrm{p}}}(1-b^{\underline{\mathrm{p}}}_{p,t}), && \text{(A.6j)}\\
p^{\mathrm{b}}_{p,t} &\leq \overline{p}^{\mathrm{b+}}_{p,t}, && \text{(A.6k)}\\
-M^{\overline{\mathrm{p}}}b^{\overline{\mathrm{p}}}_{p,t} &\leq p^{\mathrm{b}}_{p,t}, && \text{(A.6l)}\\
\mu^{\overline{\mathrm{p}}}_{p,t} &\leq M^{\overline{\mathrm{p}}}(1-b^{\overline{\mathrm{p}}}_{p,t}), && \text{(A.6m)}\\
\underline{e}^{\mathrm{b}}_{p,t} &\leq e^{\mathrm{b}}_{p,t}, && \text{(A.6n)}\\
e^{\mathrm{b}}_{p,t} &\leq M^{\underline{\mathrm{e}}}b^{\underline{\mathrm{e}}}_{p,t}, && \text{(A.6o)}\\
\mu^{\underline{\mathrm{e}}}_{p,t} &\leq M^{\underline{\mathrm{e}}}(1-b^{\underline{\mathrm{e}}}_{p,t}), && \text{(A.6p)}\\
e^{\mathrm{b}}_{p,t} &\leq \overline{e}^{\mathrm{b}}_{p,t}, && \text{(A.6q)}\\
-M^{\overline{\mathrm{e}}}b^{\overline{\mathrm{e}}}_{p,t} &\leq e^{\mathrm{b}}_{p,t}, && \text{(A.6r)}\\
\mu^{\overline{\mathrm{e}}}_{p,t} &\leq M^{\overline{\mathrm{e}}}(1-b^{\overline{\mathrm{e}}}_{p,t}), && \text{(A.6s)}\\
0 &\leq p^{\mathrm{g+}}_{p,t},\ \mu^{\mathrm{g+}}_{p,t},\ \mu^{\underline{\mathrm{p}}}_{p,t},\ \mu^{\overline{\mathrm{p}}}_{p,t},\ \mu^{\underline{\mathrm{e}}}_{p,t},\ \mu^{\overline{\mathrm{e}}}_{p,t} && \text{(A.6t)}
\end{aligned}
$$

Substituting prosumers MILP equivalent problem (A.6) with prosumer constraint in 2.4.1, the resultant MILP market model is as follows:

$$
\underset{\Omega}{\text{minimise}} \quad \sum_{t\in\mathcal{T}}\sum_{g\in\mathcal{G}}\Big(c^{\mathrm{fix}}_{g}s_{g,t}+c^{\mathrm{su}}_{g}u_{g,t}+c^{\mathrm{sd}}_{g}d_{g,t}+c^{\mathrm{var}}_{g}p_{g,t}\Big), \tag{A.7}
$$

where decision variables are as follows:

$$
s_{g,t}, u_{g,t}, d_{g,t}, b^{\mathrm{g+}}_{p,t}, b^{\underline{\mathrm{p}}}_{p,t}, b^{\overline{\mathrm{p}}}_{p,t}, b^{\underline{\mathrm{e}}}_{p,t}, b^{\overline{\mathrm{e}}}_{p,t} \in \{0,1\},
$$

$$
p_{g,t}, p^{\mathrm{g+}}_{p,t}, e^{\mathrm{b}}_{p,t}, \mu^{\mathrm{g+}}_{p,t}, \mu^{\underline{\mathrm{p}}}_{p,t}, \mu^{\overline{\mathrm{p}}}_{p,t}, \mu^{\underline{\mathrm{e}}}_{p,t}, \mu^{\overline{\mathrm{e}}}_{p,t} \in \mathbb{R}^{+},
$$

$$p_{s,t}, p^{\mathrm{b}}_{p,t}, \lambda^{\mathrm{p}}_{p,t}, \lambda^{\mathrm{e}}_{p,t} \in \mathbb{R},$$

$$\sum_{g \in \mathcal{G}} p_{g,t} = p_{c,t} + p^{\mathrm{g+}}_{p,t} \qquad \forall t, \tag{A.8}$$

$$\sum_{g \in \mathcal{G}^{\mathrm{syn}}} (\overline{p}_g - p_{g,t}) s_{g,t} \geq p^{\mathrm{r}}_t \qquad \forall t, \tag{A.9}$$

$$u_{g,t} - d_{g,t} = s_{g,t} - s_{g,t-1} \qquad \forall g,t, \tag{A.10}$$

$$\underline{p}_g s_{g,t} \leq p_{g,t} \leq \overline{p}_g s_{g,t} \qquad \forall g,t, \tag{A.11}$$

$$-r^-_g \leq p_{g,t} - p_{g,t-1} \leq r^+_g \qquad \forall g,t, \tag{A.12}$$

$$u_{g,t} - \sum_{\tilde{t}=0}^{\tau^{\mathrm{u}}_g - 1} d_{g,t+\tilde{t}} \leq 1 \qquad \forall g,t, \tag{A.13}$$

$$d_{g,t} - \sum_{\tilde{t}=0}^{\tau^{\mathrm{d}}_g - 1} u_{g,t+\tilde{t}} \leq 1 \qquad \forall g,t, \tag{A.14}$$

$$e_{s,t} = \eta_s e_{s,t-1} + p_{s,t} \qquad \forall s,t, \tag{A.15}$$

$$\underline{e}_s \leq e_{s,t} \leq \overline{e}_s \qquad \forall s,t. \tag{A.16}$$

$$\overline{p}^-_s \leq p_{s,t} \leq \overline{p}^+_s \qquad \forall s,t, \tag{A.17}$$

$$1 - \mu^{\mathrm{g+}}_{p,t} + \lambda^{\mathrm{p}}_{p,t} = 0 \qquad \forall p,t, \tag{A.18}$$

$$-\lambda^{\mathrm{p}}_{p,t} - \lambda^{\mathrm{e}}_{p,t} - \mu^{\underline{\mathrm{p}}}_{p,t} + \mu^{\overline{\mathrm{p}}}_{p,t} = 0 \qquad \forall p,t, \tag{A.19}$$

$$\lambda^{\mathrm{e}}_{p,t} - \eta^{\mathrm{b}}_p \lambda^{\mathrm{e}}_{p,t+1} - \mu^{\underline{\mathrm{e}}}_{p,t} + \mu^{\overline{\mathrm{e}}}_{p,t} = 0 \qquad \forall p,t, \tag{A.20}$$

$$p^{\mathrm{g+}}_{p,t} + p^{\mathrm{pv}}_{p,t} - p_{p,t} - p^{\mathrm{b}}_{p,t} = 0 \qquad \forall p,t, \tag{A.21a}$$

$$e^{\mathrm{b}}_{p,t} - \eta^{\mathrm{b}}_p e^{\mathrm{b}}_{p,t-1} - p^{\mathrm{b}}_{p,t} = 0 \qquad \forall p,t. \tag{A.21b}$$

$$p^{\mathrm{g+}}_{p,t} \leq M^{\mathrm{g+}} b^{\mathrm{g+}}_{p,t} \qquad \forall p,t, \tag{A.21c}$$

$$\mu^{\mathrm{g+}}_{p,t} \leq M^{\mathrm{g+}} (1 - b^{\mathrm{g+}}_{p,t}) \qquad \forall p,t, \tag{A.21d}$$

$$\overline{p}^{\mathrm{b\text{-}}}_{p,t} \leq p^{\mathrm{b}}_{p,t} \qquad \forall p,t, \tag{A.21e}$$

$$p^{\mathrm{b}}_{p,t} \leq M^{\underline{\mathrm{p}}} b^{\underline{\mathrm{p}}}_{p,t} \qquad \forall p,t, \tag{A.21f}$$

$$\mu^{\underline{\mathrm{p}}}_{p,t} \leq M^{\underline{\mathrm{p}}} (1 - b^{\underline{\mathrm{p}}}_{p,t}) \qquad \forall p,t, \tag{A.21g}$$

$$p^{\mathrm{b}}_{p,t} \leq \overline{p}^{\mathrm{b+}}_{p,t} \qquad \forall p,t, \tag{A.21h}$$

$$-M^{\overline{\mathrm{p}}} b^{\overline{\mathrm{p}}}_{p,t} \leq p^{\mathrm{b}}_{p,t} \qquad \forall p,t, \tag{A.21i}$$

$$\mu^{\overline{\mathrm{p}}}_{p,t} \leq M^{\overline{\mathrm{p}}}(1-b^{\overline{\mathrm{p}}}_{p,t}) \qquad \forall p,t, \tag{A.21j}$$

$$\underline{e}^{\mathrm{b}}_{p,t} \leq e^{\mathrm{b}}_{p,t} \qquad \forall p,t, \tag{A.21k}$$

$$e^{\mathrm{b}}_{p,t} \leq M^{\underline{\mathrm{e}}} b^{\underline{\mathrm{e}}}_{p,t} \qquad \forall p,t, \tag{A.21l}$$

$$\mu^{\underline{\mathrm{e}}}_{p,t} \leq M^{\underline{\mathrm{e}}}(1-b^{\underline{\mathrm{e}}}_{p,t}) \qquad \forall p,t, \tag{A.21m}$$

$$e^{\mathrm{b}}_{p,t} \leq \overline{e}^{\mathrm{b}}_{p,t} \qquad \forall p,t, \tag{A.21n}$$

$$-M^{\overline{\mathrm{e}}} b^{\overline{\mathrm{e}}}_{p,t} \leq e^{\mathrm{b}}_{p,t} \qquad \forall p,t, \tag{A.21o}$$

$$\mu^{\overline{\mathrm{e}}}_{p,t} \leq M^{\overline{\mathrm{e}}}(1-b^{\overline{\mathrm{e}}}_{p,t}) \qquad \forall p,t, \tag{A.21p}$$